An Exploration of Geometric and Electronic Effects in Metal Nanoparticle Catalysts

BY

David Childers

B.S.E., University of Michigan, Ann Arbor 2009

THESIS

Submitted as partial fulfillments of the requirements
for the degree of Doctor of Philosophy
in Chemical Engineering in the Graduate College of
the University of Illinois-Chicago, 2014

Chicago, Illinois

Defense Committee:

Randall Meyer, Chair and Advisor

Jeff Miller, Argonne National Laboratory

Neil Schweitzer, Northwestern University

Michael Trenary, Chemistry

Brian Chaplin, Chemical Engineering

ACKNOWLEDGEMENTS

Throughout my four and a half years as a graduate student I have changed advisors, projects and even research locations though I can honestly say that all of these events have benefitted me as a researcher. This work would not have been possible without the help of numerous individuals.

First and foremost, I would like to thank Dr. Randall Meyer who accepted me into his group and greatly influenced my ideals about research. His willingness to incorporate theoretical and experimental work in the same projects has greatly influenced my views on research and how it should be conducted. I'd also like to thank Dr. Jeff Miller for being an advisor at Argonne National Lab. I cannot state how much being able to learn from you and your wealth of experience has made me a better scientist.

Dr. Neil Schweitzer and Dr. Tianpin Wu, your knowledge, experience and willingness to help greatly aided my ability to perform experiments and analyze data. I'd also like to thank the research staffs at both the Advanced Photon Source and Research Resource Center for their assistance and knowledge of characterization techniques.

I also would like to thank Dr. John Regalbuto for taking me in initially and helping me start my path in catalysis research. To all members of the Regalbuto and Meyer groups, past and present, thank you for your help and friendship.

I'd like to thank my other committee members Dr. Michael Trenary and Dr. Brian Chaplin for their time and expertise.

I would never have accomplished any of this if not for the support of my family and friends. To my wife Amanda, you are the reason I have made it this far. Thank you.

-David

Contribution of Authors

Chapter 1 is a literature review that places my dissertation question in the context of the larger field and highlights the significance of my research question. Chapter 2 represents a published manuscript[1] for which I was the primary author and major driver of the research. Arindom Saha conducted the experiment shown in Figure 25. My research mentor, Dr. Randall Meyer contributed to the writing of the manuscript. Chapter 3 represents a published manuscript[2] for which I was the second author. I generated Figures 8, 9 and 11 and Table 2 and played a large role in the writing of the manuscript along with the first author Tianpin Wu and my supervisor at Argonne National Lab, Dr. Jeff Miller. My work was critical to the conclusions of this manuscript because the differences in catalytic behavior supported the conclusion that the surface compositions were different and gave some insight into the possible active site of the catalyst. Chapter 4 represents a series of my own unpublished experiments directed at answering the question of the role of the core metal in a bimetallic catalyst. This work has been submitted for publication to the journal *Catalysis Science & Technology* where I was the primary author. Seyed Shahari conducted the experiment shown in Figure 33b. My research mentor, Dr. Randall Meyer contributed to the writing of the manuscript. Chapter 5 represents an accepted manuscript to *Journal of Catalysis* for which I was the primary author and major driver of the research. Seyed Shahari conducted the experiment shown in Table XII. My research mentor, Dr. Randall Meyer contributed to the writing of the manuscript. In Chapter 6 represents my synthesis of the research presented in this thesis/dissertation and my overarching conclusions. The future directions of this field and this research question are discussed.

TABLE OF CONTENTS

LIST OF FIGURES

LIST OF TABLES

LIST OF ABBREVIATIONS

APS – Advanced Photon Source

BCC – Body-centered cubic

CN – Coordination number

DFT – Density functional theory

DRIFTS – Diffuse reflectance infrared Fourier transform spectroscopy

DSC – Differential scanning calorimeter

EDS – Energy dispersive spectroscopy

EELS – Electron energy loss spectroscopy

EXAFS – Extended x-ray absorption fine structure

FCC – Fluid catalytic cracking

fcc – face-centered cubic

FID – Flame Ionization Detector

FTIR – Fourier Transform Infrared

GC – Gas chromatograph

IR - Infrared

IWI – Incipient wetness impregnation

MRCAT – Materials Research Collaborative Access Team

OD – Outer diameter

PZC – Point of zero charge

SEA – Strong electrostatic adsorption

STEM – Scanning transmission electron microscopy

TCD – Thermal conductivity detector

TEM – Transmission electron microscopy

TOR – Turnover rate

UIC – University of Illinois at Chicago

UOP – Universal oil products

XEDS – X-ray energy dispersive spectroscopy

XRD – X-ray diffraction

XAS – X-ray absorption spectroscopy

XANES – X-ray absorption near edge spectroscopy

ZSM-5 – Zeolite Socony Mobile-5

SUMMARY

The goal of this thesis is to investigate the influence of geometric and electronic effects on metal nanoparticle catalysis. There are three main methods which alter a catalyst's properties: changing support material, changing nanoparticle size and alloying a second metal. This work will focus on the latter two methods using Pt-group metals and alloys. Platinum and palladium were chosen as the active metals due to a large amount of industry significance and prior literature to draw upon. Neopentane conversion and propane dehydrogenation were the two probe reactions used to evaluate these catalysts mainly due to their relative simplicity and ease of operation on a laboratory scale.

The effect of particle size was studied with Pt and Pd monometallic catalysts using neopentane hydrogenolysis/isomerization as the probe reaction. Particle size studies have been done previously using this reaction so there is literature data to compare this study's results. This data will also be used as comparison for the bimetallic studies conducted later so that particle size effects can be accounted for when attempting to determine the effect of alloying a second metal.

Bimetallic catalysts have several different possible structures depending on a number of factors from the identity of the two metals to the synthesis procedure. Homogeneous, core-shell and intermetallic alloys are the three structures evaluated in this work. Determining the surface composition of a homogeneous alloy can be difficult especially if both metals adsorb CO. PtPd homogeneous alloys were used to evaluate the ability of EXAFS to give information about surface composition using CO adsorption. These catalysts were also tested using neopentane conversion to evaluate changes in catalytic performance. Core-shell catalysts can also exhibit

unique properties although it is not clear whether the identity of the core metal is relevant or if surface changes are most important to changing catalytic behavior. PdAu catalysts were synthesized with varying Pd loadings to determine if the Au-rich core would continue to influence neopentane conversion performance with increasing Pd layers on the surface of the nanoparticle. Finally, intermetallic alloys have produced some very interesting literature results and can drastically alter catalyst surface structure. PdZn showed the potential to improve neopentane isomerization selectivity past that of Pt based on calculated electronic properties. Two PdZn catalysts with different loadings were synthesized to evaluate the electronic and geometric effects using both neopentane conversion and propane dehydrogenation.

1 INTRODUCTION

1.1 Heterogeneous Catalysis

Over the last century, heterogeneous catalysis (the use of solid catalysts with either gaseous or liquid phase reactants) has become a major component of the fuels and chemicals industry and so a great emphasis has been put on research to discover how these catalysts work. Typical heterogeneous catalysts involve the use of metal nanoparticles (e.g. Pd, Pt) dispersed on high surface area inert supports (e.g. Al_2O_3, SiO_2). Early on, many studies focused on reactions that produced a single product, i.e. carbon monoxide oxidation, ethene hydrogenation and ammonia synthesis.[3] These studies focused on improving the catalyst's activity and stability, but were limited in scope due mainly to experimental limitations. However, there are a vast number of important chemical reactions that have numerous possible pathways and multiple end products so catalyst selectivity (where selectivity is defined as the rate of reaction along a particular pathway divided by the sum of the rates along all reaction pathways) often becomes the critical aspect for catalyst performance.[4]

Altering a catalyst's selectivity can be accomplished by several different methods including: changing metal particle size, addition of other metals to the catalyst (alloying) and changing the support material. This thesis will focus primarily on the first two methods: particle size and alloying. Two different probe reactions will be used to evaluate these changes: neopentane hydrogenolysis and propane dehydrogenation. In the remainder of this chapter we will discuss the methods of altering selectivity, previous work on bimetallic catalysts, the two probe reactions stated earlier and a preview of the experiments conducted in subsequent

chapters: Chapter 2 (Pt and Pd particle size effects), Chapter 3 (PtPd bimetallic catalysts), Chapter 4 (PdAu core-shell catalysts) and Chapter 5 (PdZn intermetallic catalysts).

The performance of metal nanoparticle based heterogeneous catalysts can be linked to two intrinsic properties of the catalyst: the geometric structure and the electronic character. Geometric effects are usually thought to be dominant for structure sensitive reactions where reactive site geometry is critical to catalyst performance. Structure sensitive reactions are those whose kinetics are based upon which crystal facets of the metal nanoparticles are present. Boudart was the first to divide reactions into two groups based on structure sensitivity.[5] Boudart studied structure sensitivity on a number of different reactions including: ethane oxidation, Fisher-Tropsch synthesis, formic acid dehydrogenation and dehydration and ammonia synthesis.[6-9] Geometric effects can also be described as ensemble effects, where a reactive ensemble is the minimum number of active sites for a reaction pathway to proceed. Altering the geometry of the particles through the three methods stated earlier to provide more reactive ensembles for the desired reaction while decreasing the number of available ensembles for any undesired reactions will increase the selectivity of the catalyst. Figure 1 gives a visual representation of how ensembles and the ratio of edge/corner to terrace sites change as size is increased.[10] Corner and edge sites dominate on smaller particles while terrace sites and larger ensembles of active sites will be dominant on larger particles. With these studies came the discovery that certain reactions would occur preferentially at certain types of sites (edge sites vs. terrace sites) and so a lot of investigation began into the structure sensitivity of reactions. Ammonia synthesis over iron catalysts is an example of structure sensitivity. Dumesic et al. performed a study of ammonia synthesis over Fe/MgO catalysts varying in size from 1.5 to 150 nm.[6] In earlier work it was found that tungsten, a BCC metal, had higher ammonia

decomposition rates at 111 surfaces compared to 100 and 110 planes. Since iron is also a BCC metal and was found to preferentially form 111 planes under nitrogen, the authors reasoned that it may be a good catalyst to evaluate the structure sensitivity of this reaction. They found that activity increased by over an order of magnitude with particle size and this trend was consistent even with different pretreatment steps. It is mentioned that an electronic effect, the increasing metal-support interaction with decreasing particle size, could contribute to this trend. However, the authors believe that this change is due more to the change in the relative proportion of sites with increased activity for ammonia synthesis.

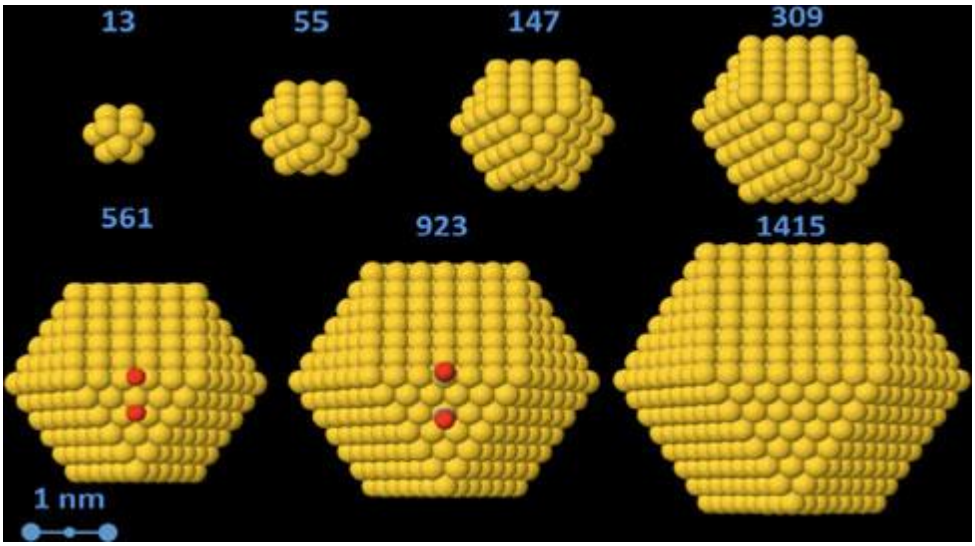

Figure 1: Closed shell cuboctahedra gold clusters of varying sizes[10]

Electronic effects are defined as changes in the chemical reactivity based on the changes in the electronic structure of the metal nanoparticle. Changing the particle size can alter the surface energy of the particles; smaller particles tend to have higher surface energies and therefore will bind adsorbates more strongly than larger particles in an attempt to lower the overall energy of the system. This can also be affected by changing supports; certain supports can bind metals more strongly which will also affect the electronic properties of the particles.

Charge transfer may also occur between the metal and support, changing the electronic structure of the metal nanoparticle.[11, 12] These effects are exacerbated as the particle size decreases. In addition, decreasing the particle size will decrease the metal-metal bond distance in the particle. This observation can be explained in two different ways: the surface tension increases with decreasing radius and lattice contraction resulting from the decrease in coordination number with decreasing particle size.[13] Although this has been proven to be true for most metals (both experimentally and theoretically), there have been conflicting studies on palladium. Some theoretical studies have calculated that Pd-Pd bonds will expand in very small nanoparticles.[14-16] Kruger et al. performed DFT studies combined with EXAFS measurements to investigate these discrepancies. Using DFT, they studied icosahedral, cuboctahedral and octahedral shaped Pd clusters and compared their results with EXAFS measurements done on plasma polymer stabilized Pd clusters. They found that palladium particles by themselves do not deviate from the expected trend, but outside factors like support effects, ligand effects, defect atoms and surface oxidation can cause elongation of Pd-Pd bonds. Oxidation in particular can cause Pd-Pd bonds to elongate by as much as 0.2 angstroms. With this study there is strong evidence that there is a consistent relationship between changing particle size and electronic effects but that these properties can also be affected by other factors. Here we see that changing the geometry via particle size (geometric effect) simultaneously changes the bonding properties of the particle (electronic effect). It is also clear that the support, defects, and impurities like oxygen can also have an effect on the electronic characteristics of the metal. Alloying with another metal can drastically affect the electronic properties of a catalyst. Two effects are present simultaneously when alloying. First, charge transfer may occur between the alloying elements due to differences in the level of filling and relative energies of the valence orbitals. Second, changes in

hybridization in the bonding between metals may result due to changes in the bond distances between metal atoms. At the same time, the orbital extents of the alloying elements are different resulting in changes in the overlap between the bonding orbitals. Therefore alloying can result in a wide range of electronic effects based on the degree of charge transfer and hybridization changes.

Although it is known that these two aspects of the catalyst are both important, it is unknown whether one factor contributes more to control of selectivity than the other. Experimentally, it is very difficult to isolate one effect from the other, as changing particle size, support or alloying all change the geometry of the particles and alter the electronic structure as well. Schuit and van Reijen studied ethylene hydrogenation over a variety of metals.[17] They found that the metals in the middle of each transition series had the maximum hydrogenation activity. The changes in lattice spacing have been ascribed to these changes in activity; however, the percentage of metallic d-character has also been suggested as a cause. These metals (Ni, Rh and Pt) have an intermediate strength of adsorption so that the adsorbate does not bind too strongly or too weakly for the reaction to occur. Despite this fact, the differences in the heats of adsorption were fairly small, making it difficult to determine whether or not this was the dominant factor in deciding activity.[18] Altering a catalyst's kinetics almost always involves altering a catalyst's geometry and electronic properties simultaneously. It is very difficult to determine whether one of these changes has a more significant impact than the other. If we can use elucidating characterization techniques to determine if one factor is dominant for a particular reaction, we can use that knowledge to better and more efficiently design catalysts.

1.2 Influencing Selectivity

1.2.1 Particle Size

Changing the metal particle size is one of the simplest and most common ways to alter a catalyst's kinetics. It has been known for a long time that when metal particles go below a certain size that their properties (even magnetism) will begin to deviate from the properties of the bulk metal.[18] Bulk metals tend to have stable crystal structures that result in only a few different low surface energy planes being present. As the metal particle size is decreased, minimum energy structures result in an increase in the percentage of undercoordinated metal atoms at the edges and corners of facets of the nanoparticle. The decrease in the coordination of edge and corner atoms of the nanoparticle can cause changes in the kinetics. Some studies have even suggested that the low coordination corner and edge sites are solely responsible for the catalyst performance.[19, 20] These arguments focus on the geometric effects through changing site geometry; however there are also electronic effects present when changing particle size. For transition metal catalysts, a decrease in coordination results in a shift of the d-band toward the Fermi level resulting in a more reactive surface increasing the adsorption energy for the reactants and products. Changes in adsorption energy will result in corresponding changes in the catalyst performance. In many cases, Norskov et al have shown that the d-band center is the single defining factor in describing the catalytic activity. Therefore particle size can have a profound effect on both the activity and selectivity.

Norskov's group has also analyzed when a particle's properties begin to change from those of the bulk solid to a nanoparticle.[10] The fact that small nanoparticles begin to behave differently than the bulk metal indicates that, for certain particle sizes, extrapolating single-crystal surface properties to nanoparticles may be incorrect. They used unsupported gold

particles in this study because of the fact that larger gold particles are essentially inactive while at smaller sizes they become active for several different reactions like CO oxidation. Through their calculations of CO and O adsorption on different size Au particles it was concluded that above 2.7 nm, gold particles would exhibit similar surface properties to the bulk metal. Below that size they found effects caused by charge density responses to adsorption events on the cluster. This indicates that single crystal studies would be viable for particles at least 3nm in diameter provided other factors like temperature, pressure and support effects were accounted for as well.

Schauermann et al. used direct calorimetric measurement of CO adsorption enthalpies to analyze particle size effects.[21] They used Pd nanoparticles supported on a Fe_3O_4(111)/Pt(111) film as the model catalyst ranging in size from 1.8 to 8 nm. They found that the initial CO heat of adsorption decreased with decreasing particle size. Changes in catalyst performance observed through particle size are generally thought to be caused by changes in the ratio of low coordination to high coordination sites, however, their theoretical calculations and experimental results suggest that the degree of coordination of surface atoms is not the important factor in determining CO adsorption energies. They offer two other possible explanations for the dependence of CO adsorption energies on particle size. The first possibility is the decrease of chemisorption energy which can cause a contraction in the lattice parameters of small nanoparticles. Calculations have been done to support the idea that this lattice contraction can reduce adsorbate binding energies by 10-15 kJ/mol compared to the bulk metal. They also found that this effect on adsorbate binding energy was not limited to certain sites (hollow or edge sites) but was a general trend throughout the particle. The second explanation offered involves the weakening of the van der Waals attraction or dispersion force caused by changes in how bulk

metal electrons interact with adsorbates. The authors concluded that the large magnitude of change in the heat of adsorption (40 kJ/mol) indicated that both of these factors most likely contributed to this behavior.

The results from the study by Schauermann et al. present a correlation between particle size and adsorption energy that is the opposite of those found by several other authors. Henry et al. performed a size effect study of CO chemisorption on Pd clusters of different sizes.[22] They found that the adsorption energy increases with decreasing size and this effect was observed for Pd nanoparticles on numerous supports (MgO, Al_2O_3, SiO_2 and TiO_2). Both geometric effects and electronic effects are invoked to explain the results. An electronic effect is attributed to the change in the valence band as the size of the nanoparticles decreased whereas a geometric effect originates from the local nature of the chemisorption bond. A number of different studies support the assertion that adsorption energies of molecules increase as the metal coordination decrease.[1, 23, 24] The increase in the proportion of low coordinated sites (corners and edges) as the particle size decreases demonstrates a geometric effect. These sites with lower coordination will bind adsorbates more strongly and the adsorption energy therefore increases with decreasing particle sizes. This relationship has been further probed by Hammer et al. using DFT calculations to study CO adsorption on Pt surfaces.[25] They calculated that the CO adsorption energy would increase by 0.7 eV at a Pt (111) step site compared to terrace sites. Calculations on a number of other possible surface sites created a linear correlation between CO chemisorption energy and the Pt d-band center. The closer the d-band center is to the Fermi level, the higher the CO chemisorption energy. CO adsorption was theoretically studied fairly extensively by Norskov's group and they found similar correlations between adsorption energy and particle size.[26-29] These theoretical results correspond to the experimental results stated

above. It is unlikely that the Pd/Fe_3O_4 samples studied by Schauermann et al. deviate from these trends without significant interaction with the support or some other unexplained phenomena changing the adsorption behavior.

Of course this change in adsorption behavior with particle size will lead to changes in the observed catalytic behavior and indeed, reports of particle size effects exist for a large number of catalyst systems and reactions. For example, Park et al. studied the effect of cobalt particle size on Fisher-Tropsch synthesis. They found that conversion and activity reached a maximum around 9.3 nm Co particle diameter.[30] Gracia et al. studied CO oxidation over Pt catalysts supported on silica and determined that changes in kinetics were due to structure sensitivity (i.e. the ratio of corner/edge sites to terrace sites) and that the activity increased with increasing particle size.[31] Claus et al. studied crotonaldehyde hydrogenation over silica and titania-supported Ag catalysts. They determined that selectivity to the desired product (crotyl alcohol) increased with increasing particle size also due to structure sensitivity.[32] Padilla-Serrano et al. studied the effect of Pt particle size on the catalytic combustion of xylenes and determined that Pt particle size was inversely proportional to xylene combustion activity.[33] These studies represent a few of the different chemistries where particle size has been proven to be an important aspect of catalysis involving both electronic and geometric effects.

1.2.2 Alloying

Bimetallic catalysts have become a significant point in catalysis research in the past few decades.[34-36] In many cases the bimetallic systems have selectivities and activities that are significantly different from what would be expected from physical mixtures of the two metals.[2, 36-38] For many reactions, bimetallic catalysts have shown enhanced stability and increased activity and selectivity compared to monometallic catalysts. Sinfelt et al. performed studies that

showed the increased stability of Pt-Ir particles compared to pure Pt over a long period for high octane gasoline production as seen in Figure 2. This change in stability is credited to the iridium's high hydrogenolysis activity, which breaks up longer chain carbonaceous molecules before they can deactivate the surface. A problem with pure Ir catalysts is that this high hydrogenolysis activity produces lighter, less valuable hydrocarbons; however the inclusion of platinum suppresses this activity enough that it prevents coking but does not break up the product molecules.

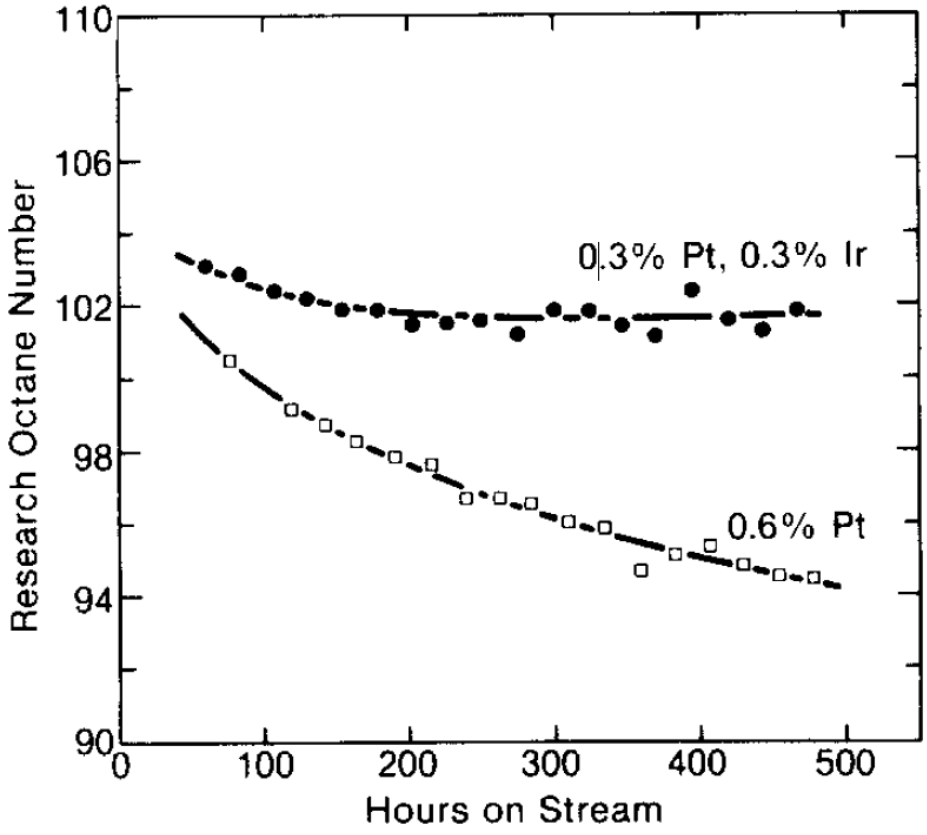

Figure 2: Stability of Pt-Ir vs. Pt for gasoline production[39]

Sinfelt also did some of the first studies analyzing altering the selectivity of specific reactions pathways. This is another aspect of bimetallic catalysts that can differ greatly from the

two single metals. An example of this is shown in Figure 3. As more copper is added to a nickel catalyst it is clear that this is impeding ethane hydrogenolysis while the cyclohexane dehydrogenation reaction activity remains constant. This catalyst's activity for one reaction involving light hydrocarbons was decreased while the desired reaction was unaffected. Another way of explaining selectivity is altering the activity of a catalyst to one pathway while the other pathway's activity increases or stays constant. The fact that bimetallic catalysts have shown an ability to turn off hydrogenolysis reactions makes them extremely relevant to industry and a major part of this work. Although there are many bimetallic systems in use today in many different processes (catalytic reforming, pollution control, alcohol oxidation and fuel cell catalysis), there is still very little known about how the combination of these metals alters the kinetics.[40] Working to understand the underlying principles of bimetallic catalysts can allow us to vastly improve how researchers attempt to find new catalysts.

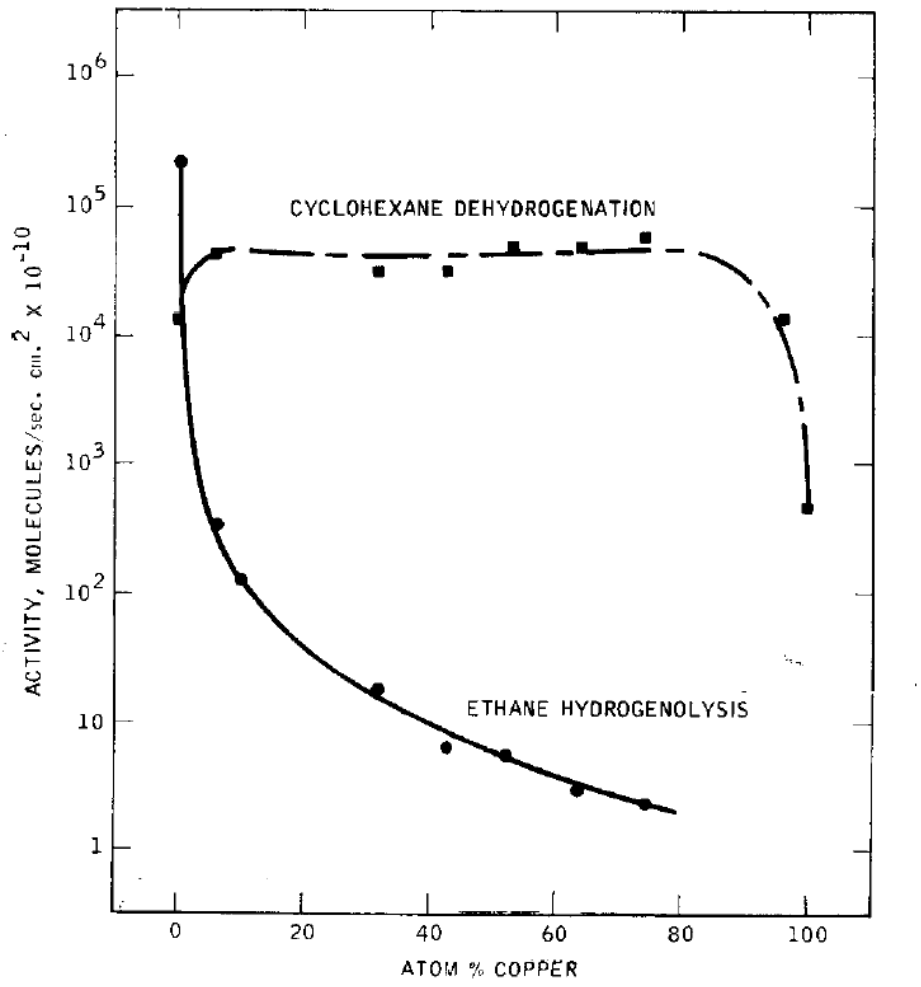

Figure 3: Effect of adding copper to nickel on ethane hydrogenolysis vs. cyclohexane dehydrogenation[41]

Sinfelt performed much of the early work on bimetallic catalysts and the work on Pt-Ir allowed for the removal of tetraethyllead from transportation fuels in the 1980s by producing higher amounts of aromatic hydrocarbons in the gasoline which greatly reduced engine knock.[36] Although monometallic Pt used to be the standard catalyst for naphtha reforming, it has since been replaced by bimetallic catalysts such as Pt-Re.[42] Both Au and Sn have been used to alloy with Pt to increase the isomerization selectivity and thereby the octane number of the fuels produced using these catalysts.[37].[38] In addition to activity and selectivity, the tolerance of the catalyst to poisoning or coking can also be changed.[28] Hammer and Norskov

have used DFT simulations to study bimetallic systems.[28, 29] Using the d-band model to interpret the changes in reactivity and selectivity observed on bimetallic systems, they proposed a relationship between the d-band center and adsorption behavior that the adsorption behavior can be described as the average d-band filling of the metal atoms in the alloy.[29] Although this relationship has been applied to bimetallic systems with two transition metal alloys it may not be applicable to an alloy with a non-transition metal.

Bimetallic catalysts can be present in several different structures including: homogenous (randomly mixed) alloys, core-shell structures and intermetallics. What structure an alloy will adopt may be determined by the thermodynamics of the system (i.e. the lowest free energy) or by the kinetics of diffusive processes during the synthesis. The free energy is a function of the surface energy of the metals, the interfacial energy with the support (as in the case of monometallic nanoparticle structures) and the strength of the bonds between the metals. If a metal bonds more strongly to the second metal that to itself, alloy formation will be exothermic[43] and intermetallic alloys may form where there is an ordered structure. For example, PdCu forms an intermetallic with a bcc structure when Pd and Cu are each present at 50 mol%.[44-46] If alloy formation is endothermic, the metals will only remain alloyed when the entropic effect is sufficiently large (requiring higher temperatures) Homogenous alloys with a more random substitution can result when the alloy formation is close to thermoneutral.[43]. Surface segregation or core-shell structures may result when the free energy of mixing is no longer favorable for intermetallic or homogenous alloy formation. In this case, the metal with the lower surface energy may segregate to form a shell around the higher surface energy metal core. However, the formation of core//shell structures are often the result of kinetic effects. For example, a core-shell structure can occur if one of the metals is more readily oxidized than the

other. For instance, gold does not oxidize very easily and so will be located in the core while a metal like palladium will migrate to the surface and oxidize. For certain bimetallic systems, the core-shell structure can be altered by the reaction environment. Tao et al. studied RhPd and PtPd nanoparticles under oxidizing, reducing and reaction environments to analyze the effect on the core-shell structure of the particles. Following synthesis, the RhPd catalyst has a structure with a Rh-rich shell and a Pd-rich core, however when exposed to different gases the core-shell structure reverses as seen in Figure 4. This process also appears to be reversible since the structure changes can be reversed by reflowing those gases. The PtPd catalyst shows that this behavior is not universal. Figure 4 shows the consistent Pd-rich shell and Pt-rich core structure regardless of environment.[40] The number of different ways that a bimetallic catalyst's structure can be affected makes understanding them on a fundamental level very difficult. However, if these systems can be understood it opens up a great number of possibilities for novel and efficient catalysts. Through understanding the properties of the different metals, we can tune the synthesis parameters or reaction environment to form a specific structure that may have enhanced kinetic effects.

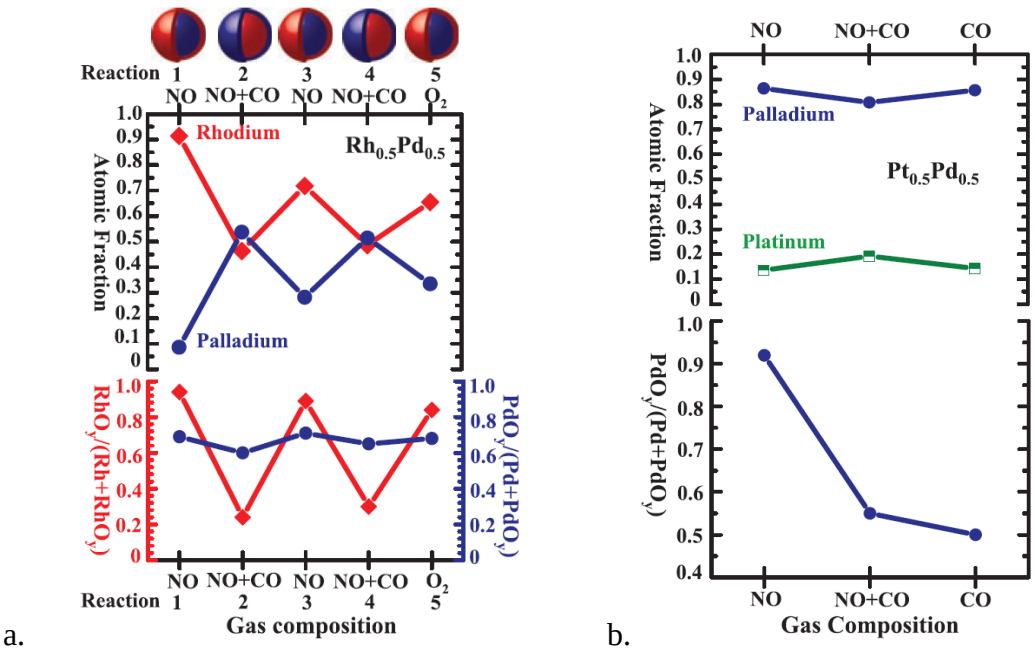

Figure 4: Changes in nanoparticle structure for a. RhPd and b. PtPd nanoparticles under varying gaseous environments studied by XPS[40]

1.3 Hydrogenolysis reactions

In general, hydrogenolysis reactions rupture carbon-carbon bonds and form carbon-hydrogen bonds. Many industrially relevant reactions involving hydrocarbons have hydrogenolysis as a potential pathway. Hydrogenolysis will convert hydrocarbons into lighter hydrocarbons which will typically be less valuable and so it can often be the undesired pathway. It has been studied on a wide array of reactants and over a number of different catalysts.[47-52] Hydrogenolysis is considered a model example of a structure-sensitive reaction where the geometry and identity of the active sites will dominate kinetics.[52] Understanding the hydrogenolysis mechanism can give insight into how to tune catalysts to prevent the reaction from happening.

Somorjai et al. studied the dehydrogenation and hydrogenolysis of cyclohexane and cyclohexene over Pt surfaces.[53] They wanted to determine which surface sites were responsible for the various bond breaking events (C-H, C-C and H-H cleavage) in these reactions,. By studying these reactions on a number of different Pt surfaces, it was possible to study the active sites for these different bond breaking steps. Using catalyst surfaces with varying kink-site density, they found that the rate of hydrogenolysis (C-C bond breaking) increased linearly with kink density; however the dehydrogenation rate (C-H and H-H bond breaking) remained constant. This behavior was described in terms of structure sensitivity, a geometric effect.

Sinfelt et al. studied cyclohexane dehydrogenation and ethane hydrogenolysis as seen previously in Figure 3.[48] This study was touched on in the previous section but will be discussed more thoroughly here. Ni catalysts were alloyed with increasing amounts of Cu to cause changes to the catalyst's properties. They found that cyclohexane dehydrogenation activity was unaffected by the addition of Cu for almost all the catalysts tested. The ethane hydrogenolysis activity was drastically reduced as Cu was added. These two reactions had completely different responses to the addition of Cu. The addition of Cu to Ni was found to decrease the average adsorption strength of hydrogen. Both an electronic effect and a geometric effect were proposed as explanations for this behavior. The electronic effect was the changes in the strength of hydrogen adsorption to Ni through the addition of Cu. A possible geometric effect was the proportion of active sites present on the catalyst surface. The surface composition must be determined in order for the possible geometric effects to be evaluated. For bimetallic catalysts, it can be very difficult to determine the surface composition of nanoparticles. Typical surface characterization methods like H_2 or CO chemisorption are not as viable when both metals

are active adsorbers of the probe molecule. In this case it becomes very difficult to determine how much adsorption each metal is responsible for on the surface.

Sinfelt described the mechanism of ethane hydrogenolysis. Ethane is chemisorbed with dissociation of carbon-hydrogen bonds and so the ethane molecule loses hydrogen to the surface. The hydrogen-deficient molecule then undergoes a carbon-carbon bond scission and at lower temperatures this is considered to be the rate limiting step. However, at elevated temperatures ethane may undergo additional dehydrogenation events that lead to the formation of strongly bound intermediates leading to more hydrogenolysis.[18] Rovik et al. studied ethane dehydrogenation/hydrogenolysis on different types of catalytic sites using Ni, Ru, Rh and Pd all co-impregnated with Ag supported on $MgAl_2O_4$.[54] Sinfelt also reported the changes in activity for hydrogenolysis for different metals.[51] Within each group the hydrogenolysis activity went through a maximum and then decreased as you went through the group as seen in Figure 5.[18] This behavior is related to the changes in percentage of d-character from one metal to another. These patterns were consistent for higher alkanes as well with only the magnitude of the activity increasing.

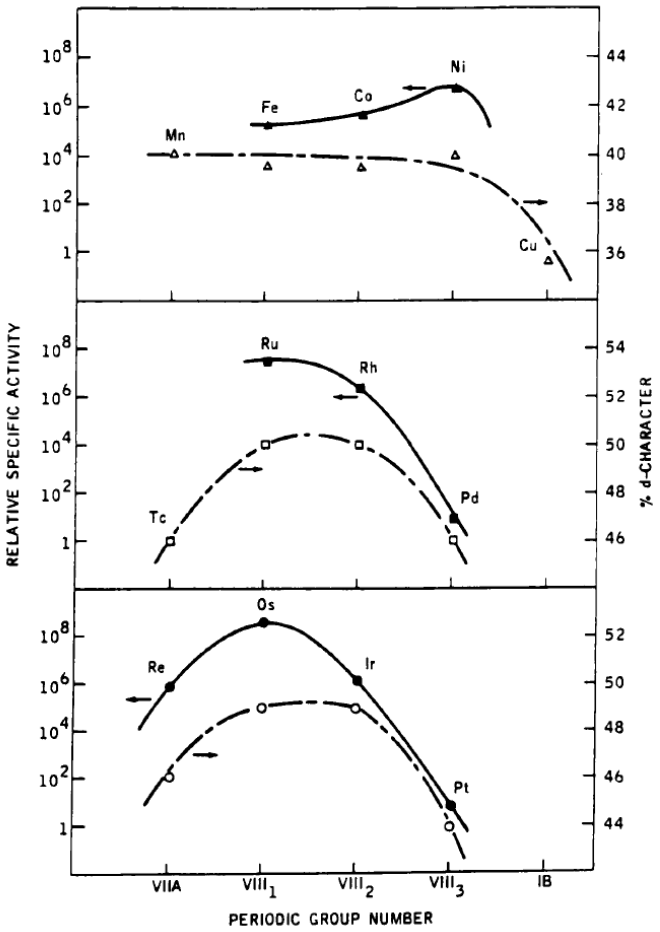

Figure 5: Activities of metals for ethylene hydrogenolysis[18]

In the case of ethane (and propane), hydrogenolysis always occurs via a terminal carbon. However, it is not clear if important site requirements change when examining higher alkanes. In the 1960s, Anderson and Avery performed mechanistic studies examining hydrocracking and isomerization reactions of ethane, n-butane, isobutene, neopentane and isopentane over Pt and Pd films.[55] Their study found that alkanes other than ethane had similar activation energies which were much lower than that of ethane. The similarity in activation energies led them to suggest a common 1,3 diadsorbed surface intermediate for these alkanes while ethane binds in a 1,2 diadsorbed state. This is driven by the differences in activation energy and the fact that

neopentane cannot bond to the surface in a 1,2 diadsorbed state. Both of these proposed surface intermediates require more than one active site and thus provide an example of how the geometry of the nanoparticle surface can become important. Ensembles of at least two sites may be required for these molecules to bind to the surface.

Although there has been work done on specific hydrogenolysis pathways, these are typically on simpler (ethane and propane) or model alkanes (neopentane) compared to those found in industrial processes (long chain isoalkanes or cycloalkanes). Finding an overall descriptor of hydrogenolysis kinetics would allow for studies on simpler molecules to be applied to a wider range of processes. Flaherty et al. attempted to find a descriptor for hydrogenolysis selectivity and activity using both experimental and theoretical techniques to study n-alkane hydrogenolysis over Ir, Rh and Pt nanoparticles.[52] They found that hydrogenolysis of a number of different alkanes required two active sites with adsorbed hydrogen to dehydrogenate the alkane before adsorbing to the surface. A relationship was found between activity and the number of carbons in the alkane; the hydrogenolysis rate constant would increase (10^8 between ethane and n-decane) with increasing chain length. This was attributed to the change in entropy between the two alkanes and these changes in entropy were also ascribed to the selectivity changes seen experimentally. While ethane and propane require C-C bond cleavage to occur at a terminal carbon bond, once the molecule has more than 4 carbon atoms hydrogenolysis occurs preferentially on nonterminal C-C bonds. The entropy of a larger alkane is less affected by adsorption to the surface and it maintains more intramolecular vibrations and configurations. Flaherty et al. developed a model using these entropy changes and this model fit the behavior of the three different metals and also with a few different particle sizes.

From these previous studies we can see that alkane hydrogenolysis requires two active sites and is related to the entropy of the adsorbate. A question that remains is what changes to catalysts will turn off the hydrogenolysis pathway. If the geometric aspect (two active sites) is the dominant factor then adjusting the surface structure so that these active sites are not present should not allow hydrogenolysis to proceed. However, if the adsorption strength and entropy of the adsorbate are significant then the electronic properties of the catalyst may be altered to inhibit hydrogenolysis. There is a possibility that both of these factors are equally important but it has not been greatly explored experimentally.

1.3.1 Neopentane Hydrogenolysis / Isomerization

The demand for fossil fuels is continuing to grow despite the increasing emphasis on finding replacement fuel sources. Therefore, advances in reforming processes will still be an important area for the foreseeable future.[56] Aside from demand, stricter regulations will require the refining process to adjust to meet higher quality standards. Selective isomerization of high n-alkanes to branched hydrocarbons is one method to improve the quality of these fuel stocks. Cracking or hydrogenolysis are other possible reactions which can occur in parallel to isomerization and so maximizing isomerization selectivity is an important goal in finding the ideal catalyst for these reactions.

Catalytic reforming is a major reaction in petroleum refining and so one of the most important reactions performed in the world today. The main purpose of catalytic reforming is to increase the octane number of a naphtha feedstock so that it will be usable in gasoline and involves the conversion of straight chain alkanes to branched alkanes as well as the dehydrogenation of cycloalkanes to form aromatics (as well as the dehydrogenation and cyclization of alkanes to aromatics).[57] Typical catalysts for hydrocarbon reforming are late d-

band transition metals such as Ir and Pt. Commercial catalysts are often complex alloys based on such late d-band transition metals which also involve inclusion of promoting metals such as Sn and Re. The study of actual naphtha reforming is difficult due to the number of products and difficulty in dealing with a multiphase system. Figure 6 shows the various reactions that naphtha can undergo. This illustrates the number of different pathways available for each molecule and so selectivity is a very important factor when making a catalyst for naphtha reforming.

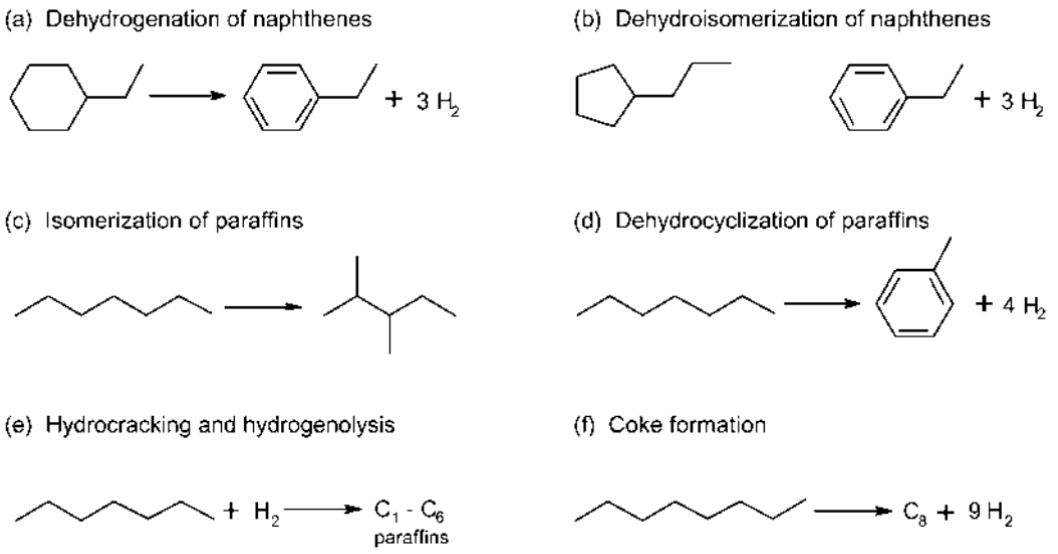

Figure 6: Naphtha reforming reactions[57]

Figure 7 illustrates a number of different processes involved in catalytic reforming. This work will focus on the isomerization unit that reforms light and straight-run naphtha. Neopentane hydrogenolysis is a widely used model reaction for characterization of noble metal catalysts.[37] Neopentane hydrogenolysis has two possible reaction pathways as shown in Figure 8, hydrogenolysis and isomerization. The former reaction involves carbon-carbon cleavage and is generally undesirable as it leads to light gas products while the latter is important for boosting octane values.[58-60]

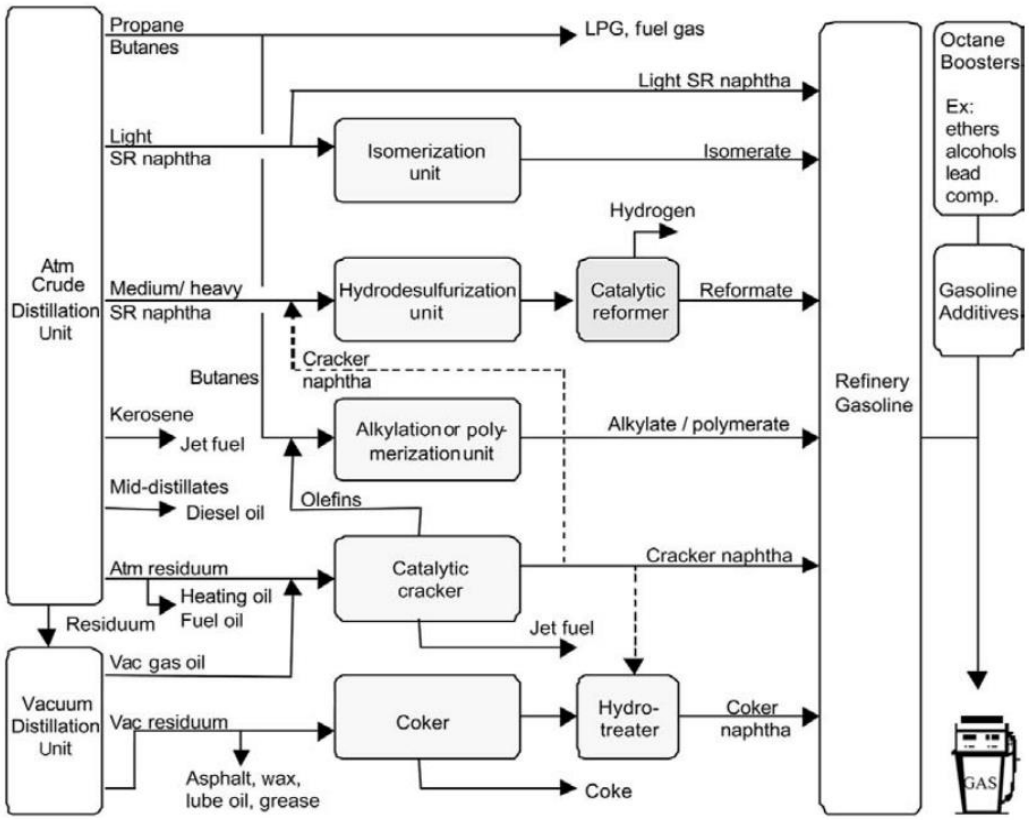

Figure 7: Process scheme for refinery production via reforming[57]

As Figure 8 illustrates, the products would be methane and i-butane for hydrogenolysis and isopentane for isomerization. In both cases, further reaction steps can occur to produce secondary products, such as propane and additional methane. Isomerization of the primary product, isopentane, can lead to formation of n-pentane. Isomerization involves a ring closure-ring opening through a cyclopropyl intermediate to produce isopentane. The selectivity for ring closure in naphtha reforming is important for the production of aromatics from paraffins, while hydrogenolysis leads to liquid yield loss.[56, 60, 61] Thus, the properties, which lead to higher isomerization selectivity for neopentane, generally lead to higher aromatic selectivity for naphtha reforming catalysts.

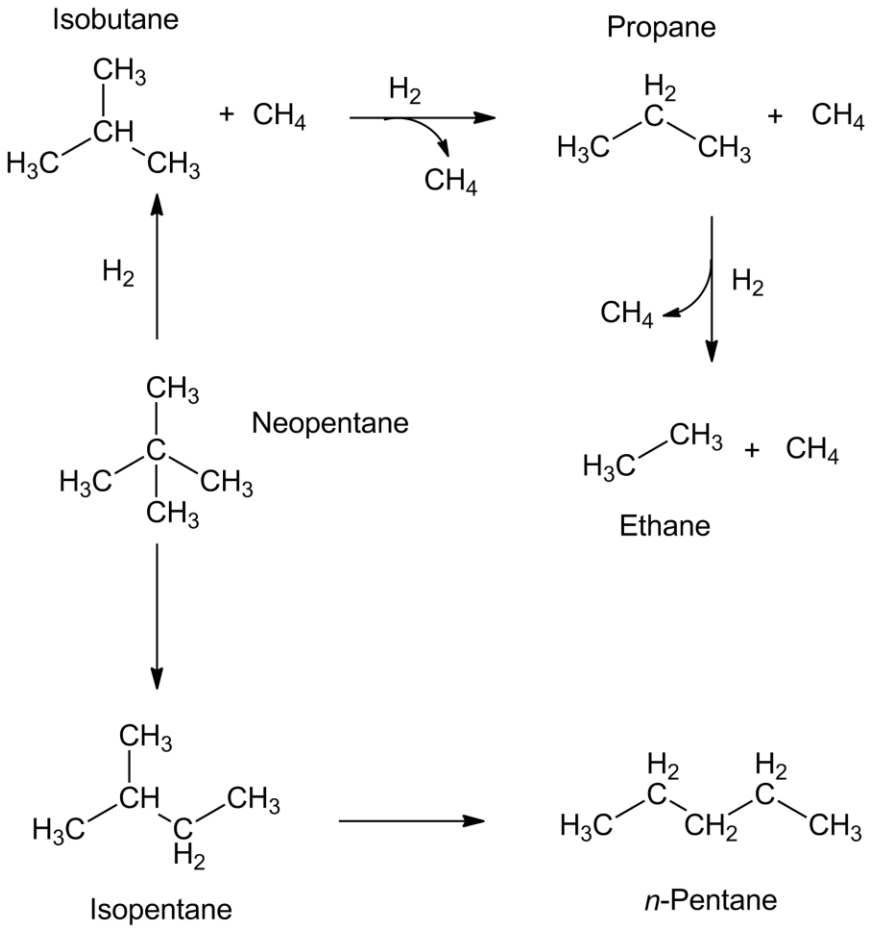

Figure 8: Reaction Pathways for neopentane hydrogenolysis

Neopentane or 2,2-dimethylpropane cannot form olefins or carbenium ions.[62, 63] Thus only metal catalyzed reactions are possible and selectivity studies are much easier to perform. In addition, neopentane hydrogenolysis is a popular test reaction due to the fact that deactivation is rarely a factor due to the lack of olefin formation (leading to coke) during the reaction.

1.3.2 Propane Dehydrogenation

Dehydrogenation of paraffins has been a major industrial reaction since the 1930s as the demand for high octane fuels emerged. A chromia-alumina catalyst developed both in Germany

and by UOP was the first industrial catalyst used for these types of reactions.[64] While chromia catalysts presented high rates of activity and selectivity, coking was the major downside which caused deactivation. Noble metal catalysts began being used for dehydrogenation around the 1960s to supply long-chain linear olefins for detergent production. Haensel had shown that platinum based catalysts had high activities for paraffin dehydrogenation as well as improved stability.[65] Bloch proved that these catalysts could also selectively dehydrogenate paraffins.[66]

At high temperature (~600°C), the selectivity tends to decrease due to the activation of the hydrogenolysis pathway and deactivation by either sintering or coke formation becomes problematic so improvements in both these aspects are desired. One way to limit coking and catalyst deactivation is to regenerate the catalyst, burn off the carbon on the surface and return the catalyst to its metallic state. This type of treatment has been in use since UOP introduced a process in the 1970's and have allowed noble metal catalysts to be used for several years without replacement. However, increasing the operation time between regeneration treatments remains a long-standing industry goal. In a similar way to neopentane hydrogenolysis, the first step in propane hydrogenolysis allows only for the formation of ethane and methane allowing us to treat the reaction as a two pathway system between hydrogenolysis (undesired) and dehydrogenation (desired).

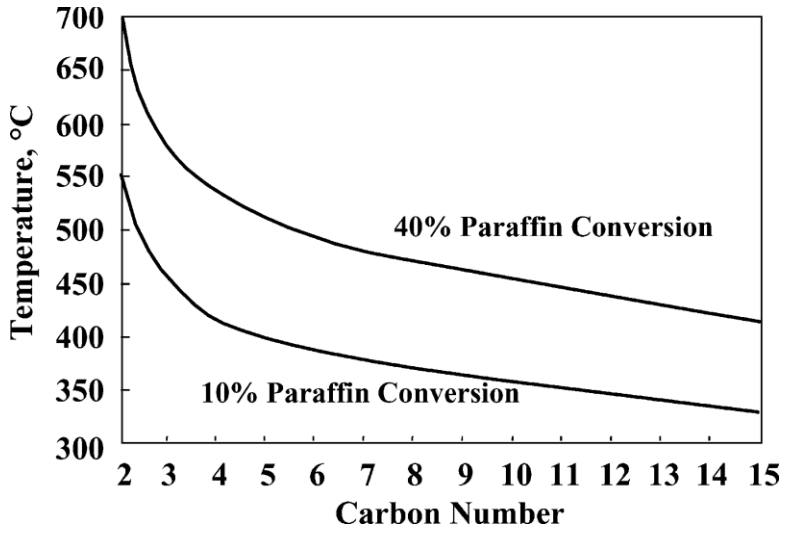

Figure 9: Temperatures required to obtain 10% and 40% alkane dehydrogenation conversion at certain length alkanes[64]

Propane dehydrogenation in particular is growing in industrial importance due to increased demand for propylene. Propylene is an important reactant in the production of polypropene, acrolein, polyacrylonitrile and acrylic acid.[67] Most propylene is now produced as a by-product of ethylene production via naphtha steam-cracking and fluid catalytic cracking (FCC) processes. Propane dehydrogenation is an endothermic reaction and so is limited by chemical equilibrium as can be seen in Figure 9. This implies that total conversion is controlled by the process conditions (temperature and pressure) and not by the properties of the catalyst. For example, the conversion can be increased by lowering the pressure or increasing the temperature.[64, 67] There is also a significant amount of study into oxidative propane dehydrogenation which is exothermic and so does not suffer from thermodynamic equilibrium limitations.[68-72] The introduction of oxygen has drawbacks however; increased danger of combustion and a significant loss in selectivity to propylene, mainly due to overoxidation which produces CO_2.[73, 74] Figure 10 shows the two possible pathways for propane conversion: hydrogenolysis and dehydrogenation. The main problems associated with this reaction are cracking selectivity, catalyst deactivation and equilibrium limitations. Both chromia and

platinum-based catalysts have these types of problems, however deactivation has been lessened through the use of Pt-Sn catalysts.[75] Ashmway studied propane dehydrogenation over chromia, palladium and platinum catalysts supported on alumina and silica in the late 1970s.[76] At this time chromia catalysts were the industry standard for propane dehydrogenation due to their high activity and selectivity. The monometallic Pt catalyst supported on silica had the lowest activity of the samples tested, while the Pd/Al_2O_3 catalyst had lower activity than the chromia catalyst but improved selectivity. The Pd catalyst also showed more resistance to coking and deactivation although the conclusions in this work were weakened since the comparisons were performed at identical conditions.

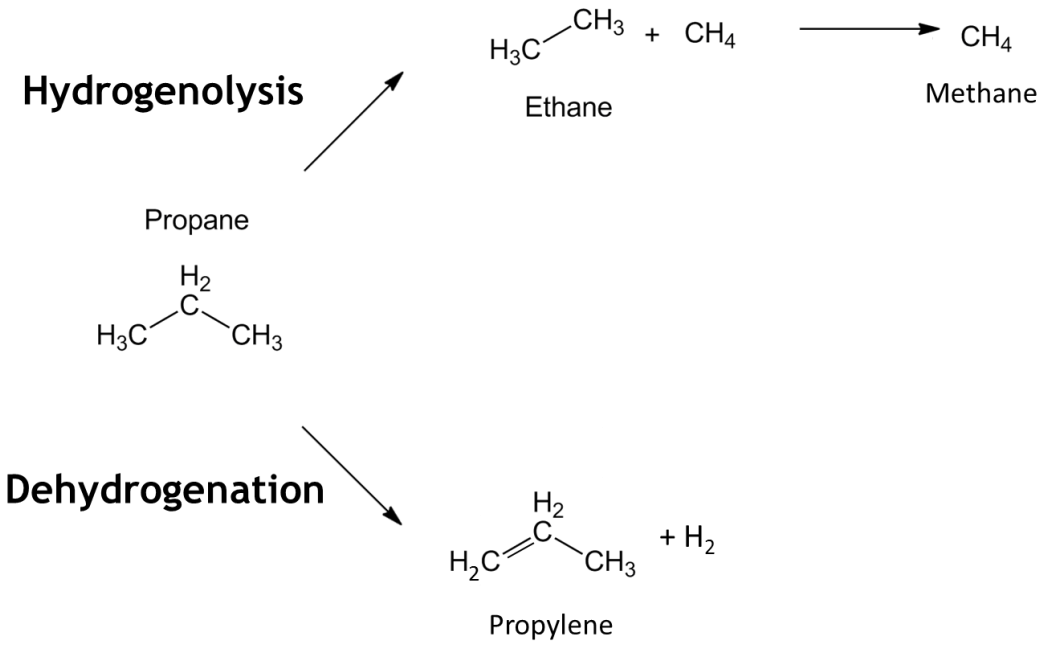

Figure 10: Propane dehydrogenation scheme

In the last few decades, bimetallic catalysts such as PtSn catalysts have become the industry standard for propane dehydrogenation due to their improved performance. Most of this improvement comes in resistance to coking and deactivation. Barias et al. studied PtSn catalysts

supported on alumina and silica in an attempt to determine why the catalyst displays the increased resistance to coking. They found that the Sn had different roles in the catalyst depending on the support. On silica, the Sn was nearly completely reduced and can therefore alloy with Pt. On alumina, the Sn is only partially reduced and so there is significant segregation of Pt and Sn on the surface. This difference results in an order of magnitude increase in the activity of the $PtSn/Al_2O_3$ catalyst over the $PtSn/SiO_2$ catalyst . The improved resistance to deactivation on the $PtSn/Al_2O_3$ catalyst is attributed to Sn poisoning the acid sites of the support, where hydrogenolysis reactions can also take place. The Sn was also suggested to help with hydrogen adsorption to the surface which also improves the catalyst stability.

Zhang et al. studied propane dehydrogenation over Pt and PtSn supported on the zeolite ZSM-5. The rigid ring structure of ZSM-5 could improve the stability of the catalyst by not allowing longer chain hydrocarbon deposits to form. Sn has already been shown to improve Pt stability for propane dehydrogenation and so PtSn supported on ZSM-5 could be a promising catalyst for this reaction. They found that the Sn promotes transfer of coking deposits from the active Pt sites to the Sn and the support resulting in improved stability. The rate of coke formation is not significantly changed; however, the active sites remain active because the carbonaceous deposits are on the support and not on the metal. These changes can be seen in Figure 11 which shows the stability of the catalysts tested by Zhang et al.[77] The addition of Sn provides a noticeable increase in stability over a long run time. The selectivity also improves as more Sn is added, from 70% for pure Pt to 82% for the 4%Sn catalyst. This work shows the number of different methods available to alter a catalyst's kinetics. It also highlights why gaining a fundamental understanding is vital to designing more effective catalysts. Finding the optimal

catalyst considering particle size, alloying and choice of support without understanding the fundamentals of selectivity change is not a practical solution.

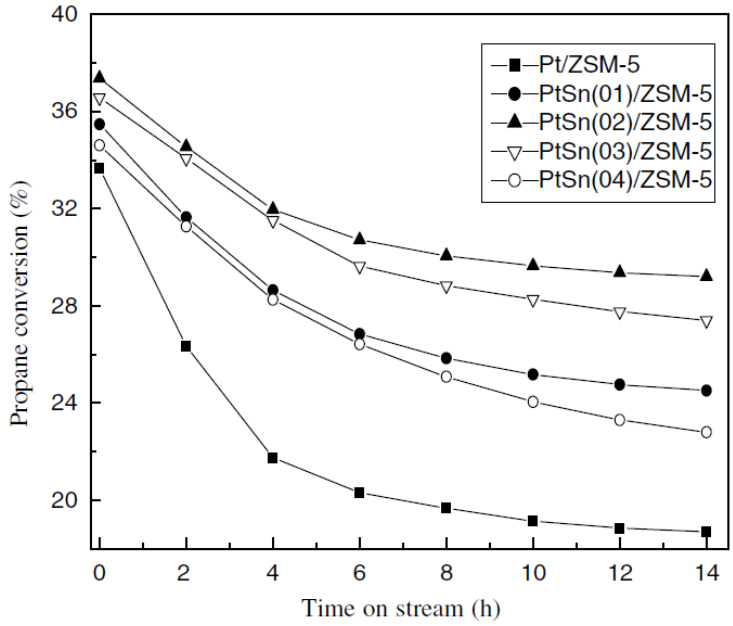

Figure 11: Propane conversion vs. time for Pt and PtSn catalysts supported on ZSM-5[77]

1.4 Preview of Experiments

In this work, we attempt to determine what factors control hydrogenolysis selectivity in both neopentane hydrogenolysis and propane dehydrogenation. In the process, we also work to understand the differences between electronic and geometric effects and if we can determine whether one is dominant. The wealth of literature information available and widespread industrial use of platinum and palladium catalysts and their alloys made them the best choice to begin our study. Initially, the effects of particle size were studied on both platinum and palladium monometallic catalysts. Secondly, a core-shell palladium-gold alloy catalyst was used to understand the role of the core of catalyst nanoparticles. Finally, a catalyst with an intermetallic structure was used.

1.4.1 Catalyst synthesis

Varying synthesis methods and parameters is the easiest way to obtain catalysts of different particle sizes and structures. Incipient wetness impregnation (IWI) and strong electrostatic adsorption (SEA) were the two methods used in this study. IWI is the most widely used industry technique and also the simplest. A support is contacted with just enough metal-precursor (generally a metal salt) containing liquid to fill the pore volume. All the metal in solution will go onto the surface due to lack of excess liquid; however, the precursor is often not evenly distributed and there can be significant particle growth during the drying process. In contrast, SEA uses excess solution and utilizes pH to facilitate metal uptake. The use of excess solution then results in a loss of some metal in that all of the metal is not guaranteed to be adsorbed to the surface. The main advantage of SEA comes in taking advantage of the point of zero charge (PZC) of oxide supports. The mechanism is shown in Figure 12. The hydroxyl groups on the surface of the oxide support will protonate and deprotonate depending on the pH of the surrounding solution. The point where there is a net neutral charge on the surface is the PZC. A support with a low PZC will have a net negative charge at high pH values while a high PZC material will have a net positive charge at low pH values.

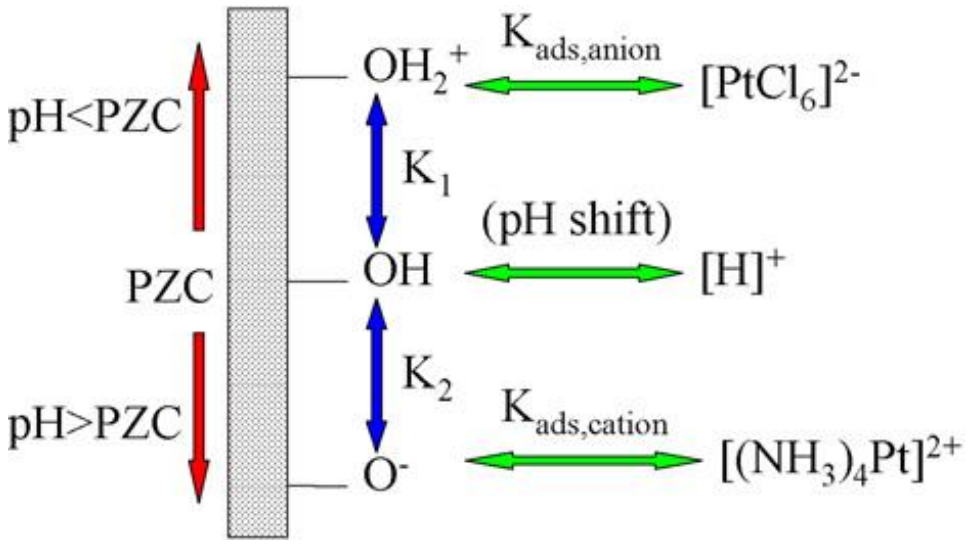

Figure 12: Strong electrostatic adsorption mechanism[78]

Precursors (either anionic or cationic as appropriate) can then be selected that will have the opposite charge as the support at a certain pH value and so the electrostatic interaction between the support and the precursor can strongly bind the metal to the surface. This allows for strong monolayer adsorption and can inhibit sintering during the post-treatment steps. However there are limitations in the types of precursors that can be used for this synthesis method as the precursor must be charged and remain stable in the solution often at extreme pH values.[79] To obtain metallic particles (and remove the salt ligands), the catalyst is subjected to a variety of treatments such as calcination and reduction after deposition. Different particle sizes, can be obtained for the same metal loading by varying the post-treatment steps' parameters (e.g.. reduction time and temperature). For example, by increasing the calcination or reduction temperatures the particles will become more mobile on the surface, making sintering more likely to occur and therefore larger particle sizes will be obtained.

For bimetallic catalysts, there were two different methods we used to synthesize these samples: sequential and co-impregnation. Sequential impregnation uses dry or wet impregnation

to adsorb one metal onto the surface, which is then dried and a second metal is then added by impregnation. Co-impregnation puts both metal precursors into the same solution and both are adsorbed to the surface at the same time. It depends greatly on the two metals being used as to which method will be the most effective to achieve the desired structure. The synthesis of bimetallic catalysts is often poorly understood with regard to the large parameter space that can be accessed (identity of the precursor, solution conditions, order of deposition, support, calcination and reduction conditions etc.) so structures are obtained largely by trial and error.[79]

1.4.2 Kinetics analysis

The determination of a catalyst's selectivity is the primary way that the catalyst's performance is evaluated and so it is paramount that the kinetics analysis is reproducible and accurate. Our first concern is that we are operating in a regime where mass transfer limitations are not present. Mass transfer limitations are present when the diffusion of the adsorbate molecules to the catalytic nanoparticle is occurring at a slower rate than the reaction itself, and therefore diffusion is the rate limiting step. If this is the case then one is unable to study the kinetics of the reaction, but rather the apparent activation energy is a function of both diffusion and reaction. The theoretical measure of the mass transfer effect is the Thiele modulus. The simple definition of the Thiele modulus is that it gives a ratio of the time for diffusion and the time for reaction. The Thiele modulus for a first-order reaction in a spherical particle is the equation[80]:

$$\Phi = \sqrt{\frac{ka^2}{D_a}}$$

k = the rate constant

a = catalyst pellet's volume-to-surface ratio

D_a = effective diffusivity in the pellet

From this equation, when the Thiele modulus is large (much greater than 1) then mass transfer is the limiting regime in the particle. In turn, when the Thiele modulus is small (much less than 1) the intrinsic kinetics are rate limiting and the true kinetics of the catalyst can be probed. The easiest way to determine if the system is in the kinetics limited or diffusion limited regime is to test the catalyst at varying grain sizes. Reducing the catalyst pellet's size changes the volume-to-surface ratio parameter (i.e. the characteristic length for diffusion) in the Thiele modulus equation. If the activity measurements are unchanged at different grain sizes it is safe to consider the catalyst to be in the kinetically controlled regime. This has been done for several of the catalysts tested and so we are confident that mass transfer did not play a role in these studies.

The next important aspect of accurate kinetics measurements is reproducibility. The selectivities and activities measured must be shown to be consistent across multiple trials. Figure 13 below shows the reproducibility of the activity measurements for one of the 2% Pd/SiO_2 catalysts. The data shown is within 5-6% error which is satisfactory for these types of studies. Reproducibility of the data also gives us confidence that the measured rates and selectivities at steady state conversions at each flow rate. Another important aspect of measuring kinetics is operation at differential conversion. This is necessary because in a plug flow reactor the rate is a function of position and therefore the rate may change as the concentration changes. Therefore, if

the conversion is high, then the reported rate is actually the result of the integrated rate as a function of reactor length and is, therefore, not single valued. Maintaining differential conversion allows us to assume a uniform concentration throughout the catalyst bed. Differential conversion is typically considered to be less than 10% though 0-5% is a better range. Differential conversion can be established by demonstrating a linear relationship between the conversion and 1/Flow rate as shown in Figure 13.

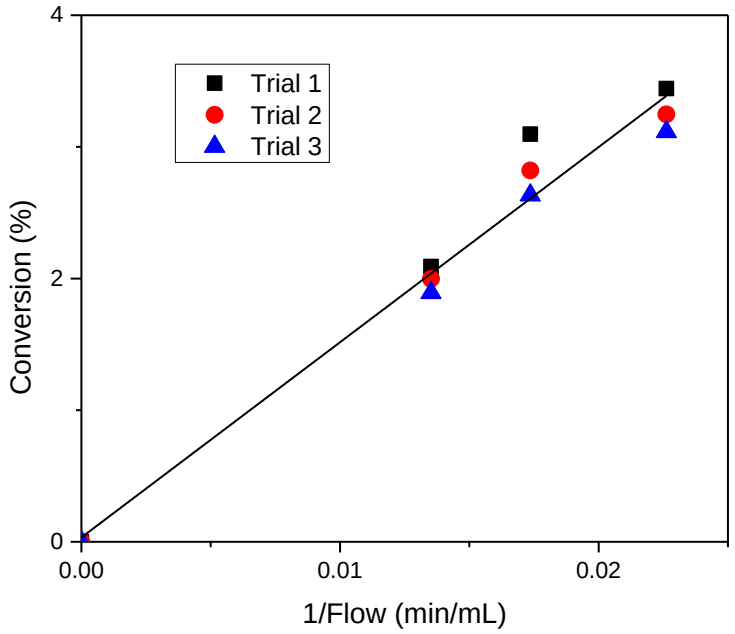

Figure 13: Reproducibility of activity measurements

In addition to stability, selectivity is critical to a successful catalyst. For selectivity measurements, differential conversion is desirable. Figure 14 shows an example of how selectivities were measured in these experiments. In order to easily compare selectivity between different catalysts all of the data was extrapolated back to 0% conversion. Selectivities have to be

compared at the same conversion to judge whether one catalyst is more selective.

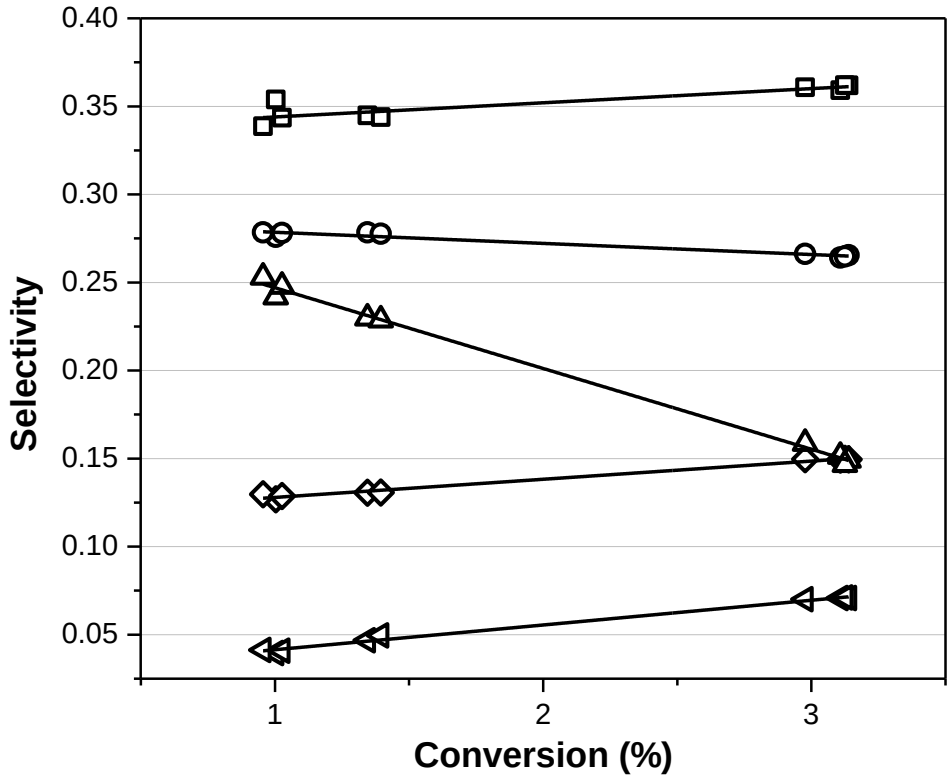

Figure 14: Selectivity for the 1% Pt(1.2nm)/SiO_2 catalyst at differential conversion. Reaction conditions were 0.35% neopentane, 3.5% H_2, balance He and 271°C. The straight lines are included as a guide. Methane (■), Ethane (♦), Propane (◄), Isobutane (●) and Isopentane (▲)[1]

Measuring selectivity in this manner can also give some insights into the reaction mechanism. Extrapolating to 0% conversion we consider any product with non-zero selectivity at 0% conversion to be a primary product. A primary product is one that forms through one adsorption event. Secondary products will have zero selectivity at zero conversion, which means these products typically form when a primary product re-adsorbs to the surface.

Kinetics analysis will be more difficult for propane dehydrogenation, as deactivation is a major problem with this reaction which must be accounted for. Therefore, a stability test is necessary. Deactivation is one of the major issues facing this reaction and so finding the catalyst's stability or steady state conversion is important when comparing to literature results. These reactions are done at a single flow rate to study the catalyst deactivation and ensure that we reach steady state conversion. Selectivity will also not be extrapolated back to 0% conversion, but rather presented as a function of conversion. In order to compare between catalysts, selectivities will be chosen for a fixed conversion that all catalysts obtain so that conclusions may be drawn about the effects on selectivity.

2 CORRELATING HEAT OF ADSORPTION OF CO TO REACTION SELECTIVITY: GEOMETRIC EFFECTS VS ELECTRONIC EFFECTS IN NEOPENTANE ISOMERIZATION OVER PT AND PD CATALYSTS

2.1 Introduction

Previously, neopentane hydrogenolysis has been studied using both Pt and Pd catalyst systems. Karpinski and Juszczyk examined Pd/SiO_2 and found a maximum isomerization selectivity of 30% for severely sintered Pd particles.[63] Neopentane hydrogenolysis was also conducted over Pd/Al_2O_3 catalysts and a max selectivity of 25% was observed which was attributed to the formation of Pd-Al alloys at the elevated treatment temperatures.[47]

Boudart et al. studied a series of transition metals (Pt, Os, Ir, Au, Ru, Rh and Pd) for neopentane hydrogenolysis and found that only Ir, Pt and Au isomerize neopentane.[81] They determined that the selectivity and activity were dependent on structure and that there were two possible ways for neopentane to adsorb onto platinum: a triadsorbed (three bonds to the surface) and diadsorbed (two bonds to the surface) state with hydrogenolysis having a lower rate in the triadsorbed state. They followed the mechanism proposed by Anderson and Avery previously (Figure 15), in which the hydrocarbon must be 1,3-diadsorbed with one sp^2 carbon forming a double bond with a surface atom and then isomerization takes place through a ring closure – ring opening mechanism on the surface.

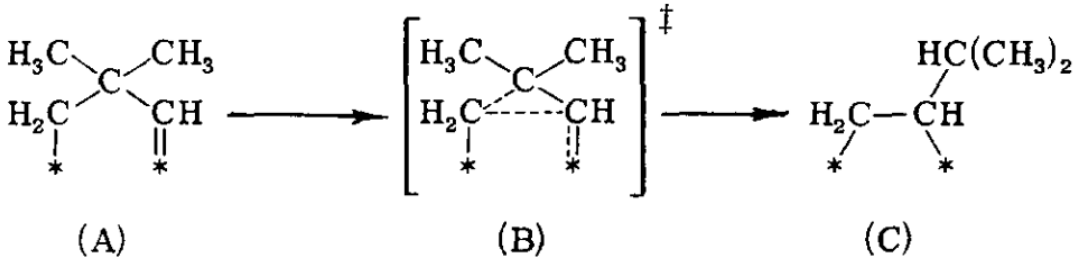

Figure 15: Isomerization mechanism proposed by Anderson and Avery[55, 81]

This mechanism requires at least 2 surface sites to bind the neopentane molecule.[81] Foger et al. performed a particle size study of Pt on silica to confirm the mechanism proposed earlier.[82] Figure 16 shows the results of the particle size study. At the largest size studied, around 20 nm, the isomerization selectivity ranges from 65 to 85%.

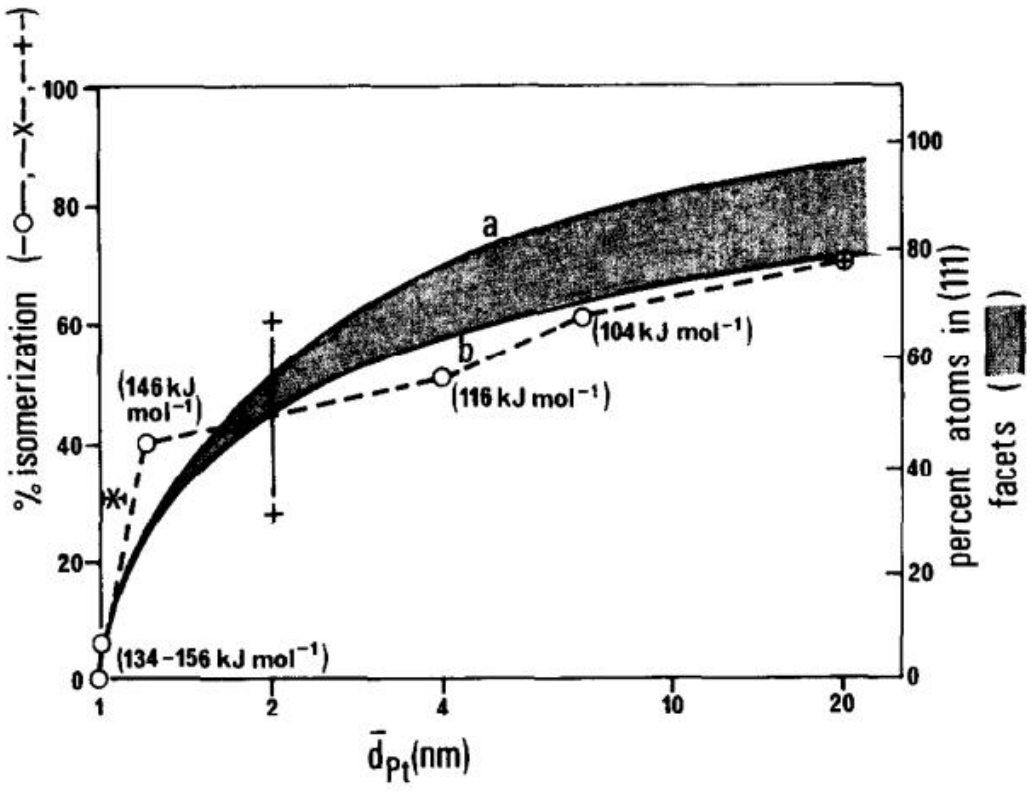

Figure 16: % isomerization and % (111) terrace atoms as a function of particle size, values in parentheses are overall activation energies for neopentane conversion[82]

They found that the isomerization selectivity increased with particle size from 1 to 20 nm. This change in selectivity was attributed to the relative increase in the proportion of Pt surface atoms that are in (111) terraces. On the low surface energy (111) face, the isomerization pathway becomes dominant. They also proposed that the hydrogenolysis pathway only needs a single Pt site to operate and at smaller particle sizes the lower coordinated Pt atoms would be the favored site for this reaction.[82] Smaller particle sizes will have a greater proportion of these

lower coordination sites on the surface compared to larger particles. Ponec et al. conducted a particle size study on Pt for 2,2-Dimethylbutane, which also has isomerization and hydrogenolysis pathways, and found that there was an increase in isomerization selectivity with increasing particle size (1 to 14 nm range).[42]

2.2 Experimental Methods

2.2.1 Synthesis of Platinum and Palladium Catalysts

Platinum and palladium samples were synthesized on a silica (Davisil A60) support. Incipient wetness impregnation (IWI) and strong electrostatic adsorption (SEA) were the two methods used.[79] IWI is the most widely used industry technique and also the simplest. During IWI, a support is contacted with just enough metal-precursor solution to fill the pore volume. All of the metal precursor solution contacts the surface due to the incipient amount of liquid used; however, there can be significant particle growth during drying and pretreatment. In contrast, SEA uses excess solution with a controlled pH to favor the uptake of the metal precursor. The use of excess solution does not necessitate that all of the metal precursor will adsorb to the surface of the catalyst support. The SEA method requires an appropriately charged metal precursor based on the point of zero charge (PZC) of an oxide support and the pH of the solution. The hydroxyl groups on the surface of the oxide support will protonate or deprotonate depending on the pH of the solution relative to the PZC of the support. Precursors can then be selected that will have the opposite charge as the support at a certain pH value and so the electrostatic interaction between the support and the precursor leads to strong binding of the metal precursor to the surface. This allows for strong monolayer adsorption and can inhibit sintering during the post-treatment steps.[79]

For the Pd catalysts, both $Pd(NO_3)_2$ and $Pd(NH_3)_4(NO_3)_2$ were used as precursors. IWI was the method of synthesis for catalysts with medium to large size particles while SEA was

used in order to obtain a catalyst with small particles. Samples were calcined and reduced at different temperatures in order to influence the final particle size. The Pt samples were made in one large batch using $Pt(NH_3)_4(NO_3)_2$ as the precursor using the SEA method. For the Pt catalysts, we varied the calcination temperature from no calcination to 525^oC in order to synthesize catalysts with various particle sizes. Catalyst reduction was accomplished in a 4% H_2/He mixture at the final temperature for 1 hr. Synthesis method and treatment steps are given in Table I.

Table I: Catalyst precursors and treatment steps

Sample	Synthesis Method	Precursor	Calcination Temperature (^oC)	Reduction Temperature (^oC)
3%Pd/SiO_2_1nm	SEA	$Pd(NH_3)_4NO_3$	----	165
2%Pd/SiO_2_2.5nm	IWI	$Pd(NH_3)_4NO_3$	125	225
2%Pd/SiO_2_3nm	IWI	$Pd(NO_3)_2$	225	225
2%Pd/SiO_2_8.1nm	IWI	$Pd(NO_3)_2$	300	225
1%Pt/SiO_2_1.2nm	IWI	$Pt(NH_3)_4(NO_3)_2$	----	300
1%Pt/SiO_2_1.5nm	IWI	$Pt(NH_3)_4(NO_3)_2$	300	300
1%Pt/SiO_2_6.6nm	IWI	$Pt(NH_3)_4(NO_3)_2$	425	300
1%Pt/SiO_2_10nm	IWI	$Pt(NH_3)_4(NO_3)_2$	525	300

2.2.2 Scanning Transmission Electron Microscopy (STEM)

STEM images were obtained at UIC's Research Resources Center facility using the JEOL-ARM 200CF aberration corrected microscope (70 pm spatial resolution and 300 meV energy resolution). Samples were dispersed into isopropyl alcohol and sonicated for 20 min. A drop of the suspension was added dropwise to a holey-carbon copper grid and dried under a heat

lamp for 20 min. Images were taken using the High Angle Angular Dark Field (HAADF) mode and particle size was counted using the Particule2 program. A minimum of 100 particles were counted to get an accurate representation of the particle size distribution for each catalyst.

2.2.3 Extended X-ray Absorption Fine-Structure Spectroscopy (EXAFS)

X-ray absorption spectroscopy (XAS) measurements at the Pd K (24350 eV), and Pt L_3 (11564 eV) edges were made on the bending magnet beam line of the Materials Research Collaborative Access Team (MRCAT) at the Advanced Photon Source (APS), Argonne National Laboratory. Measurements were made in transmission mode. A platinum or palladium foil spectrum was acquired through a third ion chamber simultaneously with each measurement for energy calibration.

Samples were prepared by grinding the catalysts into a fine powder and pressing them into the sample holder. The sample holder is a metal cylinder capable of holding up to six individual samples. The sample holder is then placed in a quartz tube with ports on each end to flow gases or isolate the sample after treatment. The sample thickness was chosen to give a total absorbance at the Pt L_3 or Pd K edge between 1-2 absorption lengths and edge steps around 0.3-0.5. Samples were reduced at 250ºC at atmospheric pressure in a 4% H_2/He mixture (50 cm^3/min). After reduction, the samples were purged with He at 100 cm^3/min and cooled to room temperature in He flow. Trace oxidants in He were removed by a Matheson PUR-Gas Triple Purifier Cartridge containing a Cu trap. All EXAFS spectra were obtained at room temperature in He.

2.2.4 Neopentane Hydrogenolysis and Isomerization

Neopentane hydrogenolysis and isomerization were studied using 0.05-0.15 grams of catalyst diluted with 0.9 grams of silica and loaded into a 0.5" OD quartz plug flow reactor. Glass wool was used for the bottom 2 cm of the bed. A 0.5 cm silica layer was placed on top of the glass wool before the catalyst and silica mixture was added to the reactor resulting in a catalyst bed height of 3 cm. The reactor was purged with He for 5 min before each run, and the catalyst was reduced in 4% H_2/He as the temperature was increased to the reaction temperature, 271 ± 2^{o}C. This temperature enabled differential (conversion) operation for all of the catalysts tested. A K-type thermocouple was inserted from the bottom of the reactor into the lower portion of the catalyst bed. Once the reaction temperature stabilized, the pre-mixed reactant feed gas consisting of 0.35% neopentane and 3.5% H_2 balanced in He was passed through the reactor. The flow rate of the feed gas was varied from 25 to 100 cm^3/min to obtain differential conversion (0.5–6 %). Each flow rate was run for at least 1 hr to ensure steady-state conversion had been reached. An Agilent 6890N gas chromatograph with an FID detector was used to analyze the products. The GC column (a J&W Scientific GS-Alumina column) was equipped with a back pressure regulator to hold the system at a constant pressure of 9 psig. Each experimental run was completed within 6 hr for consistency and multiple runs for each catalyst were performed. No appreciable deactivation was observed in any of the catalysts over this period of time. The maximum error of any selectivity measurement was 6%, with most of the data being reproducible within 2%. Turnover rates were calculated based upon the number of active sites determined by the dispersion measured by STEM (the dispersion was estimated to be 1/particle diameter (nm)). Using the EXAFS data or CO chemisorption area to determine the number of

active sites gave only slight differences with regard to the turnover frequencies and does not alter any of the conclusions reached below.

2.2.5 Diffuse Reflectance Infrared Fourier Transform Spectroscopy (DRIFTS)

Infrared spectra were obtained with an ABB Laboratory FTLA2000 FTIR spectrometer. Samples were ground to a very fine powder using a mortar and pestle, and packed into the sample chamber to create the most uniform surface possible. The chamber was purged with He, and then the gas was switched to H_2 and the temperature was raised to 250°C and held for 15 min. After reduction of the catalyst, the gas was switched back to He and the temperature was reduced to 25°C. A background scan was then recorded, which was averaged over at least 256 scans with 4 cm^{-1} resolution. Spectra were taken until signal-to-noise ratios were maximized which took anywhere from 2 to 6 hours depending on the catalyst. The sample was then exposed to 1.6% CO/N_2 and another scan was taken once equilibrium was reached, at which point the flow was changed back to He and a final scan was taken once the intensity of the adsorbed CO peak was invariant with time.

2.2.6 CO Heats of Adsorption

The heat of adsorption measurements for CO adsorption on the Pd and Pt catalysts were carried out using a volumetric adsorption apparatus (Micromeritics ASAP 2020C) that has been interfaced with a differential scanning calorimeter (Setaram Sensys EVO differential scanning calorimeter (DSC)). Pd catalysts were re-reduced at 200°C in pure H_2 for 1 hr, subsequently purged with He that had been passed through an Oxytrap at 200°C for 1 hr prior to cooling to the adsorption temperature (35°C). The Pt catalysts were subjected to a similar treatment sequence, except that the pre-reduced catalysts were re-reduced at 275°C for 1 hr in pure H_2 and purged

with oxygen-free He for 1 hr at the same temperature before cooling to the adsorption temperature (35°C).

The combined volumetric adsorption–calorimetry experiments were designed so that a significant number of low pressure data points were collected in order to measure the differential heat of adsorption at low coverage. Heat flow due to adsorption is measured simultaneously with measurement of adsorption uptake, such that a differential heat of adsorption, $\Delta H(\theta)$ can be determined by dividing the measured heat flow by the amount adsorbed determined by the Micromeritics adsorption apparatus.

2.3 Results and Discussion

2.3.1 Particle Size Analysis

Particle size was determined using STEM imaging. A STEM image for the 1% Pt/SiO_2_1.2 nm sample and the corresponding size distribution are shown in Figure 17, and demonstrate the average size is 1.2 nm. The STEM particle size of the other Pt and Pd catalysts are given in Table II.

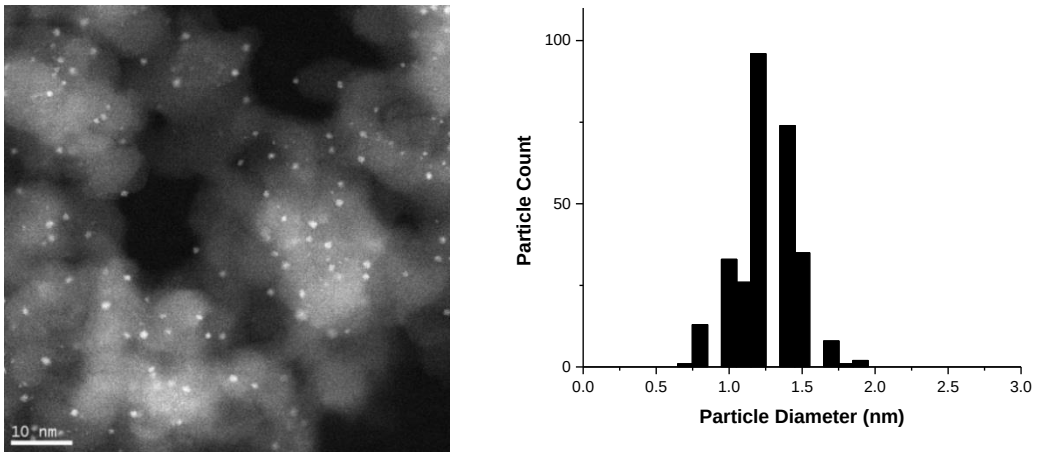

Figure 17: 1% Pt/SiO_2_1.2 nm sample image and particle size distribution determined by STEM

EXAFS spectroscopy was also used to evaluate particle size using the K edge of Pd and L_3 edge of Pt. The EXAFS component of the data was fit to obtain a coordination number and an interatomic distance. The coordination number, CN is used to estimate the particle size based on a hemispherical geometry and the lattice constant derived according to the equation:[83]

$$\log\left(\frac{H}{Pt}\right) = -0.132 \times (N_{Pt-Pt}) + 2.58$$

This equation uses the ratio of hydrogen to platinum atoms to solve for the coordination number and has been checked against STEM and other size data and is applicable to fcc Group VIII metals. Table II shows the results of the STEM, EXAFS and chemisorption particle size analysis and demonstrate there is generally good agreement between the three techniques. All three techniques indicate the average particle size of Pt and Pd varies between 1-10 nm.

Table II: Particle sizes determined by STEM, EXAFS and CO chemisorption

Sample	Particle Size by STEM (nm)	Particle Size by EXAFS (nm)	Particle Size by CO_{irr} chemisorption (nm)[a,b]
3%Pd/SiO_2_1nm	1.0 ± 0.2	1.0 ± 0.1	1.7 ± 0.2
2%Pd/SiO_2_2.5nm	2.5 ± 1.1	2.5 ± 0.3	4.3 ± 0.4
2%Pd/SiO_2_3nm	3.0 ± 0.8	5.0 ± 0.5	3.8 ± 0.4
2%Pd/SiO_2_8.1nm	8.1 ± 1.7	10 ± 1.0	9.9 ± 1.0
1%Pt/SiO_2_1.2nm	1.2 ± 0.2	1.1 ± 0.1	1.5 ± 0.2
1%Pt/SiO_2_1.5nm	1.5 ± 0.8	1.5 ± 0.2	1.3 ± 0.1
1%Pt/SiO_2_6.6nm	6.6 ± 2.6	5.0 ± 0.5	5.8 ± 0.6
1%Pt/SiO_2_10nm	10 ± 5.2	8.0 ± 0.8	8.3 ± 0.8

[a]Monolayer uptake (extrapolated to P = 0) at 35°C using the dual isotherm technique.

[b]Based on d (nm) = c/D, where c is constant and equal to 0.994 for Pd and D is the dispersion, or ratio of the number of surface atoms to the total number of atoms in the catalyst sample.

2.3.2 Reactivity results

Figure 18 shows the effect of conversion on selectivity (under differential conversion) for the 1%Pt/SiO_2_1.2nm catalyst. Product selectivity was plotted and the selectivity extrapolated to 0% conversion, these numbers are reported in Table III along with the calculated turnover rate (TOR). Products with non-zero selectivity at 0% conversion are considered primary products while products that have 0% selectivity at 0% conversion are considered secondary products. For both Pd and Pt, the amount of methane produced decreases as the particle size increases, suggesting that selectivity for hydrogenolysis decreases with increasing particle size.

Table III: TOF and product selectivity for the Pt and Pd catalysts

Catalyst	Dispersion (by STEM)	TOR(mol conv / metal site/sec)	Initial Product Distribution (%)						
			CH_4	C_2H_6	C_3H_8	n-C_4H_{10}	i-C_4H_{10}	i-C_5H_{12}	n-C_5H_{12}
3%Pd/SiO_2_1nm	1.0	1.0×10^{-3}	55	1	13	0	28	3	0
2%Pd/SiO_2_2.5nm	0.40	1.0×10^{-3}	49	1	5	2	33	9	0
2%Pd/SiO_2_3nm	0.33	7.7×10^{-4}	40	0	1	1	34	24	0
2%Pd/SiO_2_8.1nm	0.12	1.1×10^{-3}	39	1	2	1	32	26	0
1%Pt/SiO_2_1.2nm	0.83	1.4×10^{-3}	33	11	2	0	28	29	0
1%Pt/SiO_2_1.5nm	0.67	1.0×10^{-3}	29	6	2	0	25	38	0
1%Pt/SiO_2_6.6nm	0.15	8.0×10^{-4}	23	3	2	0	20	53	6
1%Pt/SiO_2_10nm	0.10	2.3×10^{-4}	19	2	2	0	16	57	5

However, the data in Table III also suggests the simple reaction scheme in Figure 8 may not be completely correct since propane and ethane are observed at zero conversion. For example, in Figure 18 (1% Pt/SiO_2_1.2nm), the initial selectivity to both ethane (11%) and propane (2%) are non-zero. This implies multiple surface reactions occur on the small Pd and all Pt catalysts before products desorb. On the Pt catalysts with ~1-2 nm particle size, the high ethane selectivity implies there is an initial isomerization to a chemisorbed isopentyl intermediate followed by selective hydrogenolysis to give ethane, but little propane. This suggests the propyl fragment is strongly bound to the surface and undergoes further reaction to ethane and methane. Unlike small Pt nanoparticles, for 1 nm Pd the selectivity to propane (13%) is greater than ethane (1%), suggesting that after the initial hydrogenolysis reaction there is second hydrogenolysis of the isobutyl surface intermediate. Davis et al. examined the conversion of neopentane over Pt single crystal surfaces and found that the (100) and (13,1,1) surfaces

produced significantly more ethane and propane than the (111), (10,8,7) and (332) surfaces. The formation of these products was attributed to a skeletal isomerization step preceding hydrogenolysis.[84] Similarly, the presence of *n*-pentane in the limit of zero conversion over large Pt nanoparticles indicates that adsorbed neopentane can also undergo two isomerization steps before desorbing. Davis et al. found significant *n*-pentane production (12-14%) on the (100) and (13,1,1) surfaces and attributed the high selectivity to *n*-pentane to two rearrangements occurring during a single adsorption to the surface.[84] In our previous study of neopentane hydrogenolysis over Pt, Pd and PdPt bimetallic catalysts, *n*-pentane formed over the monometallic Pt and the bimetallic catalysts with a particle size of ~1-2 nm.[2]

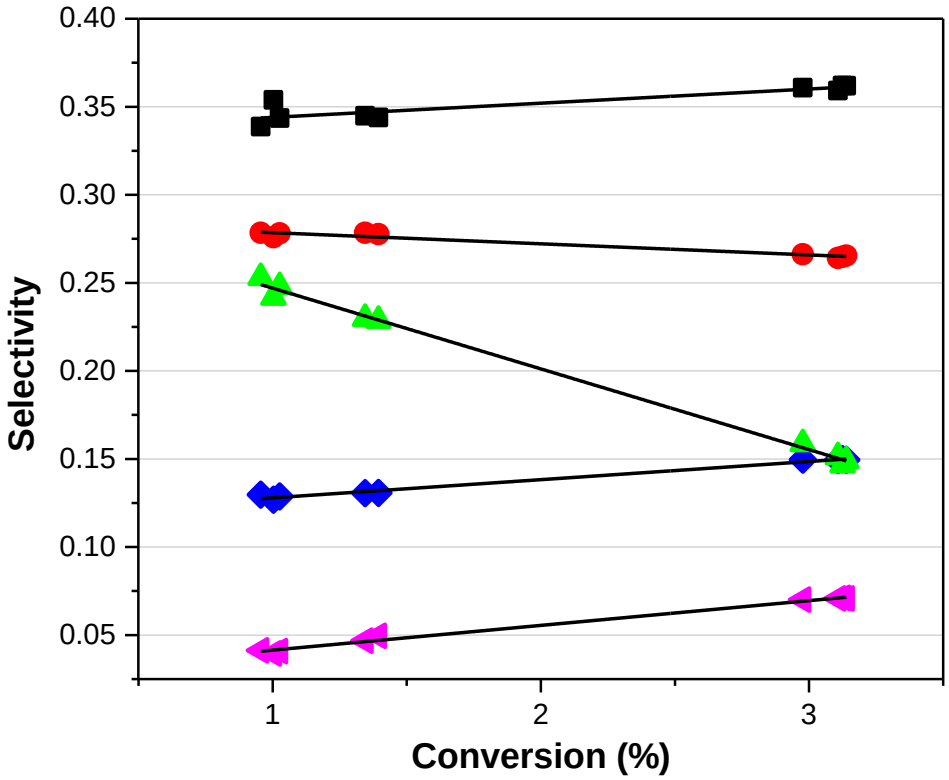

Figure 18: Selectivity for the 1% Pt(1.2nm)/SiO_2 catalyst at differential conversion. Reaction conditions were 0.35% neopentane, 3.5% H_2, balance He and 271°C. The straight lines are included as a guide. Methane (black squares), Ethane (red circles), Propane (pink side triangles), Isobutane (blue diamonds) and Isopentane (green triangles)

Figure 19 shows both the Pt and Pd particle size effect on selectivity to isopentane, the primary product of the isomerization pathway. The selectivity to isopentane over Pt catalysts is in good agreement with the previous work of Foger et al. over a comparable particle size range. Pd catalysts exhibit the same trend although the selectivity to isopentane is ~30% lower than the selectivity of a Pt catalyst with the same particle size. The isomerization selectivity (only 3%) was very low for the smallest Pd particles but increased to a maximum of 26% for the largest particle size (8 nm). The smallest Pt particles had a higher selectivity to isopentane (29%) than

the largest Pd (26%), but both metals exhibited a similar trend: isomerization selectivity increased with increasing particle size. This result seems to support Anderson and Avery's mechanism which postulates the η^3-adsorbed state is the necessary surface intermediate for isomerization and therefore it could be expected that larger (111) surface facets promote isomerization selectivity.[81] As the particle size increases there will be a greater fraction of low energy (111) surface sites as opposed to smaller particles which will contain more corners and edges that disfavor adsorption of neopentane in the tri-adsorbed state. Conversely, edges and corners are known to favor bond cleavage events (i.e. C-H and C-C bond cleavage), required events for hydrogenolysis.[85] While this model suggests selectivity is related to the presence (or absence) of particular sites on the surface and can explain the selectivity trend for a single metal, it does not account for the changes in absolute selectivity values between metals (i.e. Pt > Pd by about 30%).

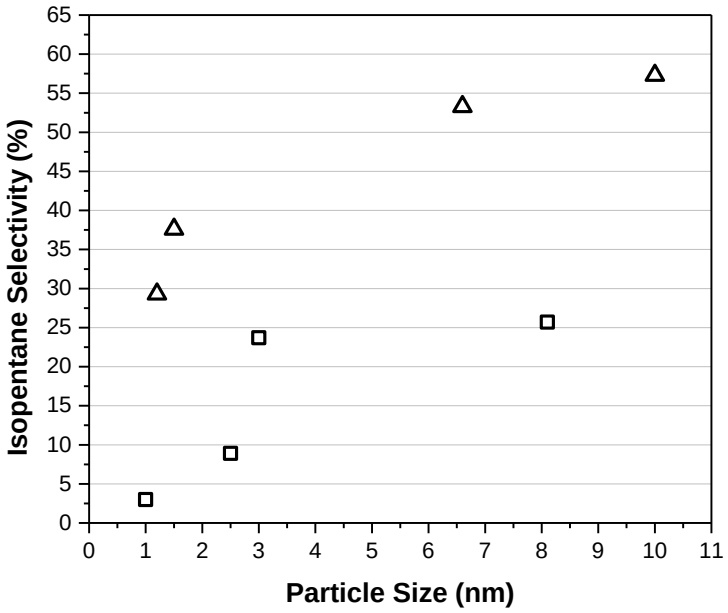

Figure 19: Isopentane selectivity as a function of particle size for silica-supported Pd (□) and Pt (Δ). Reaction conditions were 0.35% neopentane, 3.5% H_2, balance He and 271°C

The turnover rates presented in Table III are based on the molecules of neopentane converted per surface site and so activity has been normalized per surface atom. Figure 20 demonstrates the TOR of Pd catalysts for neopentane conversion varies little with particle size, while the Pt catalysts display a steady decrease in activity with increasing particle size.

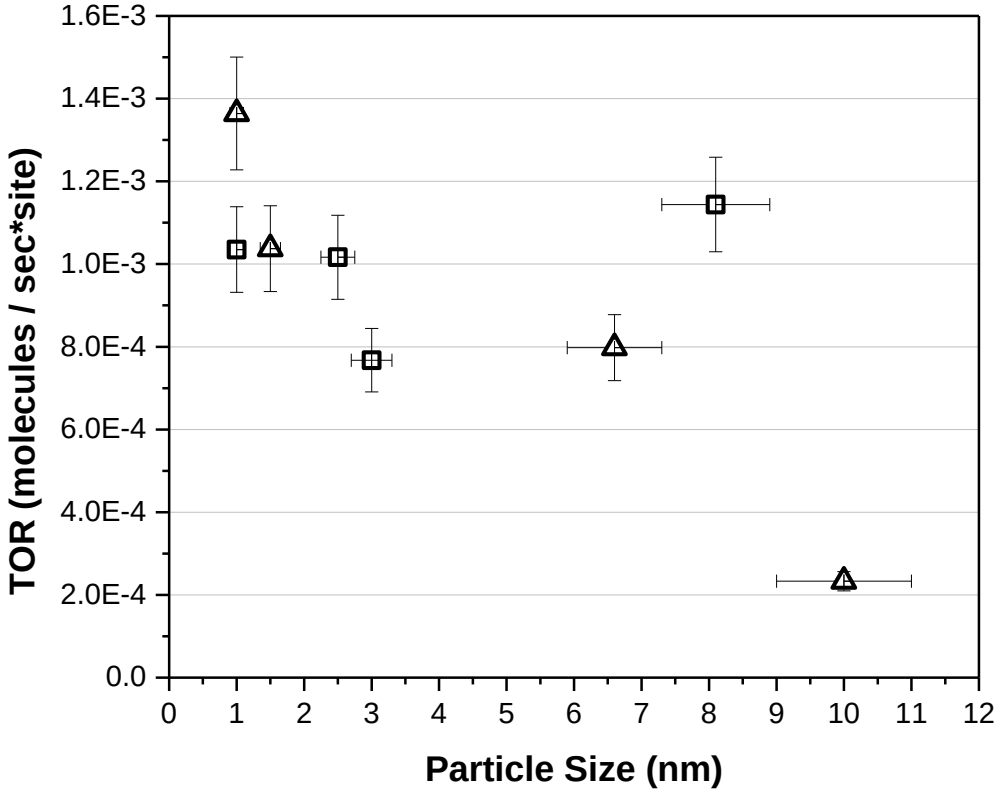

Figure 20: Overall TOR for Pd (□) and Pt (Δ) catalysts. Reaction conditions were 0.35% neopentane, 3.5% H_2, balance He and 271°C

The turnover rates for isomerization and hydrogenolysis for Pd catalysts are shown in Figure 21. For Pd, the TOR for hydrogenolysis is invariant with particle size, similar to the trend for the overall TOR. However, the isomerization TOR seems to increase with increasing particle size. The increase in the TOR for isomerization correlates with the increase in the surface area of the (111) faces. However, the magnitude of the isomerization TOR is not very significant compared to the TOR for hydrogenolysis so any trend for isomerization is obscured by the variance in the measured hydrogenolysis rate.

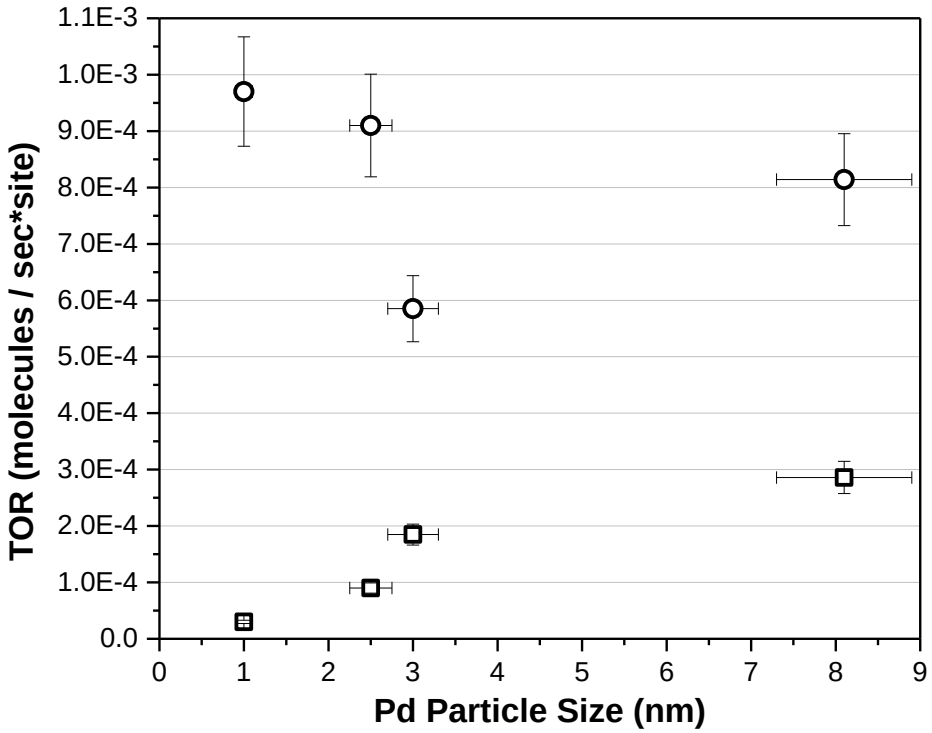

Figure 21: Isomerization (□) and hydrogenolysis (○) TOR for silica-supported Pd catalysts. Reaction conditions were 0.35% neopentane, 3.5% H_2, balance He and 271°C

Figure 22 shows the isomerization and hydrogenolysis TORs for the Pt catalysts. In contrast to Pd, there is a decrease in hydrogenolysis TOR with increasing particle size, similar to the decrease in overall TOR shown in Figure 20B. In addition, the isomerization TOR does not follow the same trend as found for Pd. From the data, one cannot conclude that there is an increase in the isomerization TOR with increasing size. For both metals, the hydrogenolysis TOR mirrors the overall TOR.

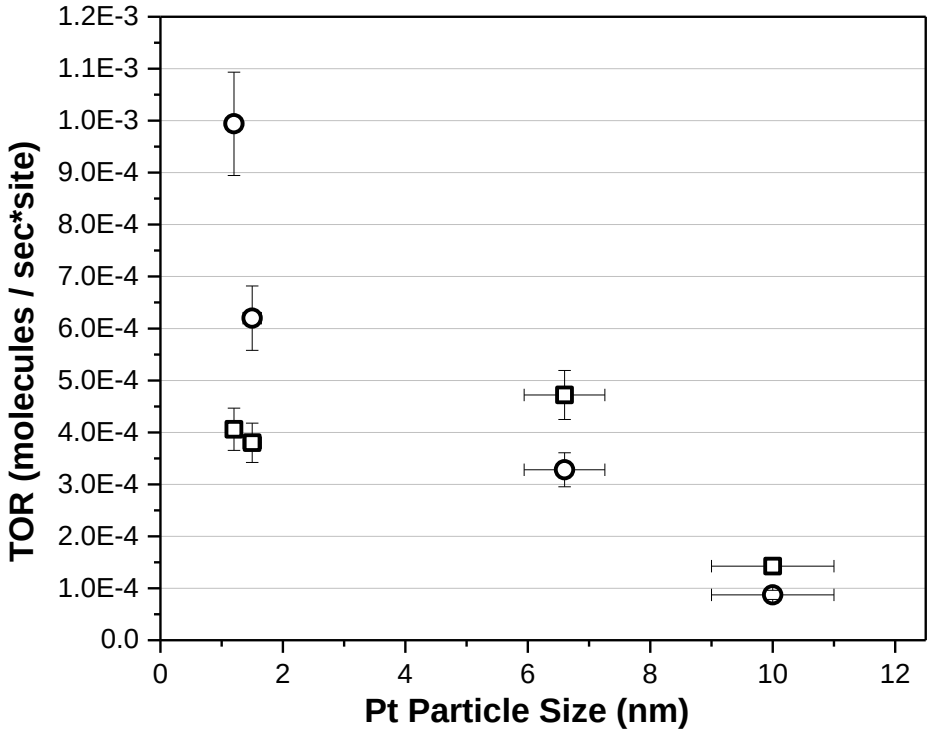

Figure 22: Isomerization (□) and hydrogenolysis (○) TOR for silica-supported Pt catalysts. Reaction conditions were 0.35% neopentane, 3.5% H_2, balance He and 271°C

2.3.3 Diffuse Reflectance Infrared Fourier Transform Spectroscopy (DRIFTS)

Figure 23 shows the compiled DRIFTS spectra of adsorbed CO on the Pd catalysts. For the catalyst with the smallest Pd particle size, there is a large absorbance around 2090 cm^{-1} which is attributed to linear bound CO, and another peak at ~1950 cm^{-1} which is assigned to bridge-bonded CO.[86-88] As the particle size increases there is a sharp decrease in the linearly adsorbed CO (~2090 cm^{-1}). The absorbance of the bridge-bonded CO peak (~1950 cm^{-1}) decreases with particle size but the overall linear-to-bridging ratio still decreases with increasing particle size (Table IV). At larger Pd sizes (> 1 nm), the bridge-bonded CO peak at ~1950 cm^{-1} splits into two distinct peaks. These two peaks can be attributed to bridge-bonded CO on terraces

and bridge-bonded CO on corner and edge sites.[89, 90] These results are consistent with an increasing ratio of large, flat surfaces (represented by bridge-bonded CO) as particle size increases. These results are consistent with those by Bradley et al.[88]

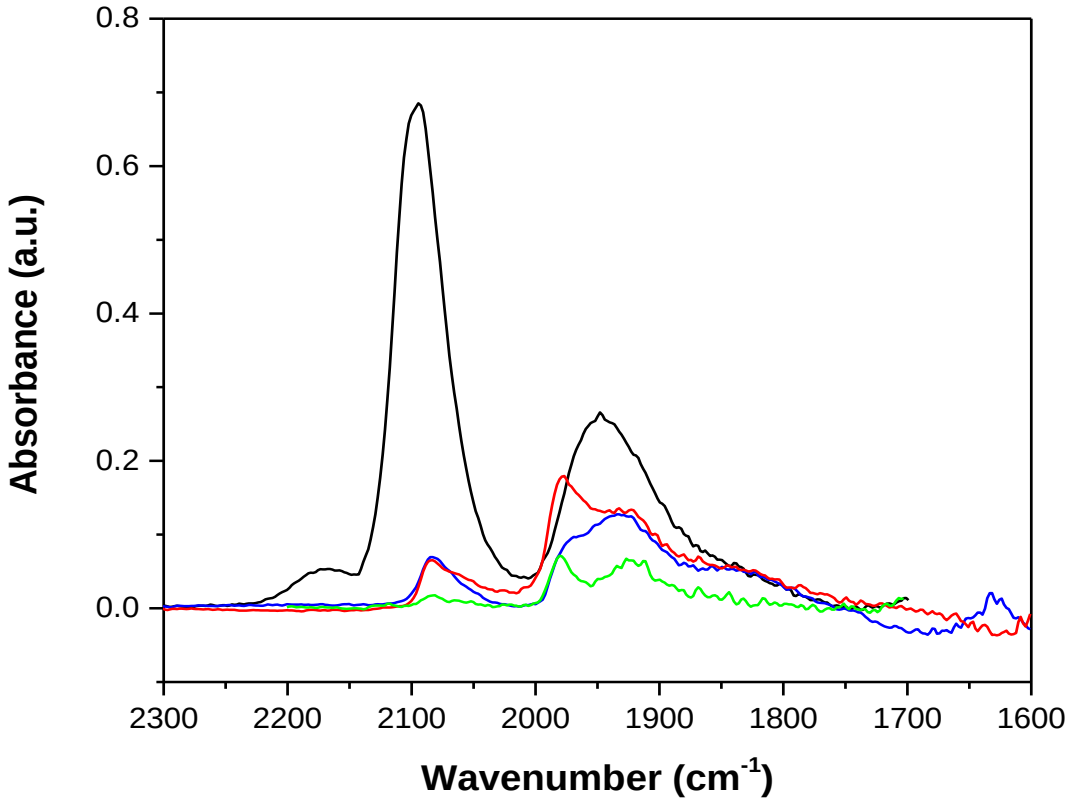

Figure 23: DRIFTS spectra of the adsorption of carbon monoxide on silica-supported Pd catalysts at room temperature. 1.0 nm (black line), 2.5 nm (blue line), 3.0 nm (red line) and 8.1 nm (green line)

Figure 24 shows the DRIFTS spectra for adsorption of carbon monoxide on the silica-supported Pt catalysts. There is a very sharp peak at ~2050 cm^{-1}, which is assigned to linear-bonded CO, and a much smaller and broader peak centered at ~1800 cm^{-1}, assigned to bridge-bonded CO.[91-96] Similar to the Pd samples, there is a dramatic decrease in the absorbance of the linear-bonded CO adsorption peak with increasing particle size while the bridge-bonded CO

peak shows a smaller decrease in absorbance over the particle size range examined. Similar to Pd, the linear-to-bridge bonded CO absorbance ratio decreases with increasing particle size. A similar trend emerges for both the Pt and Pd catalysts, although the linear peak for the Pt samples remains more prominent than Pd at the larger particle sizes. These results for Pt are also consistent with those by Singh et al. and Bradley et al.[93, 95] The linear-to-bridged bonded ratios (determined by area) for both Pt and Pd samples are given in Table IV.

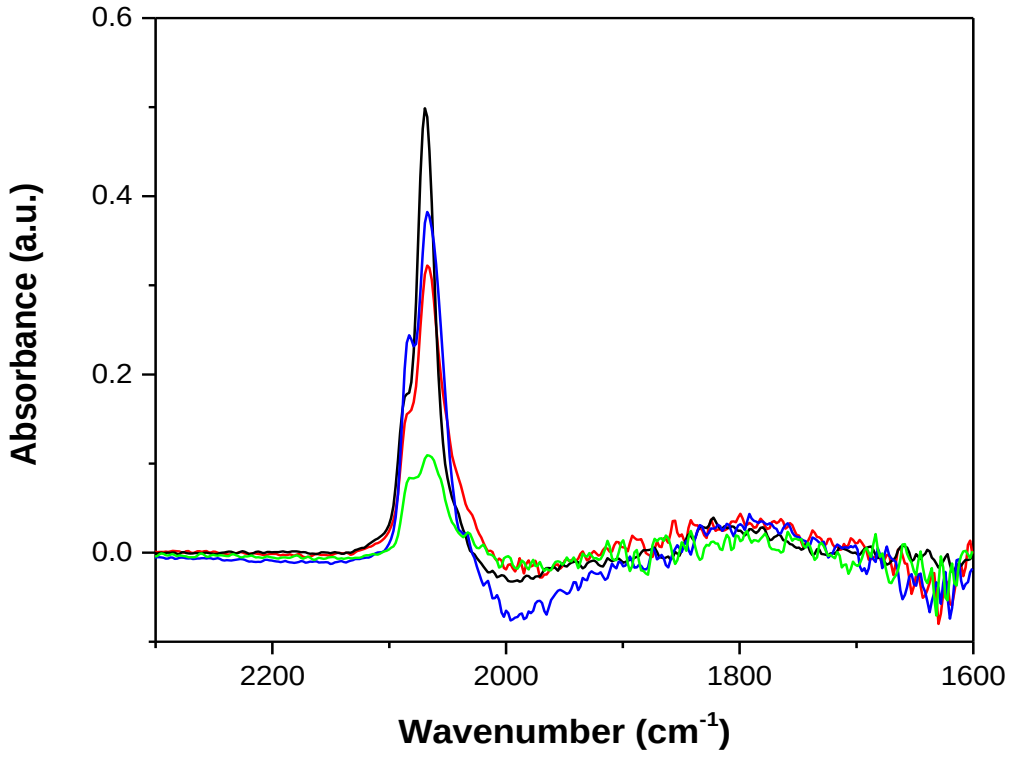

Figure 24: DRIFTS spectra of the adsorption of carbon monoxide on silica-supported Pt catalysts at room temperature. 1.2 nm (black line), 1.5 nm (blue line), 6.6 nm (red line) and 10 nm (green line)

2.3.4 Heat of adsorption of CO determined by isothermal calorimetry

Just as in the case of the DRIFTS experiments mentioned in the previous section, we have used CO as a probe molecule to examine how the heat of adsorption may relate to the activity and selectivity for neopentane conversion. Since neopentane is relatively weakly adsorbing at 35^{o}C (Kao et al. reported that neopentane desorbs from both Pt and Pd (111) surfaces at 200 K) we have chosen to use CO as a surrogate molecule.[97, 98] There is ample literature data on the heat of adsorption of CO on both Pt and Pd for comparison with the values determined in this work.[99-111] The enthalpies of CO adsorption for Pt and Pd nanoparticles of different size are given in Table IV. The uncertainty for these measurements are given as ±5 kJ/mol due to instrument error. The initial heats of adsorption of the Pd samples are similar to those reported in the literature.[112-114] Chou et al. performed a heat of adsorption study on Pd particles of various sizes supported on silica and those values are similar to the values in Table IV. Sen et al. performed a study of CO heat of adsorption on Pt/SiO_2 catalysts of different sizes and determined little to no size effect though the values obtained are similar to the ones reported here.[101] This conclusion was based mainly on the fact that the change was not as drastic as the one found for Pd; however their data does show a decreasing trend. For both Pt and Pd nanoparticles, the enthalpy of CO adsorption decreases with increasing particle size, although the relationship is more pronounced for the Pd samples.

Table IV: Particle size dependent CO heat of adsorption values and linear-to-bridging ratios

Sample	Initial CO heat of adsorption (kJ mol^{-1})	Linear-to-Bridging ratio
3Pd_1.0nm	139	1.5:1
2Pd_2.5nm	134	0.21:1
2Pd_3.0nm	126	0.16:1
2Pd_8.1nm	113	0.14:1
1Pt_1.2nm	105	3.5:1
1Pt_1.5nm	101	3.0:1
1Pt_6.6nm	97	2.3:1
1Pt_10.0nm	95	1.3:1

Now that we have established a relationship between particle size and heat of adsorption in a similar fashion to the previous observation of selectivity trends with particle size, a correlation may be made between the heat of adsorption of CO and isomerization selectivity. Figure 25 demonstrates for both Pt and Pd catalysts that there is a single correlation between the initial heat of CO adsorption and the neopentane isomerization selectivity, and that the lower the heat of adsorption, the higher the isomerization selectivity. In addition, the isomerization selectivity and enthalpy of adsorption of the 8 nm Pd (26% and 113 kJ/mol) and 1.2 nm Pt (29% and 105 kJ/mol) nanoparticles are very similar suggesting that the chemisorption energy and not the particle size, coordination geometry or ensemble size are the important factor for increasing the isomerization selectivity. Previous models suggest that large (111) surfaces are essential for high isomerization selectivity, but the smallest Pt nanoparticles (1.2 nm) are shown to have almost identical selectivity to the largest Pd nanoparticles (8.1 nm). This implies the mechanism for both isomerization and hydrogenolysis are the same at low-coordinate and high-coordinate sites or that the structure of the site is not the most relevant property of the catalyst. This idea is supported by Davis et al. who performed neopentane conversion over Pt single crystal surfaces

and found that there was little influence of surface structure on the rate and selectivity of the reaction.[84, 115] Given this strong correlation between selectivity and CO heats of adsorption, it would appear that the strength of the metal-adsorbate bond is the dominating factor for tuning selectivity.

Previously, Norskov and co-workers have shown that simple descriptors such as the oxygen binding energy can be used to predict reactivity.[116] In addition, it has been found that there is a linear relationship between the location of the d-band center and the adsorption energy of simple adsorbates. For example, Liu and Norskov demonstrated a linear relationship to describe the correlation between the d-band center of Pd surfaces and the adsorption energy of CO.[117],[26] Similarly, Nakamura and co-workers developed a linear correlation between the binding energy of a methyl fragment and the d-band center. [118] The similarity between these two correlations allowed for the two adsorption energies to be equated through a simple linear relationship.

$$E_{COads} = 0.60\ E_{CH3ads} - 0.09 \text{ (energies in eV)}$$

Expanding this idea in their study of acetylene hydrogenation, Studt et al. used the heat of adsorption of a methyl group as a simple descriptor which is correlated with the heat of adsorption of acetylene, and therefore a descriptor of acetylene hydrogenation for a large variety of metal surfaces (including Pd and Pd alloys).[26, 118, 119] Therefore since a linear relationship between hydrocarbon adsorption and CO adsorption seems evident; the linear relationship in Figure 25 implies that the adsorption energy of neopentane is a critical factor in determining selectivity. However, since relatively little is known about neopentane adsorption on metal surfaces, CO chemisorption serves as a more general predictor of isomerization selectivity.

Correlating selectivity with heat of adsorption has been demonstrated by Studt et al. in the hydrogenation of acetylene to ethylene. While the activity decreased as a function of decreasing adsorption energy of acetylene, the selectivity increased as the adsorption energy decreased. In this work, the selectivity similarly increases as the adsorption energy decreases. However, it is not clear why the activity does not exhibit a similar response as function of the adsorption energy.

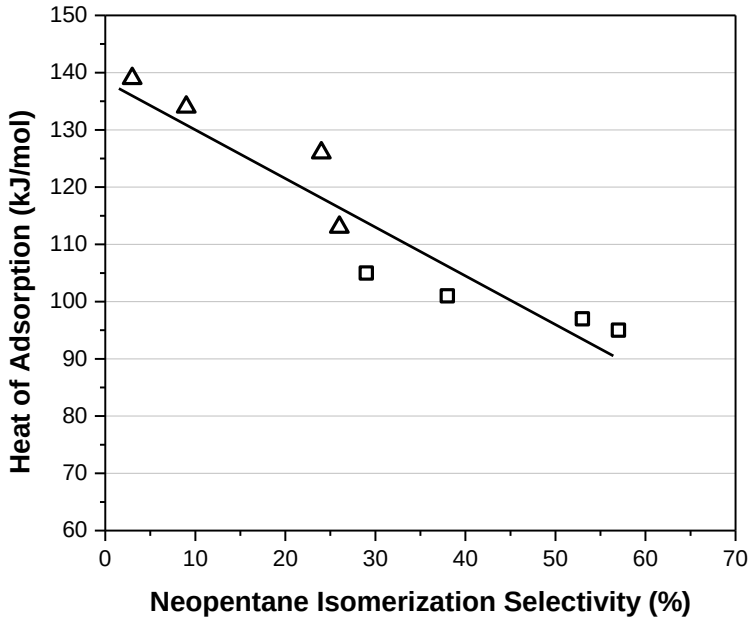

Figure 25: Isomerization selectivity versus CO heat of adsorption for Pd (triangles) and Pt (squares) catalysts

We can test this correlation by examining literature data for various metals. For example, rhodium is known to perform hydrogenolysis almost exclusively and has an initial CO heat of adsorption around 140 kJ/mol which agrees with the correlation in Figure 25.[120, 121] Iridium is shown to have some isomerization selectivity (~7%) for *n*-butane reactions and an initial CO heat of adsorption of around 146 kJ/mol.[122, 123] Although this is a slightly different reaction

and the Ir was supported on alumina rather than silica, this data still falls within our correlation. Therefore, if this correlation is true, the value for the CO heat of adsorption should be predictive for improving the isomerization selectivity of supported catalysts. Pt alloyed with Sn is widely used in industry to improve the kinetics of Pt catalysts.[108, 124] Shen et al. performed CO adsorption experiments on Pt and PtSn alloys and found a decrease of nearly 20 kJ/mol upon the addition of Sn. Schwank et al. found isopentane selectivities of 75-80% on Pt-Sn alloys supported on alumina.[37] By looking at CO heats of adsorption of various bimetallics it should be possible to predict the neopentane isomerization selectivity. Ultimately, the correlation that we observe between the CO adsorption energy and the isomerization selectivity provides a simple method for predicting catalysts which may exhibit even higher selectivity than reported here. Further work on specific bimetallic samples will be used test this relation between selectivity and bond strength and determine how far one may extend this correlation.

2.4 Conclusion

Both Pt and Pd exhibit a clear particle size effect in terms of neopentane isomerization selectivity. Both metals display increasing isomerization selectivity with increasing particle size with Pt having a significantly higher selectivity than Pd at an equivalent particle size. While such a tend might suggest this change in selectivity results from a geometric effect, the correlation between the isomerization selectivity and the initial heat of adsorption of CO suggests isomerization and hydrogenolysis selectivity are determined by the strength of the metal adsorbate bond independent of the particle size, coordination geometry of the surface atoms or the type of metal. This result implies that the observed selectivity for isomerization is primarily a function of electronic effects (i.e. the strength of the bond between the metal surface and the adsorbate) and is not a strong function of the coordination of the adsorbate to the surface. In

addition, for all catalysts, at very low conversion there are reaction products that indicate multiple surface reactions before desorption. These consecutive reactions were especially important for nanoparticles of less than 2 nm in size where the enthalpies of adsorption were largest.

3 GENERAL METHOD FOR DETERMINATION OF THE SURFACE COMPOSITION IN BIMETALLIC NANOPARTICLE CATALYSTS FROM THE L EDGE X-RAY ABSORPTION NEAR-EDGE SPECTRA

3.1 Introduction

As demonstrated by Sinfelt, bimetallic catalysts frequently possess properties that are superior to their monometallic counterparts.[36] However, the composition is not a unique descriptor of their activity. The surface composition/structure is critical to the catalyst performance.[35, 125] Bimetallic catalysts have several potential structures: core-shell, intermetallic and homogeneous (mixed) alloys. Homogeneous alloys have a less defined structure than the other two and refer to two metals mixed randomly and can exist across the full range of compositions both in the bulk and on the surface. Determining the surface composition of these homogenous alloys is an important aspect of determining their catalytic characteristics. Determining the turnover rate (TOR) is dependent on knowing the number of active sites present, which may be dependent on surface composition (and arrangement) for bimetallic catalysts. This can be simple when one of the metals adsorbs CO or H_2 while the other does not; however, the problem of quantifying the surface composition becomes more complicated when both metals (e.g. Pd and Pt) are capable of adsorption. In this case, conventional techniques like chemisorption cannot be used to effectively determine the number of active sites. However, combining CO chemisorption with an element-specific characterization technique like EXAFS or STEM-EELS could give insight into the surface compositions of these catalysts. In this work, we will demonstrate one particular example using this combination of techniques (along with infrared spectroscopy) to determine the surface composition for a homogeneous alloy of Pt and Pd.

PtPd alloys have been studied for a wide range of reactions including ethane oxidation, hydrogenation of aromatics, alcohol oxidation, hydrodesulfurization, hydrogen storage and automotive catalysis.[40, 126-132] In many of these studies, PtPd alloys exhibited increased stability, activity and selectivity. Selectivity, or the amount of one product produced divided by the total products, is an integral part of catalysis as undesired products can deactivate the catalyst and produce waste. Selectivity is typically less affected by changing reaction parameters like temperature and pressure unlike activity and stability and so the properties of the catalyst must be altered to cause changes to selectivity. Neopentane hydrogenolysis is a probe reaction that is widely used in noble metal catalysis. It is a model reaction for more complex hydrocarbon reforming reactions and is used due to neopentane's inability to form carbenium ions or olefins which cause catalyst deactivation. The reaction is simple to run on a laboratory scale as all products are gas phase and there are only two possible reaction pathways: hydrogenolysis and isomerization. It has been studied over a range of monometallic and bimetallic catalyst systems to provide comparison for the results obtained in this study.[37, 47, 81, 82, 120, 133]

3.2 Experimental Methods

The neopentane hydrogenolysis reaction was studied using 0.05−0.1 g of catalyst diluted with 0.9 g of silica and loaded into a 0.5 in. o.d. quartz plug flow reactor. Glass wool and a 0.5 cm silica layer were used to support the catalyst bed of ~3 cm height. The reactor was purged with helium for about 5 min before each run, and the catalyst was reduced in 4% H_2/He as the temperature was increased to the reaction temperature, 271 ± 2°C. A type K thermocouple was inserted from the bottom into the lower portion of the catalyst bed. Once the reaction temperature stabilized, the premixed reactant feed gas consisting of 0.35% neopentane and 3.5% H_2 balanced in He was flowed through the reactor system for 30 min to allow steady, stable operation. The

flow rate of the feed gas was varied from 25 to 100 mL/min to obtain differential conversions between 0.5 and 6%. Each flow rate was run for at least an hour to ensure that steady state conversion for that flow had been reached. An Agilent 6890N gas chromatograph with an FID detector was used to analyze the products. The GC column was a J&W Scientific GS-Alumina column equipped with a back pressure regulator to hold the system at a constant pressure of 9 psig. Each experimental run was completed within 6 hr for consistency. No appreciable deactivation was observed in any of the catalysts over this period of time. The relative error of the selectivity measurements was about 5% of the measured value. Turnover rates were calculated on the basis of the number of active sites determined by the dispersion (the dispersion was estimated as 1/particle diameter (nm)).[134] In the absence of catalyst, there was no conversion from the silica diluent.

3.3 Results

Neopentane hydrogenolysis has two possible reaction pathways as shown in Figure 8, hydrogenolysis and isomerization. Hydrogenolysis involves a carbon-carbon bond cleavage and hydrogenation resulting in isobutane and methane. Isomerization involves a ring closure-ring opening through a cyclopropyl intermediate to produce isopentane. As Figure 8 illustrates, the primary products are methane and isobutane for hydrogenolysis and isopentane for isomerization. In both cases, further reaction can occur to produce secondary products, such as propane and additional methane. Isomerization of the primary product, isopentane, can also lead to formation of n-pentane.

Figure 26 shows the selectivity plotted as a function of conversion for the 1% Pd + 2% Pt/SiO_2 catalyst. The data suggests that the reaction scheme proposed in Figure 8 is consistent with the data presented in Figure 26 as propane and ethane are not primary products since the

selectivity goes to zero as conversion goes to zero.[135] In contrast, isobutane, methane and isopentane are clearly primary products as their selectivity is non-zero in the limit of zero conversion. Although n-pentane would not be expected to be a primary product, its selectivity is non-zero at zero conversion for the Pt containing catalysts. The selectivities extrapolated to zero conversion are also given in Table V. While for Pt catalysts the initial isomerization product appears to undergo a second reaction (to n-pentane) before desorption, the initial hydrogenolysis product does not. At zero conversion there is very low selectivity to propane. For Pd, the reverse is true. There is no selectivity to n-pentane, but there is significant selectivity to propane and even ethane. In the bimetallic catalysts, the selectivity to n-pentane decreases with increasing Pd content; however, there is minimal selectivity to propane for either catalyst.

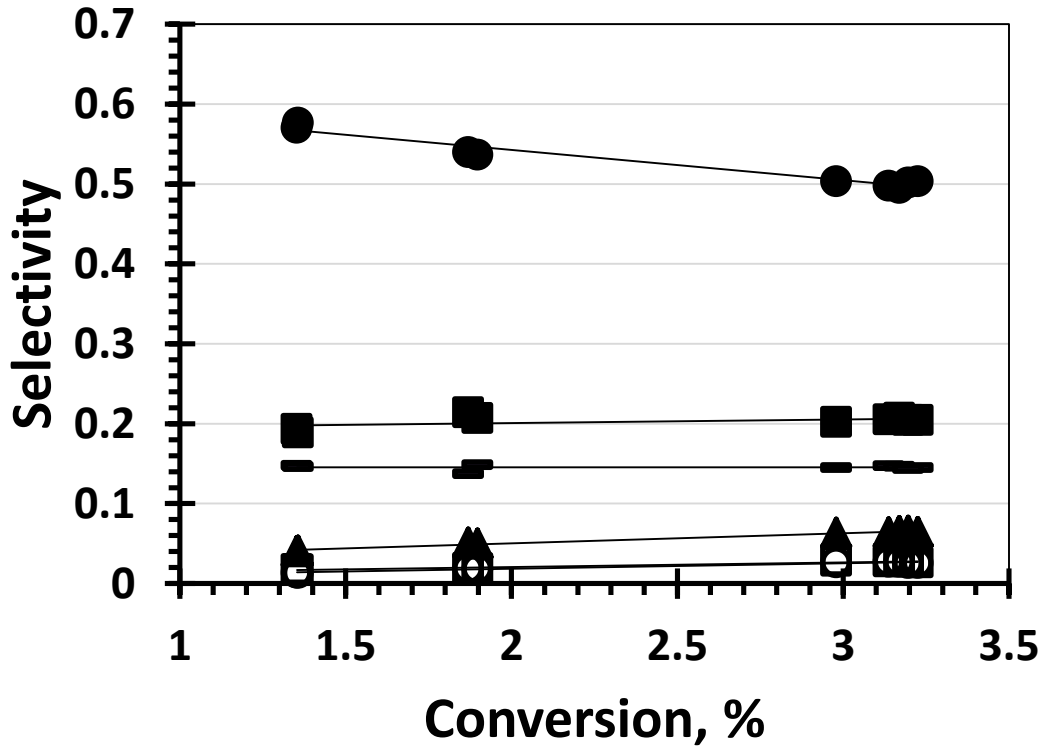

Figure 26: Selectivity vs. conversion for the 1%Pd-2%Pt/SiO_2 catalyst. Products: Methane(■) Ethane(□) Propane(○) i-Butane(-) Isopentane(●) n-Pentane(▲)

The isomerization selectivity of Pt was high at 0.64 (0.54 for isopentane plus 0.10 for n-pentane), while Pd was very low (0.05 isopentane and no n-pentane). The isomerization selectivity of the bimetallic PtPd catalysts was higher than either Pt or Pd alone. The total isomerization was approximately 0.70 for both catalysts while the selectivity to n-pentane increased with increasing Pt/Pd ratio, i.e., 1% Pd + 2% Pt < 0.75% Pd + 3% Pt < Pt.

Table V: Neopentane Turnover Rates (TOR) and Reaction Products Extrapolated to Zero Percent Conversion at 271°C

Catalyst	Dispersion	TOR (mol conv/ metal site/sec)	Initial product distribution (%)					
			CH_4	C_2H_6	C_3H_8	C_4H_{10}	i-C_5H_{12}	n-C_5H_{12}
2.06% Pt/SiO_2	0.57	1.3×10^{-3}	18	0	0	18	54	10
2.56% Pd/SiO_2	0.57	7.3×10^{-4}	53	1	9	32	5	0
0.75% Pd+3% Pt/SiO_2	0.51	6.5×10^{-4}	16	1	1	14	62	8
1% Pd+2% Pt/SiO_2	0.51	5.2×10^{-4}	16	2	1	13	68	2

The turnover rates (TOR) are also given in Table V. The total number of atoms was determined from the composition and the dispersion was calculated from the TEM average size.[136] In Table V the reported TOR for the bimetallic catalysts assumes that all surface atoms have the same TOR. The TOR of monometallic Pt is approximately 1.8 times that of Pd. The TORs of the bimetallic PtPd catalysts are slightly lower than that of Pd, and about half that of Pt.

From STEM, EDS, and EXAFS (not shown) it was confirmed that bimetallic nanoparticles have been synthesized. The TOR, however, was based on the dispersion assuming all atoms had equal rate and selectivity, rather than based on the surface composition. Since both

metals in the bimetallic catalysts adsorb CO, for example, chemisorption and FTIR cannot be used to determine the numbers of surface atoms for each metal. However, the advantage of XANES spectroscopy is that it is specific only to the amount of CO adsorbed on one metal and is essentially independent of the amount of CO adsorbed by the second metal. Adsorption of CO on Pt and Pd leads to a shift in the edge energy and change in the shape of the XANES and these changes (ΔXANES) are proportional to the amount of adsorbed CO.[137, 138] Since CO saturates the surface of Pt and Pd nanoparticles at room temperature, the ΔXANES can be calibrated, for example, with a single metal particle of known size, to determine the surface composition for that specific atom, e.g. Pt or Pd, in a bimetallic nanoparticle.

Using the ΔXANES spectrum for Pt/SiO_2 as the reference, the relative fraction of CO adsorption on Pt atoms in the PtPd bimetallic catalyst can be determined, i.e. intensity ratio of ΔXANES (PtPd) over ΔXANES (Pt).[2] An example of this technique is shown in Figure 27. The surface CO coverage on $PtPd/SiO_2$ is about 70% of coverage on Pt/SiO_2, which is determined by fitting the ΔXANES in the PtPd with that of the Pt only. In general, the ΔXANES fit also has to be corrected for any difference in particle size, or dispersion, which can be determined by TEM, and CO adsorption stoichiometry, which is determined from the IR spectra. For example, if there were an increase in size in the bimetallic nanoparticle, there would be a decrease in the ΔXANES just due to the lower fraction of surface atoms. The decrease is proportional to the ratio of the dispersions of the two catalysts. From TEM, the differences in particle size and dispersion of monometallic Pt and 1% Pt + 2% Pd/SiO_2 are small, 1.9 and 1.7, respectively. Correcting for this size (0.70 x 1.7/1.9) gives a Pt surface fraction of 0.63. In addition, from the FTIR (not shown) both catalysts have primarily linearly adsorbed CO at this particle size so there is no need to correct for the stoichiometry of CO adsorption. Therefore, the

surface composition of Pt atoms on $PtPd/SiO_2$ is unchanged on that basis and is approximately 65%.

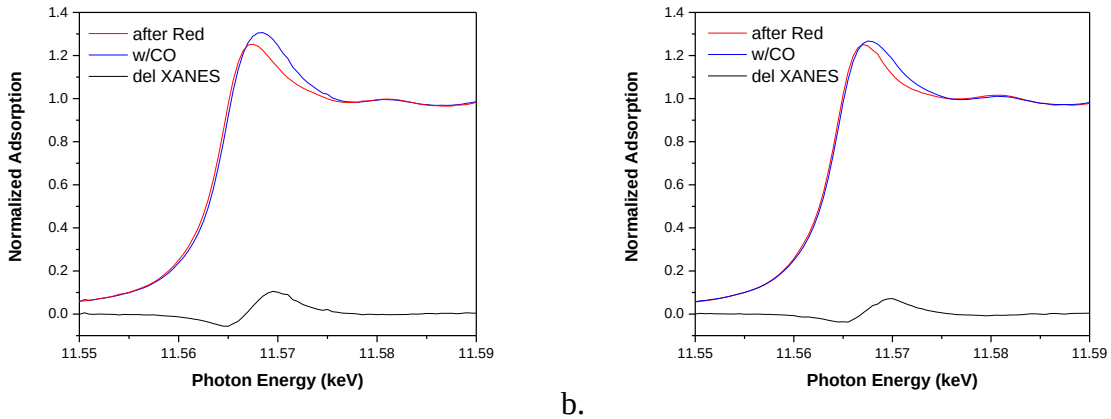

a. b.

Figure 27: XANES spectra at the Pt L_3 edge after reduction, with CO adsorption and ΔXANES spectra of CO adsorption for a) 2%Pt/SiO_2 and b) 1%Pd+2%Pt/SiO_2[2]

Similarly, the fit of the ΔXANES of CO on $PtPd/SiO_2$ is approximately 50% that on Pd/SiO_2. Again, the Pd/SiO_2 used to determine the ΔXANES was very similar in size to that of the bimetallic $PtPd/SiO_2$ catalysts. Correcting for the difference in size of Pd/SiO_2 to $PtPd/SiO_2$ (1.7/1.9), the Pd surface coverage is 0.45. However, on Pd/SiO_2 there is a significant amount of bridging CO, with a 1.33 Pd:CO ratio; while on the bimetallic catalyst CO is bound in primarily a linear configuration with little bridging CO.[139] Accounting for this difference, the surface composition of Pd atoms on $PtPd/SiO_2$ is about 0.33 (0.45/ 1.33). The sum of surface composition of Pt and Pd atoms (~65% Pt atoms and ~35% Pd atoms) is very close to 1.0 within reasonable uncertainty of the XANES, IR, TEM and EXAFS measurements. Using the same method, the Pt surface composition determined from the L_3 XANES for the 0.75% Pd + 3% Pt/SiO_2 catalyst was determined to be about 80% Pt (and therefore 20% Pd)

There are several assumptions and limitations of the described method. First, the method assumes that there is CO saturation adsorption. While this is likely for Pt and Pd, it may not be true for all metals like Au, Ag, Cu and others. For these metals, alternative adsorbates will be required. Second, the method also assumes that the surface composition is not changed by the adsorbate. Also, the method relies on the ability to determine the difference in the XANES spectra with and without adsorbate. This is generally possible for nanoparticle sizes of less than about 10 nm, but for larger particles, the fraction of surface atoms is too small to measure the amount of surface atoms (with an adsorbate) reliably. The turnover frequencies of the bimetallic catalysts reported in Table V were based on the fraction of total surface atoms independent of surface composition and were lower than both monometallic catalysts. Since the TOR of the PtPd catalysts was only slightly lower than monometallic Pd, one might conclude that the surface has a high fraction of Pd atoms. However, for the 1%Pd + 2%Pt/SiO_2 the fraction of surface Pt atoms is about 0.65. If the TOR of Pt and Pd were unchanged in the bimetallic catalyst the experimental TOR would be intermediate between that of Pt and Pd. However, the TOR is 0.4 times that of Pt and 0.71 times that of Pd. In other words, the experimental TOR is much lower than the TOR predicted using the monometallic rates and fraction of surface atoms. Similarly, if the TORs of Pt and Pd on 0.75%Pd + 3%Pt (0.80 surface Pt) were identical to that in the monometallic Pt and Pd, the expected TOR would be also between that of Pt and Pd; however, the experimental TOR that is 0.5 times that of Pt and 0.9 times that of Pd. For both catalysts the experimental TOR is lower than the expected value from the surface composition.

The neopentane isomerization selectivity in both PtPd bimetallic catalysts is slightly higher, 0.7, than for Pt, 0.64, and much higher than Pd, 0.05. Without knowledge of the surface composition, one might conclude that there is a high Pt surface coverage. Using the estimated

surface coverages and the TOF of the pure metals, one can estimate that the kinetic averaged selectivity, e.g., for isomerization, which is the isomerization rate of the surface atoms divided by the total rate. For 1%Pt + 2%Pd the kinetic average selectivity is 0.50. This selectivity is intermediate between that of Pt and Pd. Similarly, the kinetic averaged isomerization selectivity of the 0.75%Pd + 3%Pt catalyst (0.80 Pt + 0.20 Pd surface composition) is 0.55. The experimental values of 0.70 and 0.71 are significantly higher than both of these calculations and even higher than that for monometallic Pt. Thus, while the bimetallic catalysts have TORs that are lower than the monometallic catalysts, the selectivity is significantly higher than the kinetic average of the surface atoms based on the monometallic rates and selectivities.

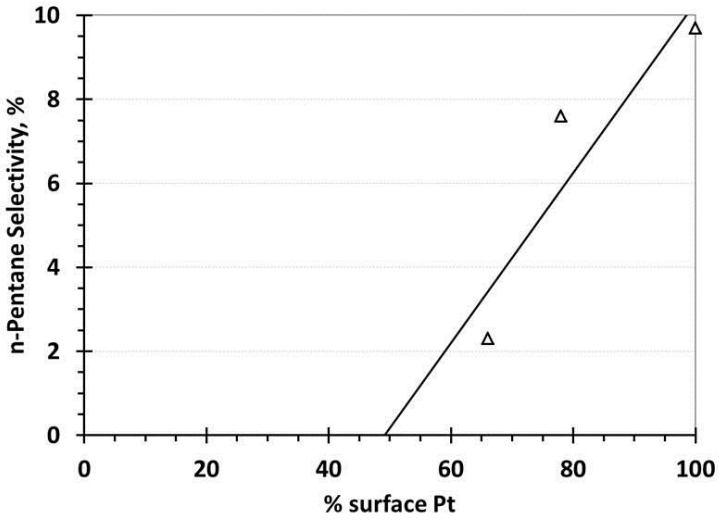

Figure 28: n-pentane selectivity vs. the fractional surface composition of Pt atoms[2]

It was previously noted that although n-pentane is not an expected primary product in the isomerization pathway; nevertheless, there were low selectivities (extrapolated to zero conversion) to this product for the Pt containing catalysts. The n-pentane selectivities were 10%, 8% and 2% for Pt, 0.75%Pd + 3%Pt and 1%Pd + 2%Pt respectively. The selectivity of n-pentane

was 0% for monometallic Pd. The most probable reaction pathway for n-pentane production involves a second isomerization step prior to isopentane desorption. The increase in the selectivity to n-pentane selectivity can be correlated with the increase in surface coverage of Pt as seen in Figure 28. The increase in n-pentane selectivity could correspond to an increase in the retention time of neopentane on the surface in the absence of hydrogenolysis. As the Pd composition decreases, the hydrogenolysis activity of the alloy decreases and neopentane which is bound to the surface may undergo further transformation. In addition, the data imply hydrogenolysis occurs through highly coordinated sites whereas isomerization may not as the addition of Pt breaks up Pd ensembles where hydrogenolysis occurs. In contrast, the presence of Pd does not disrupt the isomerization reaction. This could imply that the binding site for isomerization is more like atop binding whereas hydrogenolysis occurs via high-coordinate attachment to the surface. This would seem to run counter to our studies of monometallic catalysts where large Pd and small Pt nanoparticles displayed similar activity and selectivity (and therefore implied the sites for hydrogenolysis and isomerization were the same.[1] Perhaps the Pt is preferentially located at the more reactive corner and edge sites of the nanoparticle in the bimetallic particles and so the activity and selectivity of the Pt is similar to its presence in a small nanoparticle whereas the Pd is preferentially located in higher coordination sites that are less reactive (whose electronic structure looks then more like a large Pd particle). The TEM measurements were not able to identify such trends but DFT calculations could provide some insight into the preferred locations of the metals.[140]

The selectivity and TORs determined from the surface composition show that mixing Pt and Pd does not result in just an additive effect of the two separate metals. The TOR is lower

than the monometallic rates; while the bimetallic isomerization selectivity is higher than the monometallic catalysts.

3.4 Conclusion

The combination of CO chemisorption and XANES analysis gives a method for the determination of bimetallic catalyst surface composition regardless of adsorption properties of both metals. Knowledge of surface composition allows for better understanding of kinetics and mechanisms for bimetallic catalysts. Neopentane hydrogenolysis behavior for the PtPd catalysts was fairly similar to pure Pt in terms of activity and selectivity. This would lead to the conclusion that the catalyst structure is more of a Pd core and Pt shell rather than the mixed alloy actually present on the surface. Our result leads to the suggestion that palladium does not participate catalytically when alloyed with platinum but rather acts as a promoter.

4 CORRELATING HEAT OF ADSORPTION OF CO TO REACTION SELECTIVITY: BIMETALLIC EFFECTS OF AU ADDITION TO PD

4.1 Introduction

Bimetallic catalysts often have selectivities and activities that differ significantly from what would be expected from physical mixtures of the two metals.[2, 34-38, 141] Alloying allows the surface structure and composition to become tunable parameters to promote activity or selectivity to desired products. Both ligand (electronic) effects and ensemble (geometric) effects may be responsible for these changes in reactivity observed with alloys, but it is difficult to determine experimentally which factor is dominant since it is difficult to isolate these effects. Electronic effects are manifested as changes in the strength of surface-adsorbate interactions due to modification of the electronic structure when the two metals are alloyed. Ensemble effects arise since some reactions require a particular number or arrangement of atoms to form an active site.[38] Understanding the role of electronic and geometric effects in alloy catalysts is complicated by the fact that the two effects are often intertwined. Hammer and Norskov have interpreted changes in reactivity of d-band transition metals through the use of a single descriptor: the d-band center of the metal. Adsorption of simple molecules can be directly correlated to the d-band center and allow for an understanding of observed catalytic activity. Through DFT simulations, Hammer and Norskov separated coordination and strain effects from ligand effects in their studies of bimetallic systems and demonstrated for a given adsorption geometry linear correlations exist between the adsorbate binding energy and the position of the d-band center.[28, 29] Greeley and Norskov demonstrated this simple d-band correlation held for a large variety of alloys in their study of oxygen adsorption.[10] However, separating the influence of electronic and geometric effects experimentally for alloys is a difficult task as the

presence of a second metal not only contributes a ligand effect from the change in hybridization between neighboring metal atoms, but strain effects are often introduced due to changes in metal-metal bond distances.[142] In addition, the presence of the second metal may change the type of available sites at the surface (an ensemble effect).

We previously demonstrated that the selectivity to isomerization as opposed to hydrogenolysis in neopentane conversion follows the same type of electronic structure correlation described by Norskov et al., as the selectivity is linearly related to the CO adsorption energy (presumably directly governed by the energy of the d-band center).[1] However, it is not clear if the relationship between isomerization selectivity and the electronic structure extends beyond monometallic systems. PdAu provides an interesting test case for the electronic structure correlation as Au has previously been used as a modifier for improved selectivity in hydrocarbon reforming.[37]

PdAu alloy catalysts have been studied for a wide variety of reactions including: oxidation, hydrogen peroxide production, hydrochlorination of acetylene and butadiene selective hydrogenation.[87, 125, 143-146] Several different PdAu structural configurations are possible depending on factors like synthesis method and metal loadings. Homogeneous alloys with varying Pd and Au loadings have been synthesized by a number of different methods.[143, 145, 146] However, segregation of either Au or Pd into core-shell geometry has also been well-documented.[144, 147-150] Core-shell nanoparticles with Au-rich shells have been synthesized by sequential deposition and annealing.[148] Pd(shell)/Au(core) nanoparticles has been synthesized through a number of different methods: electrodeposition [149], colloidal synthesis [144, 150] and seeded growth (addition Pd shells to pre-made Au particles).[147] Both Pd and Au have been used as promoters to enhance the catalytic properties of the other by decorating the

surface.[151, 152] Dolle et al. studied the growth of Pd films on Au(110) surfaces; at low Pd coverage (0-0.5 ML), gold preferentially covers Pd atoms, but at higher coverage (0.5 to 3 ML), the growth of Pd introduces a small tensile strain due to the match with the Au lattice until ~9 ML when the lattice parameter of the Pd lattice relaxes significantly.[153] Li et al. performed experiments on PdAu surfaces and found at low palladium coverage, the surface restructures to form low-coordination gold ensembles that block atop palladium sites.[154] At high palladium coverage, CO adsorbs on bridge sites, similar to pure palladium. Goodman's group has investigated the structure of PdAu single crystal surfaces.[125] The addition of Pd atoms to a Au single crystal surface led to isolation of Pd atoms on the Au surface.[148, 155, 156] Electronic effects stem from the charge transfer from gold to palladium which shifts the d-band center of Pd away from the Fermi level and weakens adsorbate bonding to Pd.[157] This weakened adsorbate bonding results in improved neopentane isomerization selectivity as has been observed in previous work.[1]

A number of theoretical studies have been conducted on PdAu systems to analyze the observed changes in catalytic behavior.[125, 154, 158-161] Most findings have concluded that a combination of geometric and electronic effects contribute to Au altering the behavior of Pd. For example, Neurock et al. found that both the surface coverage and metal-adsorbate bond strength are influenced by geometric effects, since the surface coverage and bond strength are correlated (bond strength decreases as coverage increases).[162] The bond strength of ethylene to Pd is weakened by the addition of Au which makes the sites more active for ethylene hydrogenation; however, gold also reduces the binding energy of H by 130 kJ/mol which deters hydrogenation. For ethylene hydrogenation, these two effects balance each other out and the result is a negligible effect on activity but there is an effect on initial ethane dehydrogenation selectivity. Although

charge transfer was observed (an electronic effect), it was not significant and was therefore discounted as a cause for the observed change in catalytic behavior. Mazzone et al. used density functional theory to study the adsorption of CO on PdAu (111) and (100) surfaces.[157] Isolated Pd atoms on a Au surface induces a local relaxation effect that causes shortened Pd-Au bond distances compared to typical Au-Au bond distances resulting in a stronger Pd-Au bond and weakened CO binding energy by as much as 30 kJ/mol. Garcia-Mota et al. also used DFT to study the adsorption of CO on PdAu surfaces.[163] Their calculations showed that isolation of Pd on Au surfaces is thermodynamically favorable and isolation of Pd could also be stabilized by the presence of CO at high pressures ($>10^{-2}$ torr).

Gold has been previously alloyed with Pt group metals to study neopentane conversion. Schwank et al. performed a neopentane hydrogenolysis study over Pt-Au/SiO_2 and Pt-Sn/Al_2O_3 catalysts.[164] Pt-Au samples did not have a significantly different selectivity compared to the monometallic samples. Bonarowska et al. used PdAu catalysts to study neopentane conversion.[143] They synthesized two series of samples prepared by direct redox and incipient wetness impregnation. The reported dispersion of ~0.05 implies that the particles were very large (20 nm). The monometallic Pd sample showed a single-point isomerization selectivity of almost 40% at low conversion (< 1%), about a 15% increase from the selectivity found in previous work.[1] PdAu samples with lower Au content (0.05-0.20 wt%) showed either no change or a slight decrease in isomerization selectivity whereas at a loading of 0.40 wt% Au, the isomerization selectivity increased to almost 50% indicating a positive effect on selectivity. The origin of the increase in the selectivity was not explained.

Here we report on the synthesis, characterization and testing of four PdAu catalysts supported on silica with different Pd loadings. The effect of alloying palladium with gold was

investigated by electron microscopy, X-ray energy dispersive spectroscopy, diffuse-reflectance Fourier transform spectroscopy (DRIFTS), extended X-ray absorption fine structure (EXAFS), chemisorption and adsorption calorimetry of CO. Neopentane hydrogenolysis was the probe reaction used to evaluate changes in catalytic performance of Pd upon alloying with Au.

4.2 Experimental Methods

4.2.1 Catalyst Synthesis

All samples were synthesized using sequential impregnation of Au then Pd on silica (Davisil A60 silica gel from Sigma-Aldrich, 200 m^2/g and 1.15 mL/g pore volume) using both incipient wetness impregnation (IWI) and strong electrostatic adsorption (SEA). [79] During IWI, a support is contacted with just enough metal-precursor solution to fill the pore volume. All of the metal precursor solution contacts the surface due to the incipient amount of liquid used; however, this synthetic method typically leads to significant particle growth during drying and pretreatment. In contrast, SEA uses an excess amount of solution with a controlled pH to favor the uptake of the metal precursor. The SEA method requires an appropriately charged metal precursor based on the point of zero charge (PZC) of an oxide support and the pH of the solution. The hydroxyl groups on the surface of the oxide support will protonate or deprotonate depending on the pH of the solution relative to the PZC of the support. Precursors can then be selected that will have the opposite charge as the support at a certain pH value and so the electrostatic interaction between the support and the precursor leads to adsorption of the metal precursor to the surface.[79]

0.52%Pd-3%Au & 1%Pd-3%Au: Gold was added to silica using the SEA method. Silica (35 g) was added to ammonia solution (NH_4OH (5 mL)/H_2O (200 mL)). 1.7 g of $HAuCl_4$ was added to 50 mL of H_2O, 2.5 mL ethylenediamine and 5 mL of NH_4OH which resulted in a

dark orange-yellow solution. These solutions were combined and stirred for 10 min. followed by vacuum filtering of the solid catalyst, which was subsequently washed 3 times with H_2O. The sample was dried in a vacuum oven overnight at 50°C. The sample was reduced at 150°C in a flow of 4% H_2/He. For the 0.52% Pd sample, 0.55 g of 10% $Pd(NH_3)_4(NO_3)_2$ solution was then added using IWI and dried at 125°C overnight and calcined at 225°C for 3 hr and reduced at 200°C. For the 1% Pd sample, 1.42 g of 10% $Pd(NH_3)_4(NO_3)_2$ was added dropwise to 1 mL NH_4OH and 2.5 mL H_2O solution. The sample was dried at 125°C overnight followed by calcination at 225°C for 3 hr and reduced at 200°C for 30 min.

2%Pd-3.5%Au & 4%Pd-3.5%Au: Gold was added to silica using the same SEA method described above. The sample was dried in an oven overnight at 90°C. The sample was reduced at 150°C in 4% H_2/He. For the 2% Pd sample, 2.78 g of 10% $Pd(NH_3)_4(NO_3)_2$ aqueous solution was added dropwise to a solution of NH_4OH (1 mL) and H_2O (4 mL). The sample was dried at 100°C overnight and calcined at 225°C for 3 hr and reduced at 225°C. For the 4% Pd sample, Pd addition was done in two steps. Initially, 2.84 g of 10% $Pd(NH_3)_4(NO_3)_2$ was added dropwise to a solution of NH_4OH (1 mL) and H_2O (4 mL). The sample was dried at 100°C overnight and then 2.75 g of precursor was added dropwise to a solution of NH_4OH (1 mL) and H_2O (4 mL). The sample was again dried overnight at 100°C and then calcined at 225°C for 3 hr and reduced at 225°C for 30 min.

4.2.2 STEM and X-ray Energy Dispersive Spectroscopy (XEDS)

The STEM work was all done at UIC's Research Resources Center Facility using the JEOL-ARM 200CF aberration corrected microscope (70 pm spatial resolution and 300 meV energy resolution). Samples were dispersed in isopropyl alcohol and sonicated for 20 min. A

drop of the solution was added to a holey-carbon copper grid and dried under a heat lamp for 20 min. Images were taken using the High Angle Angular Dark Field (HAADF) mode. XEDS measurements were collected using an Oxford Instrument X-Max 80 mm^2 SDD detector. A 1.3 Å probe size with a 143 pA beam current was used to measure line scan data with a 1 s dwell time per step. Data was plotted using the Oxford Instrument Aztec program.

4.2.3 Extended X-ray Absorption Fine-Structure Spectroscopy (EXAFS)

X-ray absorption spectroscopy (XAS) measurements for the Pd K (24350 eV), and Au L_3 (11919 eV) edges were made on the bending magnet beam line of the Materials Research Collaborative Access Team (MRCAT) at the Advanced Photon Source (APS) at Argonne National Laboratory. Measurements were made in transmission mode. A palladium or gold foil spectrum was acquired through a third ion chamber simultaneously with each measurement for energy calibration.

Samples were prepared by grinding the catalysts into a fine powder and pressing them into a metal cylinder sample holder capable of holding up to six individual samples. The sample holder is then placed in a quartz tube with ports on each end to flow gases or isolate the sample after treatment. The sample thickness was chosen to give a total absorbance at the Au L_3 or Pd K edge between 1-2 absorption lengths and edge steps around 0.3-0.5. Samples were reduced at 300ºC in 4% H_2/He mixture (50 cm^3/min) at atmospheric pressure. After reduction, the samples were purged with He (100 cm^3/min) and cooled to room temperature in He flow. Trace oxidants in He were removed by passing through a Matheson PUR-Gas Triple Purifier Cartridge containing a Cu trap. All EXAFS spectra were obtained at room temperature in He.

4.2.4 Neopentane Hydrogenolysis and Isomerization

Neopentane hydrogenolysis and isomerization was studied using 0.05-0.15 grams of catalyst diluted with 0.9 grams of silica and loaded into a 0.5" OD quartz plug flow reactor. Glass wool was used for the bottom 2 cm of the bed. A 0.5 cm long layer of silica was placed on top of the glass wool, followed by the catalyst/silica mixture resulting in an overall catalyst bed height of 3 cm. The reactor was purged with He for 5 min before each run, and the catalyst was reduced in 4% H_2/He as the temperature was increased to the reaction temperature, 271 ± 2°C. This temperature enabled differential conversion for all of the catalysts tested. A K-type thermocouple was inserted from the bottom of the reactor into the lower portion of the catalyst bed. Once the reaction temperature stabilized, the pre-mixed reactant feed gas consisting of 0.35% neopentane and 3.5% H_2 balanced in He was passed through the reactor. The flow rate of the feed gas was varied from 25 to 100 cm^3/min to obtain differential conversions (0.5–6 %). Each flow rate was run for at least one hour to ensure steady-state conversion had been reached. An Agilent 6890N gas chromatograph (using a J&W Scientific GS-Alumina column) with an FID detector was used to analyze the products and was equipped with a back pressure regulator on the outlet to hold the system at a constant pressure of 9 psig. Each experimental run was completed within six hours for consistency and multiple runs for each catalyst were performed. No appreciable deactivation was observed in any of the catalysts over this period of time. The maximum error of any selectivity measurements was 6%, with most of the data being reproducible within 2%. Turnover rates were calculated based upon the number of active sites determined by the dispersion measured by CO chemisorption to account for the fact that surface Au sites do not adsorb CO at the experimental conditions employed and are not active for this reaction.[81, 165, 166]

4.2.5 Diffuse Reflectance Infrared Fourier Transform Spectroscopy (DRIFTS)

Infrared spectra were obtained using a Thermo Scientific Nicolet 6700 FTIR spectrometer equipped with a Harrick Scientific Praying Mantis diffuse reflectance *in*-situ cell at the Northwestern Clean Catalysis (CleanCat) Core Facility. Samples were ground to a fine powder using a mortar and pestle, and packed into the sample chamber to create a uniform surface. The chamber was purged with Ar, and then the gas was switched to 10% H_2/N_2 and the temperature was raised to 250°C and held for 15 min. After reduction of the catalyst, the gas was switched back to Ar and the temperature was reduced to 25°C. A background scan was then recorded, which was averaged over 100 scans (2 minute observation time) with 4 cm^{-1} resolution. The sample was then exposed to 1.02% CO/N_2 and another scan was taken once equilibrium was reached, at which point the flow was changed back to Ar and a final scan was taken once the intensity of the adsorbed CO peak was invariant with time. The linear-to-bridge bound ratio reported here do not take into account the differences in extinction coefficients between the adsorption sites and therefore are not quantitative, but do reflect qualitative differences between catalysts.[167]

4.2.6 CO chemisorption

The CO chemisorption measurements were conducted at the Northwestern University Clean Catalysis (CleanCat) Core Facility using an Altamira Instruments AMI-200. Catalysts (0.05-0.2 g) were loaded into a U-shaped quartz reactor tube, which was weighed before and after sample addition to ensure an accurate weight measurement. The loaded tube was then mounted in the furnace and the catalysts were reduced in H_2/Ar at 300°C for 2 hr (10°C/min ramp rate) and then flushed for 30 min in He. Using a six-way valve, 5% CO/He was then pulsed (595 μL loop volume) into the system 15 times at 30°C to ensure the surface was

saturated. Each pulse peak was integrated to find the volume of CO remaining following adsorption. Surface saturation was typically reached within 10 pulses. The dispersion determined by CO chemisorption also included average stoichiometric factor determined from the DRIFTS linear-to-bridging ratios for each catalyst. Linear bound CO accounts for one CO molecule per surface atom while bridge bound CO implies there is one CO molecule per two surface atoms. The equation used to determine the dispersion of Pd in the PdAu/SiO_2 catalysts is given below; neither CO fraction has been corrected using the extinction coefficients.

$$Dispersion = \frac{mol\ CO\ adsorbed}{mol\ metal} \times ((linear\ CO\ fraction\ \times 1) + (bridge\ CO\ fraction\ \times 2))$$

4.2.7 CO Heats of Adsorption

Determination of the initial heat of adsorption of carbon monoxide on the monometallic Pd/SiO_2 and four PdAu/SiO_2 catalysts (60-70 mg) was conducted utilizing a Setaram Sensys EVO differential scanning calorimetry interfaced with a plug-flow/breakthrough reactor. The plug-flow reactor was connected to a mass spectrometer. After reduction at 300°C in 5.11% H_2/Ar (both gases 99.999%) for 2 hr, the catalyst was cooled down to 35°C in the same gas. The catalyst was exposed to a mixture of 1% CO (99.999% research grade) in He (99.9999%, research grade) pulsed into the 5% H_2/Ar stream from a ten-way switching value with a 1000 µL sample loop. The number of moles of CO per pulse calculated from the ideal gas law was ~4 × 10^{-4} mmol. Twenty pulses of carbon monoxide were employed; the initial heat of adsorption was determined by only considering injections in which the entire pulse of carbon monoxide was consumed. The number of pulses completely consumed depended on the content of Pd in the catalyst; as the Pd content increased, the amount of adsorbed CO increased.

4.3 Results

4.3.1 Particle Size Analysis

STEM imaging was used to determine particle size. A representative STEM image for the 2% Pd+3.5% Au catalyst and corresponding size distribution are shown in Figure 29. Table VI summarizes the particle sizes for all catalysts by both STEM and chemisorption methods. The data in Table VI show that the four catalysts are similar in particle size as determined by both STEM and chemisorption. Data for similar sized monometallic Pd catalysts is taken from Childers et al. for comparison with PdAu.[1] Particle size has an effect on neopentane selectivity and activity; therefore, in order to isolate the effect of Au alloying, it is critical that catalysts with varying composition have similar particle sizes.[1]

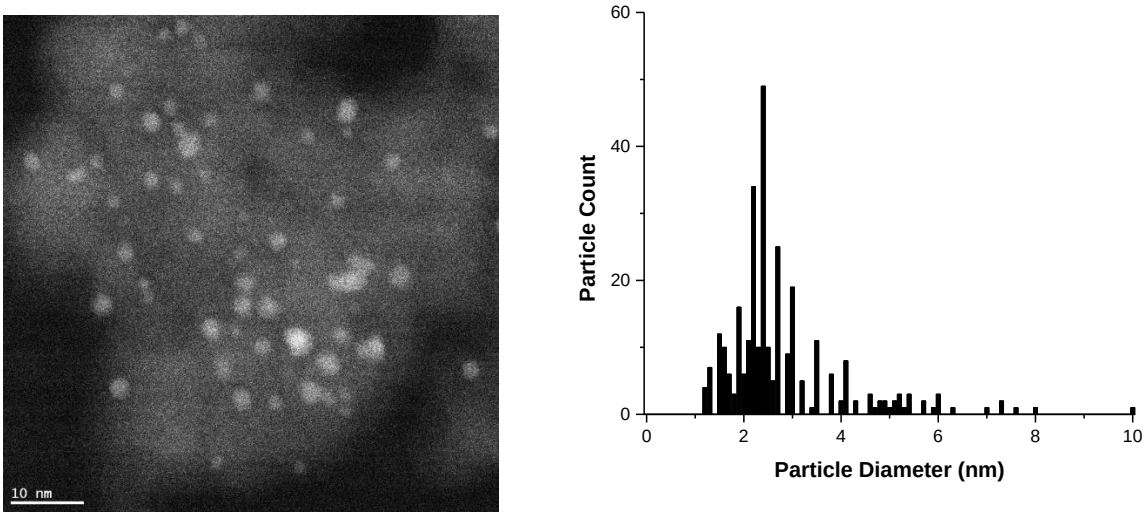

Figure 29: 2%Pd-3.5%Au sample image and particle size distribution determined by STEM

Table VI: Particle size determined by STEM and CO chemisorption

Sample	Particle Size by STEM (nm)	Particle Size by CO chemisorption (nm)
2%Pd_2.5 nm	2.5 ± 1.1	4.3 ± 0.4
2%Pd_3 nm	3.0 ± 0.8	3.8 ± 0.4
0.52%Pd+3%Au	2.9 ± 1.4	1.7 ± 0.2
1%Pd+3%Au	2.8 ± 1.2	2.2 ± 0.2
2%Pd+3.5%Au	3.3 ± 1.1	2.3 ± 0.2
4%Pd+3.5%Au	4.1 ± 1.0	3.8 ± 0.4

Figure 30 shows a line scan and the corresponding STEM image for the 0.52% Pd+3% Au and 1% Pd+3% Au catalysts, respectively. Line scans demonstrate an increased concentration of Pd on the outer shells of the nanoparticles while the Au is concentrated in the core. Analysis performed on several particles per catalyst sample confirmed that a majority of the nanoparticles have a Au-rich core and Pd-rich shell structure.

a.

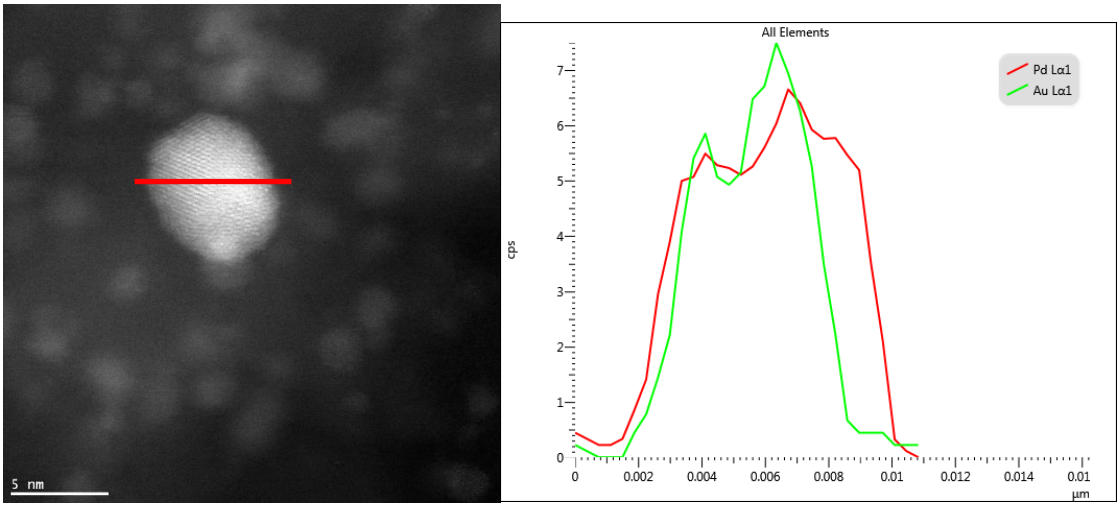

b.

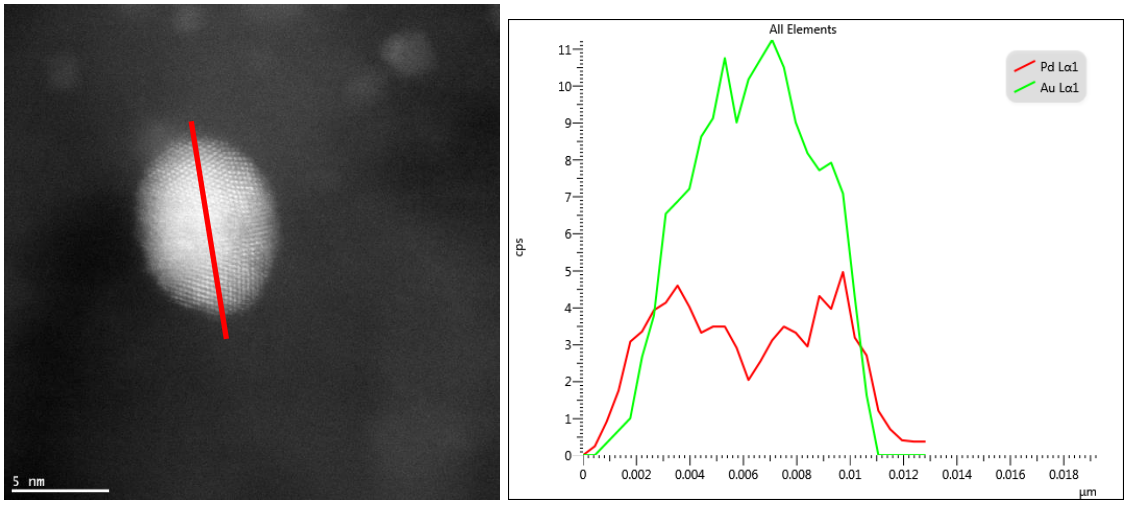

Figure 30: Linescan data for 0.52%Pd-3%Au catalyst (a) and 1%Pd-3%Au catalyst (b) Pd (red) and Au (green).

4.3.2 EXAFS

Extended X-ray absorption fine structure (EXAFS) spectra were collected for each catalyst following reduction at 300°C and fit to determine bond distances and coordination numbers (CN). The EXAFS spectra for the Pd K-edge and the Au-L_3 edge spectra are given in Figure 31 and the fitting parameters are summarized in Table VII. The reference Pd and Au foil spectra (black dotted lines) are included for comparison. The Pd foil EXAFS in Figure 31a show

two prominent peaks at 1.97 and 2.47 Å with an intensity ratio of 2:1, typical of metallic Pd.[168] The PdAu catalysts have small shifts in these peaks to 2.00 and 2.55 Å respectively; however, these shifts are not unexpected due to slight changes in particle size amongst samples. The 4%Pd-3.5%Au catalyst also has the 2:1 peak intensity ratio typical of metallic Pd. However the other PdAu catalysts show a change in that ratio to about 1.6:1. This change indicates that there are Au atoms in contact with Pd in the catalyst. The Pd-Pd bond distance in all of the catalysts is 2.80 Å, an expansion by 0.05 Å from the metallic bond distance of 2.75 Å.[1] This expansion in the Pd-Pd bond distance could be the result of strain from epitaxial growth of Pd over Au.[153] The differences in coordination number between Pd-Pd and Pd-Au show the majority of the palladium atoms in this catalyst are bonded to other palladium, as would be expected for a core-shell configuration. The fraction of Pd atoms which interact with Au decreases with increasing palladium loading. A Pd-Au bond distance of 2.82 Å is approximately the average of the bulk Pd-Pd and bulk Au-Au bond distances. Figure 31b shows the Au L_3-edge spectra of all catalysts and the Au foil reference. The Au foil spectra show two peaks at 2.45 and 2.95 Å, and these peaks shift to 2.37 and 3.00 Å in the PdAu catalysts, respectively.[83, 169] The spectra show almost no variation from metallic Au except the peak at 2.45 Å is shifted lower by 0.075 Å and the peak at 2.95 Å is shifted higher by 0.025 Å. The fitting parameters in Table VII show that there are very few Au-Pd interactions and no change to the bulk properties of Au in the bimetallic catalysts. The Au-Au bond distance contraction from 2.88 to 2.86 Å is not unexpected for smaller Au particles.[150] This lack of change indicates that nearly all gold present in the catalysts are surrounded by other gold atoms.

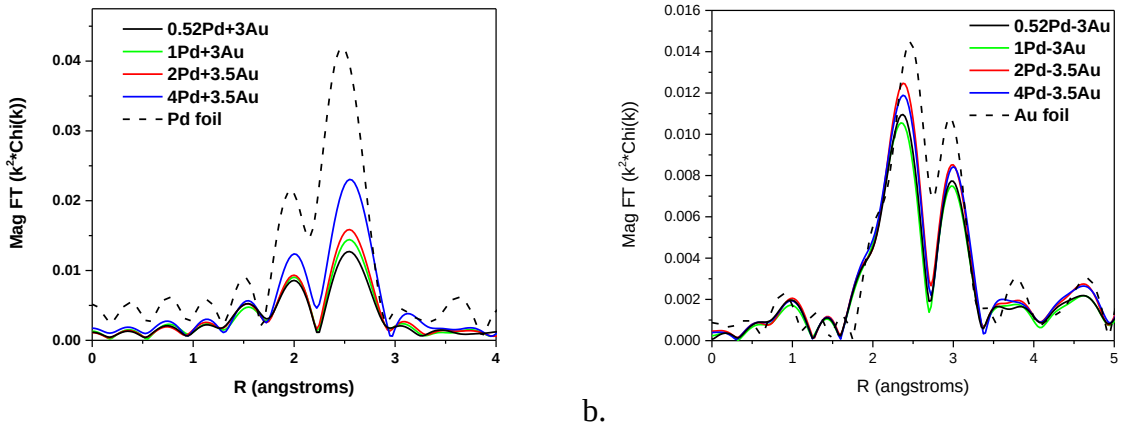

a. b.

Figure 31: EXAFS spectra for (a) Pd K-edge and (b) Au L_3-edge

Table VII: EXAFS fitting parameters for Pd K-edge and Au L_3-edge

Catalyst	Pd Edge Energy (keV)	Scatter	Coordination Number	Bond Distance (Å)
0.52Pd-3Au	24.350	Pd-Pd	6.2	2.80
		Pd-Au	3.4	2.82
1Pd-3Au	24.350	Pd-Pd	6.4	2.80
		Pd-Au	2.9	2.82
2Pd-3.5Au	24.350	Pd-Pd	7.0	2.80
		Pd-Au	2.6	2.82
4Pd-3.5Au	24.350	Pd-Pd	10.0	2.80
		Pd-Au	1.7	2.82

Catalyst	Au Edge Energy (keV)	Scatter	Coordination Number	Bond Distance (Å)
0.52Pd-3Au	11.919	Au-Au	10.2	2.86
		Au-Pd	1.1	2.80
1Pd-3Au	11.919	Au-Au	9.8	2.86
		Au-Pd	1.4	2.83
2Pd-3.5Au	11.919	Au-Au	11.2	2.87
		Au-Pd	1.0	2.83
4Pd-3.5Au	11.919	Au-Au	11.3	2.87
		Au-Pd	1.1	2.82

4.3.3 Diffuse Reflectance Infrared Fourier Transform Spectroscopy (DRIFTS)

Characterization of CO adsorption on the PdAu/SiO_2 catalyst was conducted with DRIFTS to determine changes in CO bonding to the catalyst surface with the addition of increasing amounts of Pd to the catalyst. Peaks in the range of 1800-2000 cm^{-1} are assigned to bridge bound CO. Within this range, peaks between 1800 and 1900 cm^{-1} are attributed to CO bound on terrace sites while peaks between 1900 and 2000 cm^{-1} are believed to be due to the presence of CO bound to corner and edge sites.[170, 171] The linear bound region can also have two peaks typically occurring around 2080 and 2050 cm^{-1} which Lear et al. have assigned to linear bound CO on corner sites and edge sites respectively.[170]

Figure 32 shows the DRIFTS spectra for the PdAu catalysts as well as monometallic Pd catalysts with similar particle sizes. The linear bound CO peak in each spectrum was normalized to facilitate direct comparison amongst catalysts. Palladium is known to have more bridge bound CO than linear bound CO and alloying with gold caused an increase in the linear-to-bridge ratio, suggesting division of large Pd ensembles into smaller ones. All catalysts have a peak centered at 2082 cm^{-1} which is attributed to linear bound CO on diluted Pd atoms on a Au-Pd surface.[148, 172] CO bound on Au surfaces shows a linear peak around 2110 cm^{-1} which is not seen in any of the catalysts.[145] All catalysts possess two peaks in the bridge bound region though the peak position shifts. The 0.52% Pd-3% Au catalyst has a peak at 1955 cm^{-1} which is assigned to bridge bound CO on corner and edge sites and another peak at 1860 cm^{-1} which is assigned to bridge bound CO on terrace sites.[86-88] These peaks are in the same positions as the monometallic Pd (2.5 nm) catalyst and all other catalysts have two bridge bound peaks centered at 1970 cm^{-1} and 1930 cm^{-1}. Both of these peaks are in the range of bridge bound CO on corners and edges, but Lear et al. have further defined these two distinct peaks as bridge

bound CO on (100) facets (1970 cm^{-1}) and CO bridge bound on (111) facets (1930 cm^{-1}) specifically.[170] These PdAu catalysts have similar peak positions to the monometallic Pd (2.5 nm) catalyst, except that the bridge bound CO peak on terrace sites is located at 1830 cm^{-1}. All PdAu catalysts lose the bridge bound CO peak on terrace sites centered at 1830 cm^{-1} suggesting that gold breaks up palladium ensembles. The resolution of two distinct peaks in the bridge bound region and the loss of the peak around 1830 cm^{-1} are evidence for bimetallic formation.[148, 161, 172] The similarity of these spectra to the monometallic Pd spectra suggests that there is not much surface Au which adsorbs CO. Marx et al. found a similar trend when combining Pd and Au and found little contribution to the DRIFTS spectra from CO adsorbed on Au sites.[173]

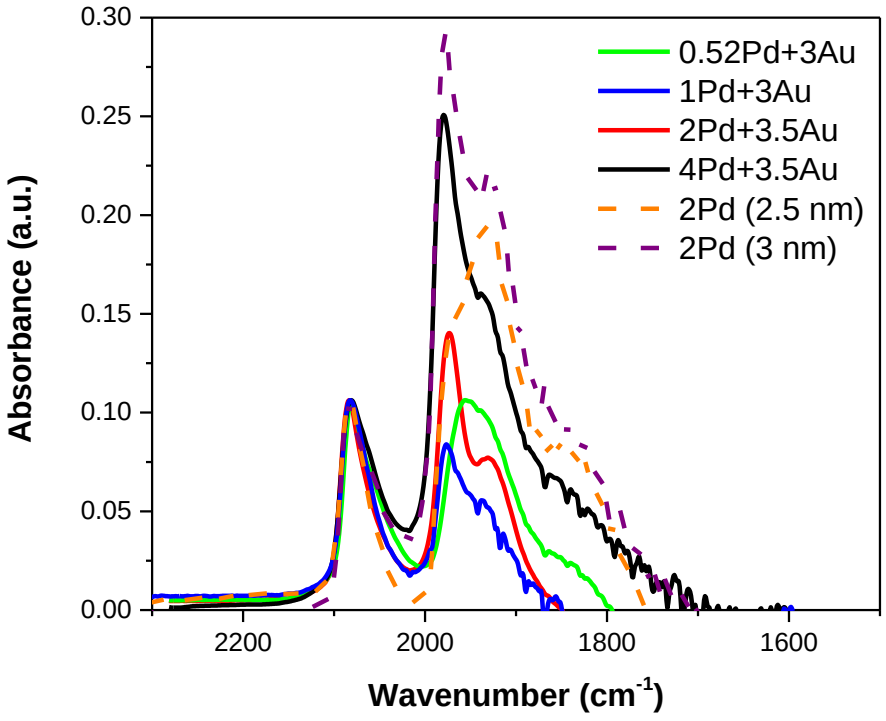

Figure 32: DRIFTS spectra of the adsorption of carbon monoxide on silica supported PdAu catalysts: 0.52%Pd-3%Au (green), 1%Pd-3%Au (blue), 2%Pd-3.5%Au (red) and 4%Pd-3.5%Au (black) and monometallic Pd catalysts of similar particle size (dotted lines): 2.5 nm (orange) and 3 nm (purple). Intensity of linear bound CO peak at 2082 cm^{-1} normalized for each catalyst for comparison.

The linear-to-bridge ratios of adsorbed CO are calculated by comparing the area of the different peaks and are presented in Table VIII. All PdAu catalysts have a higher linear-to-bridge ratio than the monometallic Pd catalyst with similar particle size determined by STEM.[1] Alloying with gold causes a decrease in bridge bound CO, further indication that palladium ensembles break up. There is not a smooth correlation between palladium weight loading and linear-to-bridge ratio as the 1%Pd-3%Au catalyst has the highest ratio. However, the addition of Pd above the 1 wt. % loading causes the linear-to-bridge ratio to decrease to a value similar to monometallic Pd catalyst, consistent with a contiguous overlayer of Pd on the Pd(shell)/Au(core)

nanoparticle. The change in the DRIFTS spectra are another indication that the palladium is altered by alloying with gold and has been seen in literature.[172, 174]

4.3.4 Calorimetric determination of CO Heat of Adsorption on PdAu/SiO_2

The initial heat of adsorption determined previously for a pair of Pd/SiO_2 catalysts with a mean TEM particle size of 2.5-3 nm was ~ 130 kJ mol^{-1}.[1] The heat of CO adsorption on Pd was previously determined for the catalysts reduced in H_2, evacuated at the reduction temperature, followed by cooling in vacuum to the adsorption temperature (35°C). In the previous work, the differential (initial) heat of adsorption was determined using a volumetric adsorption instrument (Micromeritics ASAP 2020C) interfaced with a Setaram Sensys EVO differential scanning calorimeter. For the PdAu catalysts studied in this work, calorimetric measurements of CO were conducted in a plug-flow reactor interfaced to a mass spectrometer using the same Setaram Sensys EVO differential scanning calorimeter. Attempts to measure the heat of adsorption of CO on the PdAu catalysts in an inert environment were unsuccessful due to the large heat flow associated with the oxidation of CO by the oxygen in He (UHP, 99.999%). The heat flow observed calorimetrically was accompanied with a nearly identical increase in the CO_2 (44 m/z) signal in the mass spectrometer. All attempts to eliminate the CO oxidation reaction were unsuccessful including utilizing a CO/He mixture containing research grade He (99.9999%). In order to reduce the oxidation of carbon monoxide, we introduced pulses of CO into a 5% H_2/Ar stream. The Ar contained significantly less oxygen than both grades of He. Reduction of the catalyst and cooling down to the adsorption temperature in the H_2/Ar ensured that Pd was covered with chemisorbed hydrogen. Therefore, the CO heat of adsorption values reported in Table VIII are reported for H-covered Pd surfaces. Chemisorbed hydrogen will lower the heat of adsorption of CO compared to an adsorbate-free surface of Pd.[175] For the

monometallic Pd sample, the heat of adsorption of CO decreased by ~40 kJ mol^{-1} in the presence of chemisorbed H. At this point, we do not know to what extent the potential incorporation of Au in the Pd shell layer influences the energetics of H adsorption, but the reported initial heats of adsorption of CO are approximately the same across all samples demonstrating Pd dominates the interaction with CO.[176-178] The results in Table VIII also show that increasing Pd wt% decreased the heat of adsorption to a value similar to monometallic Pd.

Table VIII: Initial Heat of CO Adsorption Values (± 10 kJ/mol) in the presence of chemisorbed hydrogen and Linear-to-Bridge ratios from DRIFTS.

Sample[a]	CO (initial) heat of adsorption on H-covered surface (kJ/mol CO)[b]	Linear to Bridge Ratio
2Pd/SiO_2[c]	92	0.20 : 1
0.52Pd-3Au/SiO_2	104	0.59 : 1
1Pd-3Au/SiO_2	97	0.94 : 1
2Pd-3.5Au/SiO_2	99	0.37 : 1
4Pd-3.5Au/SiO_2	90	0.25 : 1

[a]Catalysts were initially reduced under 5.11% H_2/Ar (both gases, 99.999% UHP) for 2 hr at the specified reduction temperature, followed by subsequent cooling in H_2.
[b]Initial heat of CO adsorption determined by microcalorimetry on a reduced H-covered Pd or PdAu surface.

4.3.5 Neopentane Hydrogenolysis and Isomerization

Neopentane conversion was performed at 275°C, 9 psig and varying flow rates (25-100 cc/min) in order to maintain differential conversion (< 6%) behavior. Two reaction pathways are possible for this reaction: hydrogenolysis and isomerization. Isomerization products include isopentane (single isomerization) and n-pentane if isopentane undergoes a second isomerization. A single hydrogenolysis step results in the formation of isobutane and methane, and secondary hydrogenolysis reactions produce additional methane and lighter hydrocarbons (propane and ethane). The selectivity values (extrapolated to 0% conversion) and calculated turnover rates

(TOR) based on Pd surface concentration determined from CO chemisorption are provided in Table IX. Since the activity of gold is several orders of magnitude lower for neopentane hydrogenolysis than Pd [81], CO chemisorption is required to determine the surface concentration of palladium for the calculation of nominal turnover rates. Products with non-zero selectivity at 0% conversion are considered primary products while products that have 0% selectivity in the limit of 0% conversion are considered secondary or higher order products.[179] The isomerization selectivity is defined as the selectivity to isopentane since no n-pentane was observed, and hydrogenolysis products are < C_5 molecules.

Table IX: TOR and product selectivity data for PdAu and Pd catalysts

Catalyst	Dispersion[a]	TOR (mol conv / metal site / sec)	Initial Product Distribution (%)					
			CH_4	C_2H_6	C_3H_8	n-C_4H_{10}	i-C_4H_{10}	i-C_5H_{12}
0.52%Pd+3%Au	0.59	6.2×10^{-4}	38	2	3	0	33	26
1%Pd+3%Au	0.45	3.0×10^{-4}	43	3	6	0	29	20
2%Pd+3.5%Au	0.43	5.8×10^{-4}	43	0	4	1	33	19
4%Pd+3.5%Au	0.26	1.3×10^{-3}	45	0	3	4	36	12
2%Pd/SiO_2_3nm	0.33	7.7×10^{-4}	40	0	1	1	34	24
2%Pd/SiO2_2.5nm	0.40	1.0×10^{-3}	49	1	5	2	33	9

[a]Dispersion determined by CO chemisorption for PdAu catalysts and by STEM for Pd catalysts.

The isomerization selectivity for all of the PdAu/SiO_2 catalysts falls within the range of the two monometallic Pd catalysts (Table IX). There is a trend of increasing isomerization selectivity with decreased palladium weight loading. Primary hydrogenolysis (i.e., increase in methane selectivity) increases as the amount of Pd increases in the PdAu/SiO_2 catalysts, but the

secondary hydrogenolysis product selectivity doesn't show a consistent trend with Pd content in the bimetallic catalysts.

4.4 Discussion

4.4.1 Explanation of activity and selectivity change

XEDS measurements demonstrated particles had Pd-rich shells and Au-rich cores. EXAFS data revealed palladium in the bimetallic catalysts is under expansive strain compared to monometallic palladium. The data from EXAFS shows that Pd-Pd bond length increases from 2.75 to 2.80 Å when alloyed with Au. This type of lattice expansion has been documented previously for Pd-shell/Au-core catalysts.[147, 150, 180] The activity of the bimetallic catalysts also falls within the monometallic Pd behavior for neopentane hydrogenolysis established in our previous work.[1] Although the selectivity is not significantly improved compared to monometallic palladium, the dependence of the selectivity with the effective particle size has changed. An isomerization selectivity of ~25% requires a monometallic palladium particle of ~3 nm, whereas the 0.52% Pd-3% Au catalyst with comparable isomerization selectivity has an effective particle size of 1.7 nm as determined by CO chemisorption. Dispersion determined by chemisorption is a more relevant determination of the number of active sites than STEM since Au has an almost negligible neopentane hydrogenolysis activity compared to Pd.[47, 81] In addition, CO does not bind well to Au under the conditions of the chemisorption experiment; the temperature is too high, enabling the number of Pd surface atoms to be determined.[165, 166] Increasing the weight loading of palladium also increases the particle size determined by chemisorption since more of the Au nanoparticle surface will be covered by Pd. The increase in the Pd surface composition results in a decrease in isomerization selectivity to the extent that the 4% Pd-3.5% Au catalyst performs almost identically to the monometallic Pd (2.5 nm) catalyst.

This behavior indicates gold must be in close contact to the surface palladium to influence the catalysis.

4.4.2 Comparison of geometric and electronic effects

Figure 33a shows the dispersion determined by chemisorption for the pure Pd data from the previous study combined with the PdAu selectivity data.[1] The figure demonstrates the addition of gold alters the behavior of palladium when it is in direct contact with the surface palladium. A similar sized monometallic palladium catalyst (by STEM) has an isomerization selectivity of 3% compared to the 0.52% Pd-3% Au catalyst which has a selectivity of 26%. Figure 33b shows the heat of adsorption behavior for both Pd and PdAu catalysts. There is a similar behavior seen here where an increasing wt% of Pd results in heats of adsorption closer to Pd. The 4% Pd-3.5% Au catalyst has a heat of adsorption that fits well with our correlation from previous work, suggesting that the catalyst adsorbs CO more like Pd as the amount of added Pd increases.[1] Ward et al. also found that the heat of adsorption of CO did not change significantly with the alloying of Pd and Au.[165] The small changes were attributed to electronic effects through electron transfer from Pd to Au; however, the differences in heats of adsorption were not larger than the standard deviation given in their data. Neurock et al. performed a theoretical study of PdAu for ethylene hydrogenation and found the electronic effect due to rehybridization was negligible compared to the contribution from geometric effects caused by the weakening of carbon and hydrogen bonding to Au.[162] Both figures suggest the gold must be close to the surface to have an effect on the catalytic performance and that the composition of the core of the particle is not important if the shell is thick enough to be contiguous and effectively function as a monometallic nanoparticle.

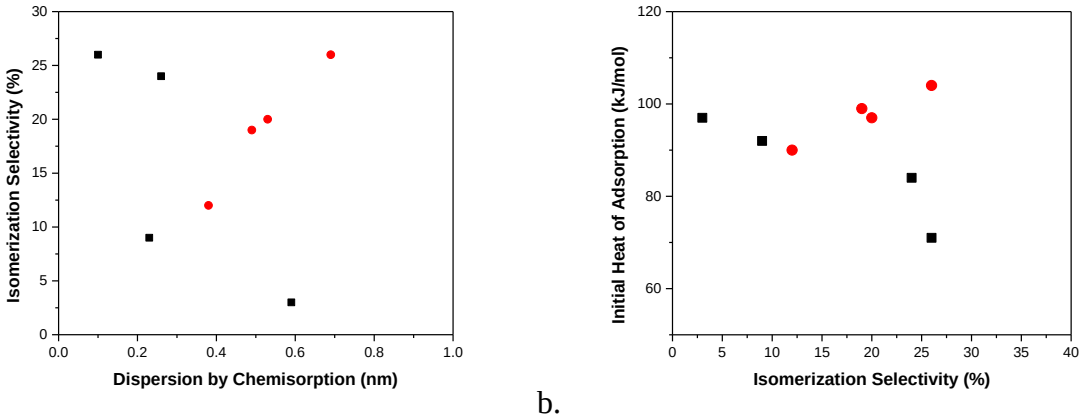

a. b.

Figure 33: a) Isomerization selectivity vs. Particle size determined by CO chemisorption and b) Initial CO heat of adsorption vs. Isomerization selectivity of monometallic Pd (black squares) and PdAu (red circles) catalysts

The expansion of the Pd-Pd lattice seen in EXAFS may explain the changes in reactivity since the expansion may influence the adsorption configuration of neopentane to the surface. This is observed in DRIFTS data for CO.[162] The de-emphasis of the hydrogenolysis pathway would explain the increase in isomerization selectivity and similarity of the turnover rate for neopentane disappearance due to the loss of ensembles for C-H and C-C bond cleavage. Although the performance of Pd has not been improved significantly by the addition of Au, two catalysts were created (the 3.0 nm Pd and the 0.52% Pd-3% Au) with significantly different surface bonding characteristics but with very similar isomerization selectivity. This data also highlights the influence of the near-surface composition compared to the bulk properties of a nanoparticle on the catalytic performance.[181] The presence of gold alters the behavior of palladium relative to a monometallic nanoparticle with a similar effective diameter. However, the further the gold is from the catalyst surface the effect on the catalyst performance is lessened such that the 4% Pd-3.5% Au catalyst performs like pure Pd.

Corner and edge sites typically bind adsorbates more strongly and are more active for bond-breaking reactions compared to terrace sites.[19, 182, 183] To interrogate the types of sites available, CO adsorption on these catalysts monitored by DRIFTS has been used. The addition of gold decreases the amount of bridge-bound CO as seen in Figure 32, which would indicate an increase in the fraction of low coordination corner and edge sites. From previous work, Pd catalysts with low linear-to-bridge ratios resulted in higher isomerization selectivity.[1] However, the PdAu catalysts do not follow this trend, the 0.52% Pd-3% Au and 1% Pd-3% Au catalysts had the highest linear-to-bridge ratio and the highest isomerization selectivity of all of the catalysts. Both these catalysts have an isomerization selectivity similar to the largest Pd particles tested in our previous work; however, the linear-to-bridge ratios are significantly different. The best Pd catalysts in terms of isomerization selectivity had a linear-to-bridge ratio of ~0.15:1 while the PdAu catalysts with similar selectivity behavior have a ratio of 0.59:1 (0.52%Pd-3%Au) and 0.94:1 (1%Pd-3%Au).[1] Figure 34 shows the isomerization and hydrogenolysis turnover rates versus the linear-to-bridging ratio for the PdAu catalysts. The neopentane hydrogenolysis rate decreases with increasing linear bound CO while the isomerization rate is insensitive to changes in surface structure. Hydrogenolysis is a well-known structure-sensitive reaction which requires a minimum ensemble of two active sites.[18, 53, 184] The increase in linear bound CO suggests that large Pd ensembles are broken up by Au. Although our previous work with neopentane conversion suggests that the active site for hydrogenolysis and isomerization are similar, apparently, the presence of Au does not prevent formation of the transition state for isomerization. This suggests that the hydrogenolysis activity is altered by geometric effects although the overall neopentane conversion activity is not greatly affected.

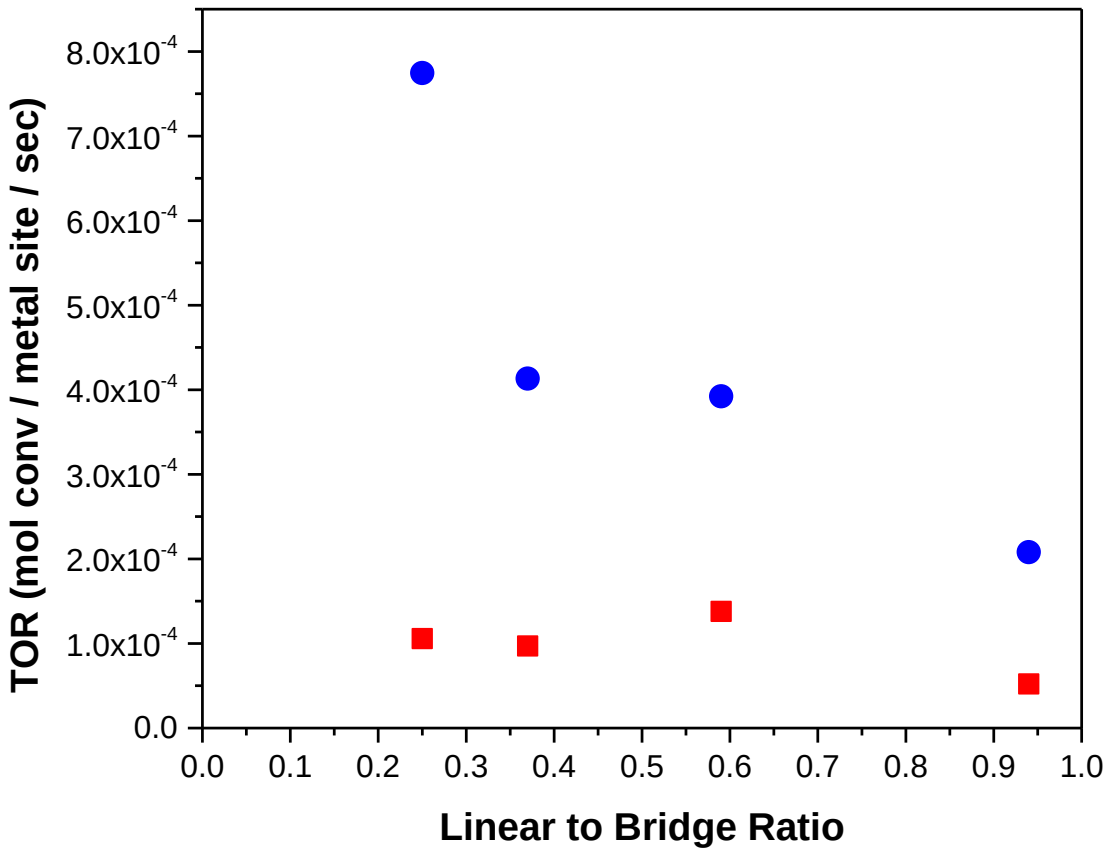

Figure 34: Hydrogenolysis (blue circles) and isomerization (red squares) turnover rate versus the linear to bridge ratio from DRIFTS of CO adsorption

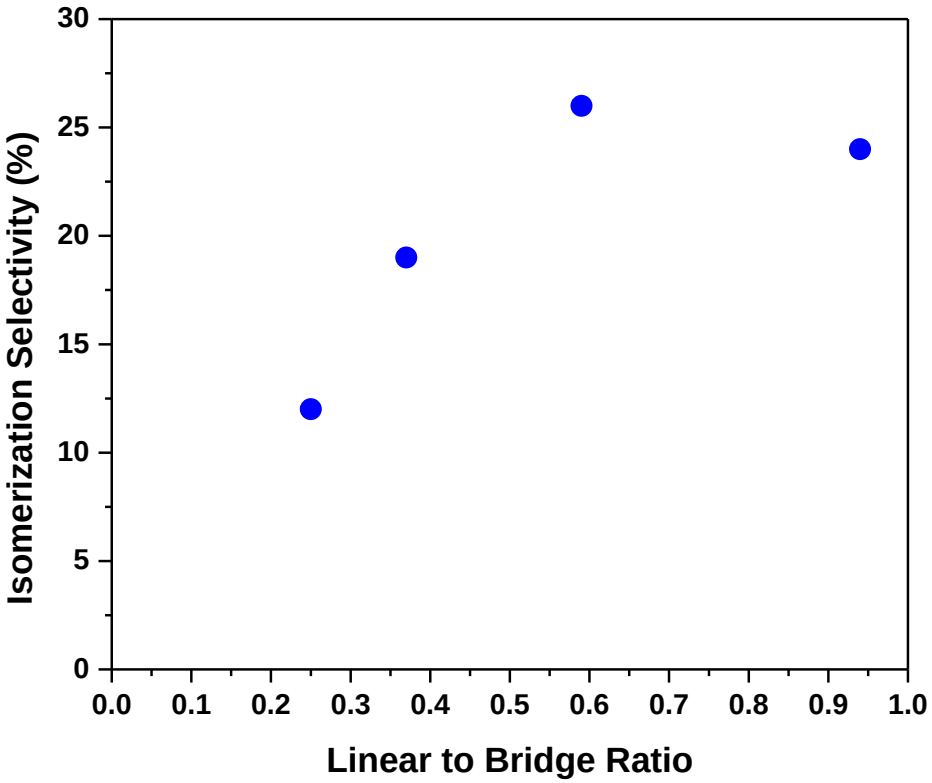

Figure 35: Linear-to-Bridge ratio from DRIFTS of CO adsorption vs. Isomerization selectivity for PdAu catalysts

Figure 35 shows the relationship between neopentane isomerization selectivity compared to the surface structure assessed by DRIFTS. Decreasing bridge bound CO results in an increase of isomerization selectivity but this effect appears to reach a maximum at around 0.55 where the selectivity levels off. This suggests that breaking up large Pd ensembles on the surface is desirable, but limited as an approach to increase isomerization selectivity.

4.5 Conclusion

Alloying palladium with gold on a silica support to form a Au(core)-Pd(shell) nanoparticle improved the neopentane isomerization selectivity compared to a silica-supported monometallic palladium catalyst with a similar particle size. This improvement was more

significant when the Pd shell was influenced by the underlying Au core (i.e., lower Pd weight loading catalysts). As the amount of palladium added to the catalyst increased, the catalytic behavior was similar to monometallic Pd. The turnover rate for hydrogenolysis decreased as the fraction of Au increased which correlated with an increase CO linear-to-bridging ratio as seen in Figure 34. Calorimetry showed that the electronic effect of Au addition lessened with increasing Pd wt%. Although both electronic and geometric effects have been observed, the changes in catalytic performance correlate more with changes in geometry. The identity of the metal atoms in the core of the particle appears to be less significant to catalytic properties than the surface composition and metal atoms near the surface.

5 INTERMETALLIC CATALYSTS: ADDITION OF ZN TO PD AS A DETERRENT FOR HYDROGENOLYSIS

5.1 Introduction

The catalytic performance of metal nanoparticles can be modified by changes in the surface geometry due to modification of the particle size, or changes in the electronic properties by the addition of promoters or alloy formation. Boudart was the first to divide reactions into two groups based on sensitivity of the catalytic activity to particle size.[5] Structure-sensitive reactions are those for which the kinetics is dependent on the particle size (due to changes in the coordination of surface atoms with particle size); while structure-insensitive reactions are independent of the particle size. For structure-sensitive reactions the turnover rate (TOR), or rate per surface atom, changes with size. This geometric effect results because the active site for structure-sensitive reactions requires an ensemble of active atoms and the number of these ensembles changes with particle size. For structure-insensitive reactions, every surface atom is an active site, thus the rate is directly proportional to the dispersion.

Electronic effects alter the chemical reactivity of the metal nanoparticle due to changes in the electronic structure. These two effects are often interrelated as changes in surface geometry often lead to changes in electronic properties. For example, as the size of a metal cluster is reduced, the cluster exhibits quantum confinement effects that perturb the electronic structure and in some cases, can even give rise to a band gap.[185-187] The reduced coordination of the cluster often results in changes in the energy of the valence orbitals that alter the bond strength of adsorbates.[188-190]

Alloying with another metal can also affect the electronic properties of a catalyst.[142] Two effects appear simultaneously when metals are alloyed. First, charge transfer may occur

between the alloying elements due to differences in the level of filling and relative energies of the valence orbitals. Second, changes in hybridization of the bonding between metals may result due to changes in the bond distances between metal atoms. At the same time, the orbital extent or the size of the valence orbitals of the alloying elements is different, resulting in changes in the overlap between the bonding orbitals. Therefore, alloying can result in both electronic effects (degree of charge transfer and hybridization) and geometric effects due to the creation of specific reaction ensembles. Although it is well-known these two aspects of the catalyst are important, it is often unknown whether one factor contributes more than another with respect to selectivity control for a particular reaction. However, understanding which factor is dominant for a particular reaction can be used to design improved catalysts.

Previous work on Pt and Pd catalysts of different particle sizes yielded a correlation between neopentane isomerization selectivity and the initial CO heat of adsorption.[1] Isomerization selectivity increased with decreasing CO heat of adsorption and this correlation appears to be independent of metal, nanoparticle size and the configuration of adsorbed CO. Large Pd particles have primarily bridge-bound CO, while small Pt particles have primarily linear-bound CO, but they have similar catalytic behavior. This provides strong evidence that the selectivity is dependent on electronic effects and the strength of adsorbate chemisorption. Extending this correlation, high selectivity to isomerization should be achieved by materials which bind CO even less strongly than Pt terrace sites. From previous DFT calculations, an intermetallic 1:1 PdZn (111) surface was shown to have a lower CO adsorption energy compared to Pt(111).[191] In addition, experimentally by Sarkany et al. found that the CO heat of adsorption on a PdZn alloy was 67 kJ/mol lower than that of monometallic Pd.[192, 193] Using our correlation between the heat of adsorption and the neopentane isomerization selectivity, it is

anticipated that alloy formation between Pd and Zn would lead to a lower heat of adsorption and also improve neopentane isomerization selectivity.[191]

PdZn alloys have been studied for a number of different reactions, including methanol steam reforming, water-gas shift, alkene hydrogenation and auto-thermal reforming.[168, 192, 194-199] Pd and Zn form a large number of bimetallic structures each with their own unique crystal structure and stoichiometry. At a 1:1 ratio of Pd:Zn, a face centered tetragonal structure forms, which is present for a wide range of Pd compositions (30-70%).[168, 194, 198, 200] Improved selectivity and stability were the main benefits that PdZn catalysts exhibited for these various reactions. These improvements were credited to both geometric changes caused by zinc altering the catalyst surface by expanding the palladium bond distance and electronic effects observed by the weakening of the Pd-CO bond.[168, 193] Chen et al. performed DFT studies on the surface structure of PdZn alloys and found that the (111) surface was the most energetically favorable.[201] Calculations also suggested that the Pd d-band valence width was significantly reduced compared to pure Pd which was linked to improvements in methanol steam reforming performance. Many of these studies used ZnO as a support or supported ZnO, e.g., from a $Zn(NO_3)_2$ precursor, as a source of zinc for alloy formation. PdZn intermetallic structures are typically synthesized with excess zinc and not in nominal molar ratios close to 1:1. Iwasa et al. were unable to form the PdZn intermetallic structure on silica at temperatures up to 700°C due to a lack of zinc reduction in ZnO.[202] Fottinger et al. performed methanol steam reforming over Pd/ZnO catalysts and found that reaction conditions caused PdZn intermetallic formation which resulted in improvements to selectivity.[199] Through *in situ* XAS it was also shown that the PdZn intermetallic structure was also reversible upon exposure to oxygen.

Here we report on the synthesis, characterization and testing of two PdZn nanoparticle catalysts supported on silica with different Pd:Zn molar ratios. The catalysts were characterized by electron microscopy, diffuse-reflectance infrared Fourier transform spectroscopy (DRIFTS) of adsorbed CO, X-ray absorption spectroscopy (XAS), CO chemisorption and isothermal calorimetry. Neopentane hydrogenolysis/isomerization and propane hydrogenolysis/dehydrogenation reactions were used to evaluate the influence of Zn on the hydrogenolysis selectivity of Pd.

5.2 Experimental Methods

5.2.1 Catalyst Synthesis

PdZn bimetallic catalysts supported on silica (Davisil 646 silica gel from Sigma-Aldrich, 300 m^2/g and 1.15 mL/g pore volume) were synthesized by two different synthesis methods – sequential and co-incipient wetness impregnation (co-IWI) under controlled pH conditions.[79, 203] During IWI, the support is contacted with just enough metal-precursor solution to fill the pore volume. All of the metal precursor solution contacts the surface due to the incipient amount of liquid used. Sequential impregnation requires the two metals be added in separate incipient wetness impregnation steps while co-impregnation combines the metals into a single solution. The 2% Pd catalyst was synthesized using a procedure described in previous work.[1]

2%Pd-10%Zn: This catalyst was synthesized by sequential impregnation. Zinc was first added to silica using the IWI method. 18.1 g of $Zn(NO_3)_2 \cdot 6H_2O$ was dissolved in 15 mL of H_2O. 15M NH_4OH was then added to this solution to initially form a white precipitate which dissolved when additional NH_4OH was added bringing the total volume to 50 mL. This solution was added dropwise to 40 g of silica and stirred. The catalyst was dried overnight at 125°C and then calcined at 300°C for 3 hr. Palladium was also added by the IWI method. 2.81 g of 10%

$Pd(NH_3)_4(NO_3)_2$ solution from Aldrich was added dropwise to 5 g of the 10% Zn/SiO_2 catalyst. This catalyst was then dried overnight at 125°C, calcined at 500°C for 3 hr and reduced at 550°C in 4% H_2/He at 30 cc/min for 30 min.

3%Pd-1.8%Zn: The catalyst was synthesized by co-IWI with both zinc and palladium precursors added simultaneously. 0.42 g of $Zn(NO_3)_2 \cdot 6H_2O$ was dissolved in 1.5 mL of 15M NH_4OH and this solution was added to 4.21 g of 10% $Pd(NH_3)_4(NO_3)_2$ solution in H_2O. This solution was then added dropwise to silica (5 g) and mixed between drops. The catalyst was dried overnight at 125°C, calcined at 225°C for 3 hr and then reduced at 300°C at 30 cc/min in 4%H_2/He for 30 min.

5.2.2 STEM

The STEM images were taken at UIC's Research Resources Center facility using the JEOL-ARM 200CF aberration-corrected microscope (70 pm spatial resolution and 300 meV energy resolution). Samples were dispersed in isopropyl alcohol and sonicated for 20 min. A drop of the solution was added to a holey-carbon copper grid and dried under a heat lamp for 20 min. Images were taken using the High Angle Angular Dark Field (HAADF) mode and particle size was counted using the Particule2 program. A minimum of 100 particles were counted to get an accurate representation of the particle size distribution for each catalyst.

5.2.3 X-ray absorption spectroscopy (XAS)

X-ray absorption spectroscopy (XAS) measurements for the Pd K (24350 eV) edge were made on the bending magnet beam line of the Materials Research Collaborative Access Team (MRCAT) at the Advanced Photon Source (APS), Argonne National Laboratory. Measurements

were made in transmission mode. A palladium foil spectrum was acquired through a third ion chamber simultaneously with each measurement for energy calibration.

Samples were prepared by grinding the catalysts into a fine powder and pressing them into the sample holder. The sample holder is a metal cylinder capable of holding up to six individual samples. The sample holder is then placed in a quartz tube with ports containing Kapton windows on each end to flow gases or isolate the sample after treatment. The sample thickness was chosen to give a total absorbance at the Pd K edge between 1-2 absorption lengths and edge steps around 0.3-0.5. The XAS spectra were obtained following reduction at 275°C and 550°C at atmospheric pressure in a 4% H_2/He mixture at 50 cm^3/min flow rate. After reduction, the samples were purged with He at 100 cm^3/min at the reduction temperature and cooled to room temperature in He flow. Trace oxidants in He were removed by passing through a Matheson PUR-Gas Triple Purifier Cartridge containing a Cu trap. All spectra were obtained at room temperature in He.

WINXAS 3.1 software was used to fit the XAS data. The EXAFS coordination parameters were obtained by a least-squares fit in k-space of the k^2- weighted Fourier transform data from 2.6 to 12.1 $Å^{-1}$, and the first shell fit of the magnitude and imaginary parts were performed between 1.6 and 3.0 Å. Because of the limited data range and number of allowed fit parameters of the two-shell fit in the bimetallic nanoparticles, the error in the fits was determined by fixing $\Delta\sigma^2$ at values typical of 2.5-3 nm nanoparticles, that is, 0.001−0.002 greater than metallic foils. The error in N was ±10% and in R was ±0.02 Å, within the typical fitting errors of EXAFS. Fits were performed by altering the coordination number (CN), bond distance (R), σ^2 and energy shift (E_0). The σ^2 value was kept constant through all sample fits and CN and R were allowed to vary in turn to determine the correct fit.

5.2.4 Neopentane Hydrogenolysis and Isomerization

Neopentane hydrogenolysis and isomerization kinetics and selectivity were determined using 0.05-0.15 grams of catalyst diluted with 0.9 grams of silica and loaded into a 0.5" O.D. quartz plug flow reactor. Glass wool was used for the bottom 2 cm of the bed. A 0.5 cm silica layer was placed on top of the glass wool before the catalyst and silica mixture was added to the reactor resulting in a catalyst bed height of 3 cm. The reactor was purged with He for 5 min before each run, and the catalyst was reduced in 4% H_2/He as the temperature was increased to the reaction temperature, 273 ± 2°C. This temperature allowed for all the catalysts to be tested at differential conversion. A K-type thermocouple was inserted from the bottom of the reactor into the lower portion of the catalyst bed. Once the reaction temperature stabilized, the pre-mixed reactant feed gas consisting of 0.35% neopentane and 3.5% H_2 balanced in He was passed through the reactor. The flow rate of the feed gas was varied from 25 to 100 cm^3/min to obtain differential conversions (0.5–6 %). Each flow rate was run for at least one hour to ensure steady-state conversion had been reached. An Agilent 6890N gas chromatograph (J&W Scientific GS-Alumina column) with an FID detector was used to analyze the products and was equipped with a back pressure regulator at the outlet to hold the system at a constant pressure of 9 psig. Each experimental run was completed within six hours for consistency and multiple runs for each catalyst were performed. No appreciable deactivation during neopentane hydrogenolysis was observed in any of the catalysts over this period of time. The maximum relative error of any selectivity measurements was 6%, with most of the data being reproducible within 2%. Turnover rates were calculated based upon the moles of neopentane converted divided by the number of active sites determined by the dispersion calculated from CO chemisorption.

5.2.5 Propane Dehydrogenation

Propane dehydrogenation selectivity and rate were determined using 0.2-0.5 grams of catalyst diluted with 0.9 grams of silica and loaded into the same 0.5" O.D. quartz plug flow reactor used for neopentane hydrogenolysis. The reactor was purged with He for 5 min before each run, and the catalyst was reduced in 4% H_2/He as the temperature was increased to the reaction temperature, 550 ± 2°C. Once the reaction temperature stabilized, the pre-mixed reactant feed gas consisting of 2% propane and balance Ar was passed through the reactor. The flow rate of the feed gas was set to 50 cm^3/min and held constant throughout the test so that the deactivation of each catalyst could be determined. The test was run until a steady-state conversion was reached. Each experimental run was completed within six hours for consistency and multiple runs for each catalyst were performed. The maximum relative error of any selectivity measurements was 6%, with most of the data being reproducible within 2%.

5.2.6 Diffuse Reflectance Infrared Fourier Transform Spectroscopy (DRIFTS)

Infrared spectra were obtained using a Thermo Scientific Nicolet 6700 FTIR spectrometer equipped with a Harrick Scientific Praying Mantis diffuse reflectance *in*-situ cell at the Northwestern Clean Catalysis (CleanCat) Core Facility. Samples were ground to a fine powder using a mortar and pestle, and packed into the sample chamber to create a uniform surface. The chamber was purged with Ar, and then the gas was switched to 10% H_2/N_2 and the temperature was raised to 250°C and held for 15 min. After reduction of the catalyst, the gas was switched back to Ar and the temperature was reduced to 25°C. A background scan was then recorded, which was averaged over 100 scans (2 minute observation time) with 4 cm^{-1} resolution. The sample was then exposed to 1.02% CO/N_2 and another scan was taken once equilibrium was reached, at which point the flow was changed back to Ar and a final scan was taken once the

intensity of the adsorbed CO peak was invariant with time. The linear to bridge-bound ratios reported here do not take into account the differences in extinction coefficients between the adsorption sites and therefore do not represent quantitative coverages, but rather reflect qualitative differences between catalysts.[167]

5.2.7 CO Heats of Adsorption

Determination of the initial heat of adsorption of carbon monoxide on the two Pd-Zn catalysts (60-70 mg) reduced at two different temperatures (300 and 550°C) was conducted utilizing a Setaram Sensys EVO differential scanning calorimetry interfaced with a plug-flow reactor. The plug-flow reactor was connected to a mass spectrometer. After reduction at the specified temperature in 5.11% H_2/Ar (both gases 99.999%) for 2 hr, the catalyst was cooled down to 35°C in the same gas, and the catalyst was exposed to a mixture of 1% CO (99.999% research grade) in He (99.9999%, research grade) pulsed into the 5% H_2/Ar stream from a ten-way switching value with a 1000 µL sample loop. The number of moles of CO per pulse calculated from the ideal gas law was ~4×10^{-4} mmol. Twenty pulses of carbon monoxide were employed; the initial heat of adsorption was determined by only considering injections in which the entire pulse of carbon monoxide was consumed. The 3Pd-1.8Zn/SiO_2 adsorbed entirely 5-6 pulses depending on the reduction temperature, while the 2Pd-10Zn/SiO_2 adsorbed entirely ~1 pulse of carbon monoxide.

5.2.8 CO chemisorption

The CO chemisorption measurements were conducted at the Northwestern University Clean Catalysis (CleanCat) Core Facility using an Altamira Instruments AMI-200. Catalysts (0.05-0.2 g) were loaded into a U-shaped quartz reactor tube, which was weighed before and after sample addition to ensure an accurate weight measurement. The loaded tube was then

loaded into the furnace and the catalysts were reduced in H_2/Ar at 300°C or 550°C for 2 hr (10°C/min ramp rate) and then flushed for 30 min in He. Using a six-way valve, 5% CO/He was then pulsed (595 μL loop volume) into the system 15 times at 30°C to ensure the surface was saturated. Each pulse peak was integrated to find the volume of CO remaining following adsorption. Surface saturation was typically reached within 10 pulses. The dispersion determined by CO chemisorption also included average stoichiometric factor determined from the uncorrected DRIFTS linear-to-bridging ratios for each catalyst. CO bound linearly account for one CO molecule per surface atom while bridge bound CO implies there is one CO molecule per two surface atoms. The equation used to get the dispersion is given below.

$$Dispersion = \frac{mol\ CO\ adsorbed}{mol\ metal} \times ((linear\ CO\ fraction\ \times 1) + (bridge\ CO\ fraction\ \times 2))$$

5.3 Results

5.3.1 Particle Size Analysis

STEM imaging was used to determine metal nanoparticle size. A representative STEM image for the 3%Pd-1.8%Zn catalyst and corresponding size distribution are shown in Figure 36. The particle sizes for the three catalysts tested are reported in Table X and show that the average particle sizes are similar. The 3%Pd-1.8%Zn catalyst was also reduced at the propane dehydrogenation reaction temperature (550°C) to determine if any sintering occurred. The particle size did not appreciably change, between the two temperatures. Having similar particle sizes between catalysts enables the changes caused by alloying to be studied without having to account for changes in particle size which are known to alter the kinetics of structure-sensitive reactions. From our previous studies, there are results for similar sized monometallic Pd catalysts for comparison with these PdZn bimetallic catalysts.[1]

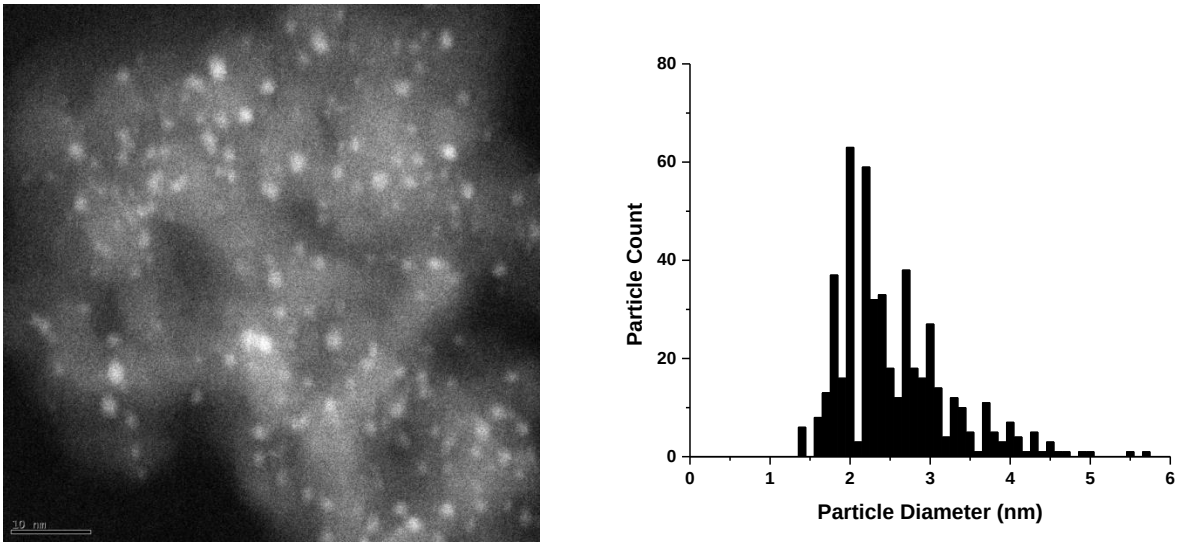

Figure 36: 3%Pd-1.8%Zn sample image and particle size distribution determined by STEM

Table X: Particle sizes determined by STEM

Sample	Particle Size by STEM (nm)
2%Pd	2.5 ± 1.1
2%Pd-10%Zn 300°C	2.2 ± 0.8
3%Pd-1.8%Zn 300°C	2.7 ± 0.8
3%Pd-1.8%Zn 550°C	2.6 ± 0.7

5.3.2 XAS

Extended X-ray absorption fine structure (EXAFS) and X-ray absorption near-edge (XANES) spectra were gathered for each catalyst following reduction at 275°C and fitting done to determine bond distances and coordination numbers (CN). The XANES spectra are shown in Figure 37a and an expanded view to the leading edge is shown in Figure 37b. XANES were analyzed to determine the Pd K-edge position of each catalyst and evaluate the oxidation state of

palladium. The edge energy is defined as the inflection point of the leading edge and is determined by taking the maximum of first derivative of the spectra in Figure 37a. The edge energy for all three catalysts is summarized in Table XI. A K-edge energy of 24.350 keV corresponds to metallic Pd and the PdZn catalysts are slightly shifted as seen in Figure 37b (to 24.349 keV) from Pd which is consistent with the presence of bimetallic nanoparticles.[142] The intensity of the first absorption peaks are similar indicating that the palladium is metallic rather than oxidized which would cause the peak intensity to increase. The small differences in the spectra following the first peak, changes in intensities and peak shifts, also indicate that non-Pd neighbors are near to Pd.

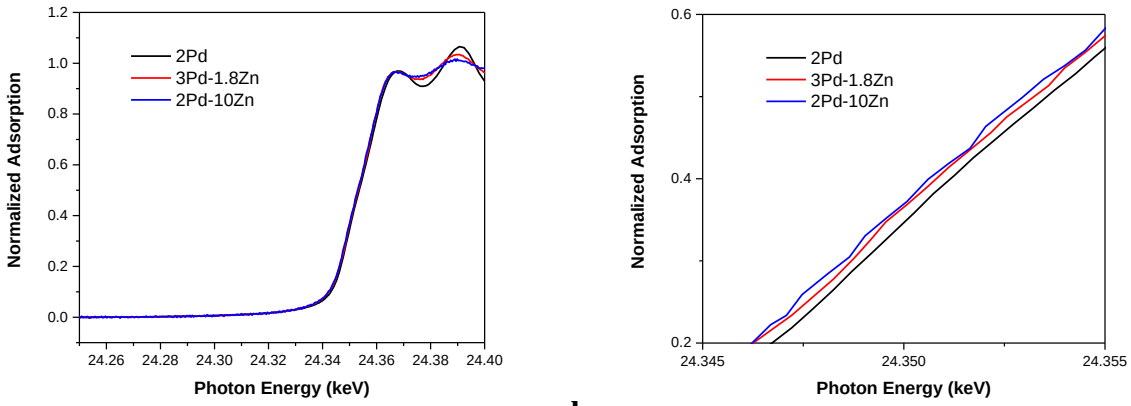

Figure 37: Pd XANES K-edge spectra for catalysts reduced at 275°C a. full edge b. Expanded view of the leading edge of the XANES near the inflection point

Figure 38 shows the EXAFS spectra for the Pd foil reference and all three catalysts reduced at 275°C, and Table XI summarizes the parameters calculated from the fitting of the spectra. Coordination numbers and bond distances were determined by fitting the magnitude and imaginary parts of the Fourier transform of the k^2-weighted first shell spectra. Although the total coordination numbers for each of the samples are identical, the identity of the neighbors and their

distances change between the three catalysts. The monometallic Pd catalyst shows two prominent peaks at 2.05 and 2.50 Å (phase uncorrected distances) at a ratio of 2:1, typical of metallic Pd and also observed for the Pd foil spectra seen in Figure 38a.[168] The Pd-Pd bond distance of 2.75 Å in Table XI also corresponds to metallic Pd. Figure 38b shows both bimetallic PdZn catalysts; the 3%Pd-1.8%Zn spectra looks similar to metallic Pd, however, a change in the peak ratio to 1.45:1 is consistent with a small number of non-Pd scattering atoms. The fit confirms there are Pd-Zn bonds with a coordination number of 2.3 and a bond distance of 2.56 Å. The coordination number for the Pd-Pd scatters is 5.3 with a bond distance of 2.73 Å (similar to metallic Pd). The differences in the coordination numbers between the Pd-Pd and Pd-Zn scatterers indicate that the majority of the palladium atoms in this catalyst are still surrounded by other palladium atoms with a few Zn neighbors. The 2%Pd-10%Zn catalyst also has two prominent peaks, but these peaks deviate from the pure Pd spectra significantly. Although the peak positions are similar, the ratio of the peaks has changed, suggesting that the bonding environment of Pd has changed with the addition of zinc . The fits in Table XI confirm this shift from Pd-rich particles to a catalyst with significant interaction between Pd and Zn as the Pd-Zn coordination number increases to 5.3 and the Pd-Pd coordination number decreases to 2.7. The bond distances have not changed significantly in the two Pd-Zn catalysts and these bond distances are also similar to those found in the literature.[168] Although the average coordination environment in these catalysts is different, EXAFS is a bulk characterization technique, therefore the surface composition and structure, which is responsible for the catalytic activity, is uncertain.

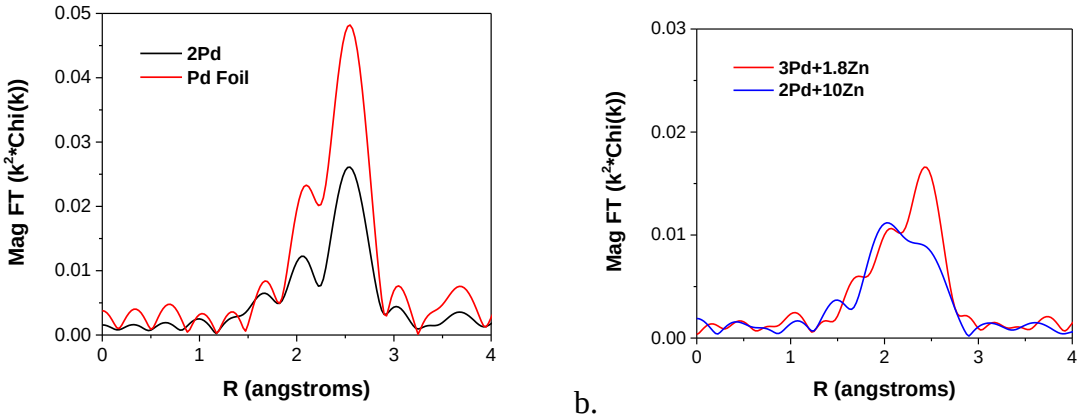

a. b.

Figure 38: Pd K-edge spectra and fitting parameters following 275°C reduction a. 2%Pd (black) and Pd foil (red) and b. 3%Pd-1.8%Zn (red) and 2%Pd-10%Zn (blue)

Table XI: XANES and EXAFS fitting parameters following 275°C reduction

Catalyst	Edge Energy (keV)		Coordination Number	Bond Distance (Å)
2Pd	24.3500	Pd-Pd	7.5	2.75
		Pd-Zn	---	---
3Pd-1.8Zn	24.3496	Pd-Pd	5.3	2.73
		Pd-Zn	2.3	2.56
2Pd-10Zn	24.3494	Pd-Pd	2.7	2.72
		Pd-Zn	5.2	2.56

5.3.3 Diffuse Reflectance Infrared Fourier Transform Spectroscopy (DRIFTS)

DRIFTS of CO adsorption was used to evaluate changes in surface composition and structure of the catalysts. Figure 39 shows the DRIFTS spectra for the PdZn catalysts as well as the monometallic Pd catalyst with a similar particle size. Bridge-bound CO has previously been assigned to the peaks in the range of 1800-2000 cm^{-1}. Within this range, peaks between 1800 and 1900 cm^{-1} are attributed to CO bridge-bound on terrace and hollow sites; while, peaks

between 1900 and 2000 cm^{-1} are assigned to CO bridge-bound to corner and edge sites.[170, 171] Linear bound CO is characterized by two peaks typically appearing around 2080 and 2050 cm^{-1} which Lennon et al. have assigned to corner and edge adsorption sites respectively.[170]

The 2%Pd catalyst, with an average particle size of 2.5 nm, has one very prominent bridge-bound CO peak at 1936 cm^{-1}, a shoulder centered around 1835 cm^{-1}, and one linear CO peak at 2084 cm^{-1}. The presence of two bridge-bound CO peaks is typical of pure Pd catalysts.[170, 171] The 3%Pd-1.8%Zn catalyst has one bridge-bound CO peak located at 1975 cm^{-1}. The loss of the bridge-bound CO peak around 1835 cm^{-1} peak suggests zinc breaks up palladium terraces on the surface typically responsible for bridge bound CO. Since the tail of the peak extends into the terrace site range, there may be a small percentage of Pd ensembles remaining. The shift of the linear peak to 2075 cm^{-1} from 2084 cm^{-1} indicates there is a small fraction of CO linearly bound to edge sites since most is still bound to corner sites. These shifts have also been reported for other PdZn catalysts.[168, 204] The 2%Pd-10%Zn catalyst has a small bridge-bound CO peak at 1960 cm^{-1} corresponding to corner and edge sites. The peak position has shifted from the other PdZn catalyst; however, it is still in the range of bridge-bound CO on corner and edge sites and there are no longer peaks for CO in the terrace region. The linear region has two distinct peaks at 2080 cm^{-1} and 2050 cm^{-1} which indicates that CO is linearly bound to edge sites as well as corner sites suggesting further zinc addition continues to reduce the number of surface palladium ensemble sites. Two peaks in the linear region have also been observed for PdZn catalysts.[168]

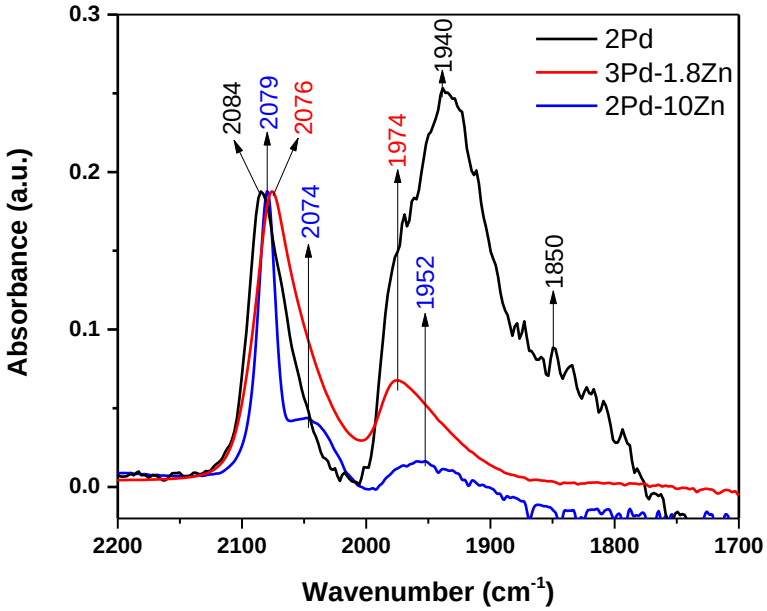

Figure 39: Normalized DRIFTS spectra of CO adsorption on: 2%Pd (red), 2%Pd-10%Zn (blue) and 3%Pd-1.8%Zn (black) reduced at 250°C

The linear to bridge bound ratio calculated by comparing the raw areas of the different peaks, are presented in Table XII. The addition of zinc causes a dramatic shift in the CO adsorption resulting in greatly reduced concentration of bridge-bound CO. While the monometallic Pd catalyst has mostly bridge-bound CO, the addition of zinc causes a significant increase in linear-bound CO. The addition of excess zinc in the 2%Pd-10%Zn catalyst leads to a minor increase in the overall ratio of linear-to-bridge bound CO (2.5:1) compared to the lower Zn sample (2.1:1), but there are differences in the peak positions as discussed previously. The shift in the linear-to-bridge ratio indicates that zinc breaks up palladium ensembles on the surface and decreases the number of Pd ensemble sites capable of adsorbing bridge bound CO. Weilach et al. used DFT to study CO adsorption on PdZn surfaces and found that adsorption on top sites was preferred on the intermetallic surface past ½ ML CO coverage.[205]

5.3.4 Heat of Adsorption of CO Determined by Isothermal Calorimetry

The initial heat of adsorption determined previously for a pair of Pd/SiO_2 catalysts with a mean TEM particle size of 2.5-3 nm was ~ 130 kJ mol^{-1}.[1] The heat of CO adsorption on Pd was previously determined for the catalysts reduced in H_2, evacuated at the reduction temperature, followed by cooling in an inert gas to the adsorption temperature (35°C). In the previous work, the differential (initial) heat of adsorption was determined using a volumetric adsorption instrument (Micromeritics ASAP 2020C) interfaced with a Setaram Sensys EVO differential scanning calorimeter. For the Pd-Zn catalysts studied in this work, calorimetric measurements of CO adsorption led to abnormally large heat flow which was associated with the oxidation of CO by small quantities of oxygen in He (99.999% UHP) led to the oxidation of CO. Enthalpy measurements in He were unreliable since the oxidation reaction is highly exothermic and contributed significantly to the measured heat. All attempts to eliminate the CO oxidation reaction were unsuccessful including utilizing a CO/He mixture containing research grade He (99.9999%). As a result, the PdZn bimetallic catalysts were cooled in a 5% H_2/Ar mixture to the adsorption temperature of 35°C. Due to the small particle size and alloy formation with Zn, the formation of a hydride is not expected, but there will be an adsorbed layer of hydrogen on the surface of these PdZn catalysts.[206-209] Chemisorbed hydrogen will lower the heat of adsorption compared to an adsorbate-free surface of Pd.[175] The results in Table XII also show that increasing reduction temperature slightly lowered the heat of adsorption. The monometallic Pd catalyst was measured using the same procedure to allow for comparison of the heat of adsorption values.

Table XII: Initial Heat of CO Adsorption Values (± 5 kJ/mol) in the presence of chemisorbed hydrogen and Linear-to-Bridge ratios from DRIFTS.

Sample[a]	Reduction Temperature (°C)	CO (initial) heat of adsorption with chemisorbed H (kJ/mol CO)[b]	Linear to Bridge Ratio
2Pd/SiO_2[c]	225	92	0.2 : 1
2Pd-10Zn/SiO_2	300	102	2.5 : 1
3Pd-1.8Zn/SiO_2	300	99	2.1 : 1
	550	93	1.8 : 1

[a]Catalysts were initially reduced under 5.11% H_2/Ar (both gases, 99.999% UHP) for 2 h at the specified reduction temperature, followed by subsequent cooling in H_2.
[b]Initial heat of CO adsorption determined by microcalorimetry on a reduced Pd or PdZn surface containing chemisorbed hydrogen.
[c]Monometallic Pd catalyst from previous work studied using the modified procedure

5.3.5 Neopentane Isomerization and Hydrogenolysis

Neopentane conversion was conducted at 273 ± 2°C, 9 psig and varying flow rates in order to vary conversion within range of differential conversion (< 10%). There are two possible reaction pathways: hydrogenolysis and isomerization. Isomerization products include isopentane produced from an initial isomerization reaction and n-pentane if isopentane undergoes a second isomerization reaction before desorption from the surface. A single hydrogenolysis reaction will produce isobutane and methane, and any subsequent steps will produce additional methane and lighter hydrocarbons (propane and ethane). All selectivities given in Table XIII are extrapolated to 0% conversion. Calculated turnover rates (TOR) using the same method described previously are also given in Table XIII.[1] Products with non-zero selectivity at 0% conversion are considered primary products while products that have 0% selectivity are considered to be secondary products.[179] The isomerization selectivity is defined as the selectivity to isopentane and hydrogenolysis products are any molecule lower than C_5 shown in the Table XIII. The 2%Pd catalyst has an isomerization and hydrogenolysis selectivity of 9% and 91%, respectively.

The 3%Pd-1.8%Zn catalyst has a similar isomerization selectivity (13%) and hydrogenolysis selectivity (87%). The product distributions are also similar for the various hydrogenolysis products. If a single hydrogenolysis event occurs per converted neopentane molecule, equal amounts of methane and isobutane should be identified in the product distribution. An excess of methane can be seen for both catalysts in Table XIII which indicates that further hydrogenolysis is occurring, as evidenced by the presence of small amounts of ethane and propane at 0% conversion.

Since zinc does not adsorb CO, the amount of surface palladium was determined by chemisorption and used to calculate the TOR values in Table XIII.[210-212] Despite the similar selectivity distribution and particle size, the TOR of 3%Pd-1.8%Zn is an order of magnitude lower than that of the 2%Pd catalyst. The 2%Pd-10%Zn catalyst had negligible activity for neopentane conversion despite reduced palladium on the nanoparticle surface as observed by DRIFTS, CO chemisorption and calorimetry.

Table XIII: Neopentane hydrogenolysis TOF and product selectivity data

Catalyst	Dispersion (by CO chemisorption)	TOR (mol conv / metal site / s)	Initial Product Distribution (%)					
			CH_4	C_2H_6	C_3H_8	n-C_4H_{10}	i-C_4H_{10}	i-C_5H_{12}
2%Pd	0.23	1.0×10^{-3}	49	1	5	2	33	9
3%Pd-1.8%Zn	0.35	1.3×10^{-4}	46	1	5	2	32	13
2%Pd-10%Zn	0.12	0	No measurable products					

5.3.6 Propane Dehydrogenation

The catalysts were also evaluated for propane dehydrogenation at 550°C. In addition to propane dehydrogenation to form propylene, hydrogenolysis may also occur under these

conditions producing methane and ethylene. The latter hydrogenolysis product can also be hydrogenated to ethane. In order determine differences in catalyst performance, all catalysts are compared at a similar level of conversion. The product selectivities in Table XIV are all reported at a propane conversion of 15%. The 2%Pd catalyst has a propylene selectivity of 11% and an overall hydrogenolysis selectivity of 89%. Within the hydrogenolysis product distribution, the selectivity to methane is 75%, 8% to ethylene and the remainder (6%) to ethane. The high hydrogenolysis selectivity is consistent with the results for neopentane.

The two PdZn catalysts have a similar dehydrogenation selectivity of 98%. The very low propane hydrogenolysis selectivity of 2%Pd-10%Zn is consistent with the low selectivity for hydrogenolysis of neopentane; however, the low hydrogenolysis selectivity of 3%Pd-1.8%Zn differs from the selectivity measured during neopentane conversion on the same catalyst. The selectivity for dehydrogenation over both PdZn catalysts is comparable to those reported for PtSn catalysts and chromia catalysts, the two industry standard catalysts.[64, 75-77, 213]

Table XIV: Propane dehydrogenation product selectivity data

Catalyst	**Dispersion (by CO chemisorption)**	**Product Distribution at 15% conversion (%)**			
		CH_4	**C_2H_6**	**C_2H_4**	**C_3H_6**
2Pd	0.23	75	6.3	8.1	10.7
3Pd-1.8Zn	0.27	0.3	0	1.7	98.3
2Pd-10Zn	0.08	1.2	0	0.7	98.4

Although both PdZn catalysts have similar selectivity, there are some differences in their time-on-stream performance (Figure 40a). The 2%Pd catalyst begins with an initial conversion of 54%, but deactivates to 2% conversion within one hour. The 2%Pd-10%Zn (35%) and 3%Pd-1.8%Zn (31%) catalysts start with lower initial conversions and deactivate to a steady-state conversion of 7% and 15%, respectively. Propane dehydrogenation is an endothermic reaction and equilibrium-limited to a conversion of 40% at 550°C.[64] The high conversion observed initially for Pd and 3%Pd-1.8%Zn are a result of the hydrogenolysis pathway; while the steady-state conversion for dehydrogenation are below the equilibrium conversion.

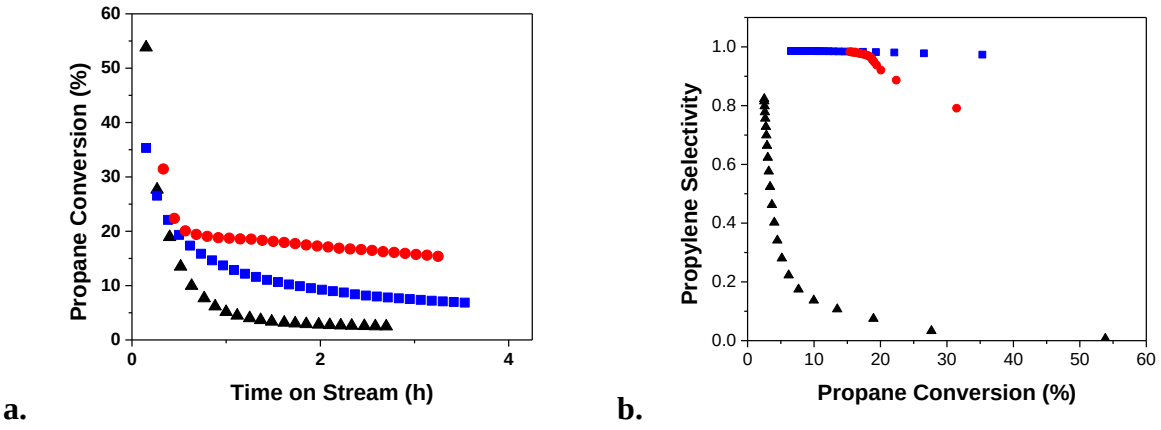

a. **b.**

Figure 40: Plots of a) Propane dehydrogenation conversion vs. time and b) propylene selectivity vs. propane conversion for the 2%Pd (black triangles), 2%Pd-10%Zn (blue squares) and 3%Pd-1.8%Zn (red circles)

Figure 40b shows the change in propylene selectivity vs. conversion. At high conversion, which also corresponds to early time-on-stream, the 2%Pd catalyst has low selectivity to propylene (0%) and methane is the most abundant product. The selectivity improves as the catalyst deactivates; although the 2%Pd catalyst doesn't begin to improve until about 10%

conversion. The 2%Pd-10%Zn catalyst had stable propylene selectivity at 98% while the 3%Pd-1.8%Zn catalyst increases in propylene selectivity from 79% as the conversion decreases..

The 3%Pd-1.8%Zn catalyst has a low selectivity towards propane hydrogenolysis at 550°C, which is in contrast to the high selectivity to hydrogenolysis for neopentane at 275°C. This difference in selectivity suggests a change in the surface composition may be occurring between these two reaction temperatures. Additional characterization was done after reduction at this elevated temperature in order to evaluate these changes. The XANES spectra (not shown) do not indicate any change in Pd K-edge energy position but there are small changes in the peaks following the edge, consistent with a change in the nearest neighbors to Pd.

Figure 41 shows the differences in the magnitude of the Fourier transform of the EXAFS region of the XAS spectra taken at both reaction temperatures (275 and 550 °C) for the two PdZn catalysts. The EXAFS of the 3%Pd-1.8%Zn catalyst shown in Figure 41a undergoes a change in the EXAFS from a Pd-rich PdZn bimetallic catalyst to one that looks similar to the 2%Pd-10%Zn catalyst reduced at 275°C, i.e., a structure with an increased number of Pd-Zn bonds. The fits in Table XV confirm the number of Pd-Pd scatters decreases form 5.3 to 2.7 and the number of Pd-Zn increases from 2.3 to 4.9 with increasing reduction temperature. After high temperature reduction, the structure of the metallic nanoparticles on the 3%Pd-1.8%Zn catalyst have very similar composition to those on the 2%Pd-10%Zn catalyst reduced at 275°C. Figure 41b also shows a change in the composition of the 2%Pd-10%Zn nanoparticles reduced at 550°C with the appearance of a single peak centered at 2.19 Å (phase uncorrected distance). This single peak spectrum is characteristic of a PdZn intermetallic alloy.[168, 200] The coordination numbers and bond distances given in Table XV show a majority of Pd-M scatterers in the catalyst are now Pd-Zn interactions and the Pd-Pd bond increases from 2.75 Å to 2.84 Å. A

similar change in EXAFS has been observed in the literature which used increasing amounts of Zn to form the intermetallic structure.[168, 214] After high temperature reduction, the structure of the 2%Pd-10%Zn nanoparticles are similar to that of a 1:1 PdZn intermetallic alloy.[168]

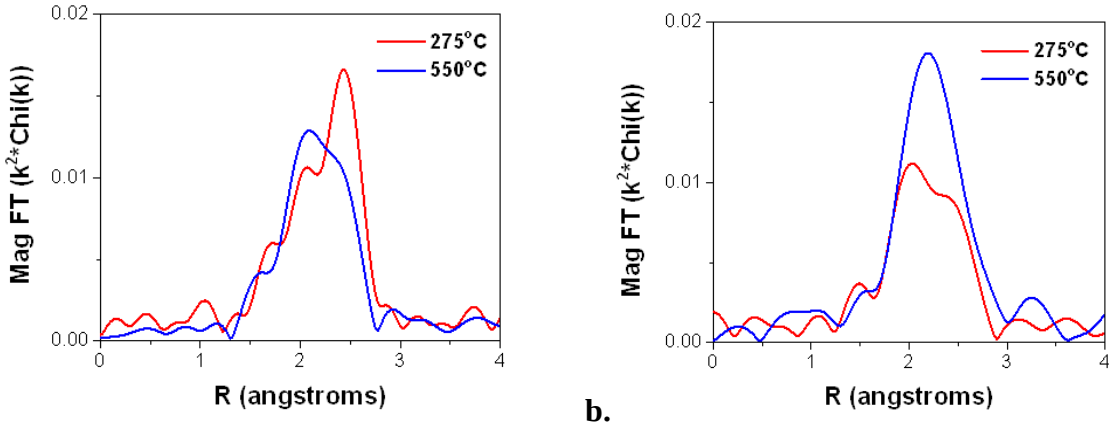

Figure 41: EXAFS spectra following reduction at both reaction temperatures 275°C (red) and 550°C (blue) of a. 3%Pd-1.8%Zn and b. 2%Pd-10%Zn (right plot)

Table XV: EXAFS fitting parameters after reduction 550°C for both PdZn catalysts

Catalyst	Edge Energy (keV)		Coordination Number	Bond Distance (Å)
3Pd-1.8Zn	24.3495	**Pd-Pd**	2.7	2.72
		Pd-Zn	4.9	2.56
2Pd-10Zn	24.3492	**Pd-Pd**	2.6	2.84
		Pd-Zn	8.0	2.57

DRIFTS of the 3%Pd-1.8%Zn catalyst pre-reduced at 300 and 550°C is shown in Figure 42. The linear CO peak shifts from 2075 cm^{-1} to 2070 cm^{-1} at the higher reduction temperature which indicates a slight increase in linear-bound CO at edge sites. The bridge-bound CO peak also shifts when the reduction temperature is increased from 1975 cm^{-1} to 1965 cm^{-1} and the peak broadens. There is also a shift in the linear CO peak which brings the peak position in line with

the linear CO peak of the 2%Pd-10%Zn spectra seen in Figure 39. The overall linear-to-bridge ratio calculated from the areas of each peak did not change significantly at the higher reduction temperature, from 2.1:1 at 275°C to 1.8:1 at 550°C.

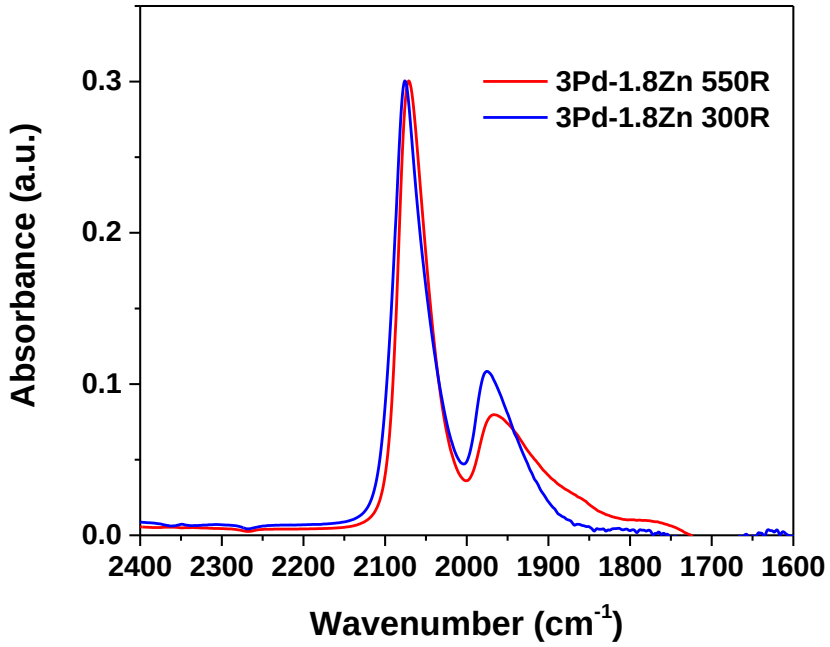

Figure 42: Normalized DRIFTS spectra taken of the 3%Pd-1.8%Zn catalyst pre-reduced at 300°C (red) and 550°C (blue)

5.4 Discussion

The 2%Pd catalyst had a high hydrogenolysis selectivity during neopentane (91%) and propane (89%) conversion. Results for both reactions were expected as palladium is well-known to have high hydrogenolysis selectivity.[1, 18, 47, 133, 215-217] For propane, the initial conversion of a 2%Pd catalyst is high, but deactivates quickly due to coking (Figure 40) with high selectivity to methane during this period. Pd ensemble sites, as evidenced by bridge-bound CO, promote hydrogenolysis and coking reactions, rather than dehydrogenation of propane.

While the Pd catalyst performed as expected, the 2%Pd-10%Zn PdZn catalyst exhibited behavior not characteristic of monometallic Pd. It proved to be unreactive toward neopentane despite evidence for the presence of surface (metallic) Pd. Although the PdZn intermetallic alloy was inactive for neopentane conversion, it was highly active for propane dehydrogenation with high propylene selectivity and stability. From Table XIV, propane dehydrogenation is a structure-insensitive reaction and the high selectivity results from the ability to catalyze dehydrogenation but not the structure-sensitive propane hydrogenolysis reaction.

The EXAFS and IR spectra are consistent with the formation of a PdZn intermetallic alloy. The changes in performance are likely related to differences in the surface structure of Pd and PdZn, i.e., geometric effects. Hydrogenolysis is a well-known example of a structure-sensitive reaction, where a certain ensemble size or geometry is required for the reaction to occur.[18, 52, 53, 218] From previous literature, it has been proposed that the hydrogenolysis pathway requires a minimum of two active sites.[48, 52, 53] Figure 43 shows the structure and bond distances for the bulk PdZn intermetallic alloy. In this intermetallic composition, Pd has only Zn neighbors and the Pd-Pd bond distance is 0.15 Å larger than in monometallic Pd nanoparticles. In the ideal structure there are no Pd ensemble sites since Pd atoms are at a non-bonding distance. The lack of adjacent Pd atoms results in no catalytic activity for neopentane conversion. While hydrogenolysis is a well-known structure-sensitive reaction, the lack of neopentane isomerization suggests this is also a structure-sensitive reaction. This conclusion is consistent with the mechanism postulated by Anderson and Avery where neopentane isomerization requires ensembles with more than one attachment point for the neopentane molecule.[55]

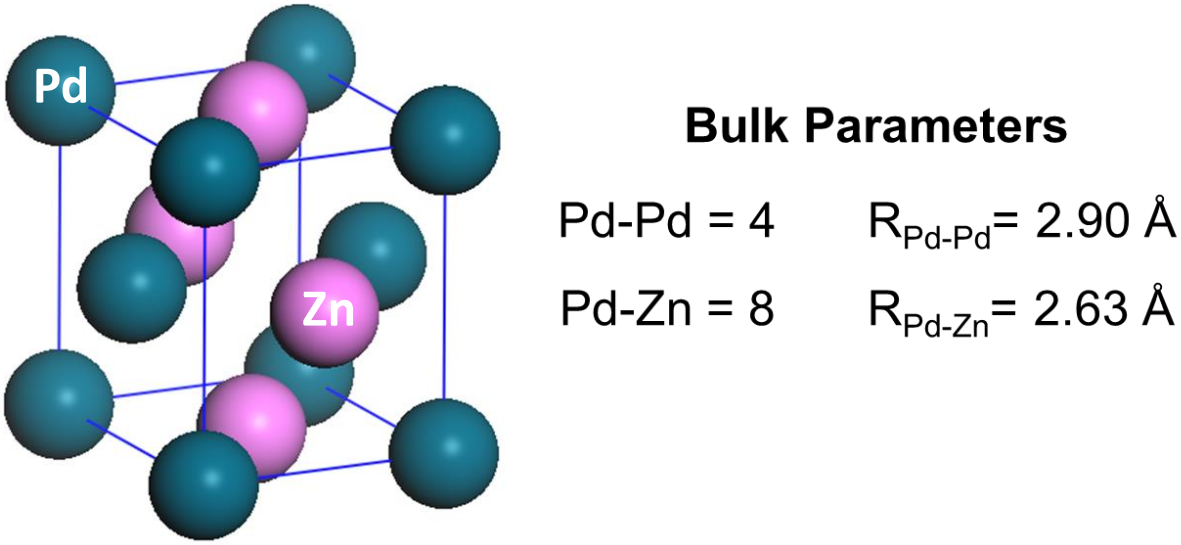

Figure 43: Structure of PdZn intermetallic alloy, coordination numbers and bond distances of the bulk alloy. Pd atoms are blue and Zn atoms are purple.

For the 3%Pd-1.8%Zn catalyst reduced at low temperature, the selectivity during neopentane conversion is very similar to monometallic Pd nanoparticles. The lack of significant change in neopentane selectivity suggests there are active Pd ensembles similar to those in the Pd nanoparticles. While the selectivity is similar, the TOR of 3%Pd-1.8% Zn is 10 times lower than that of Pd. If the surface of the 3%Pd-1.8% Zn is high fraction of (unreactive) ordered PdZn intermetallic alloy and a small fraction of the surface covered with Pd ensemble sites, then the IR would look very similar to the 2%Pd-10%Zn catalyst, and the selectivity would look similar to that of Pd, but with a reduced TOR. This also implies that even when there is a small amount of reduced Zn, i.e., at low temperature, the surface layer forms an ordered PdZn intermetallic alloy leading to isolation of the active Pd atoms. This geometric effect is primarily responsible for the changes in catalytic performance.

For propane dehydrogenation, it might be expected that the Pd and 3%Pd-1.8%Zn catalysts would have similar catalytic performance; however, the latter has high propylene selectivity with little hydrogenolysis selectivity similar to that of the 2%Pd-10%Zn catalyst. The EXAFS shows there is an increase in the number of PdZn neighbors while there is only a small increase in the linear-to-bridge ratio of adsorbed CO, which indicates a change in the structure of the bimetallic nanoparticle at elevated temperatures. The high propylene selectivity similar to the intermetallic catalyst suggests there are very few Pd ensembles left on the surface. In order to verify this conclusion, the 3%Pd-1.8%Zn catalyst was first reduced at 550°C and reactions of neopentane at 275°C were conducted. Although the catalyst was active after reduction at low temperature, there is no neopentane conversion after reduction at high temperature.

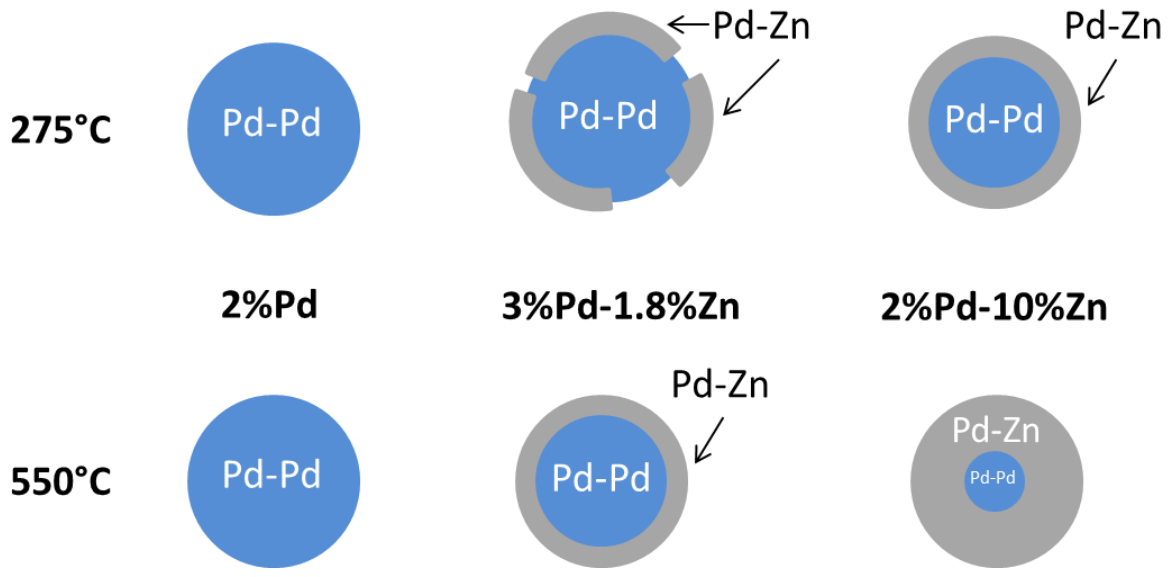

Figure 44: Simplified cross section of Pd and PdZn catalysts showing structure change as reduction temperature increased

The above results are summarized by the scheme shown in Figure 44. The structure of the 3%Pd-1.8%Zn catalyst reduced at 275°C has a Pd core with a small number of surface Zn (metallic) atoms. The high ratio of linear-bound CO peaks in the DRIFTS suggests that this

PdZn film has an intermetallic alloy structure. The catalytic performance suggests that approximately 90% of the surface is the Pd-Zn alloy with the remaining 10% of the surface consisting of Pd ensembles. At 550°C, there is an increase in the surface coverage of the PdZn intermetallic alloy with few remaining Pd ensembles, although the nanoparticle core is still Pd-rich.[219] The inability to form a fully intermetallic PdZn alloy nanoparticle is due to a limited amount of Zn interacting with the Pd. Datye et al. and van Bokhoven et al. have also shown that PdZn intermetallic formation increases with reduction temperature.[214, 220]

For the 3%Pd-1.8%Zn catalyst, there is a high surface coverage of the PdZn alloy with a Pd-rich core at 275°C. For both Pd-Zn catalysts, it appears that even under conditions which lead to a small amount of reduced Zn, the PdZn surface forms an ordered alloy structure rather than a random distribution of metallic Pd and Zn surface atoms. At 550°C, there is little change in the IR spectra, but the EXAFS shows an increase in the number of PdZn bonds with near complete formation of the PdZn alloy nanoparticles. For each PdZn catalyst with complete surface coverage of the PdZn intermetallic alloy, the isolated Pd atoms are active for structure-insensitive reactions, but are inactive for structure-sensitive reactions. The large change in catalytic performance is due to a geometric effect, i.e., isolation of the active Pd atoms, rather than an electronic effect due to alloy formation.

5.5 Conclusion

Bimetallic PdZn on silica catalysts can form an intermetallic alloy with isolated active palladium atoms. At low reduction temperature and with limited amounts of zinc near the Pd nanoparticles, there are small regions of the surface with Pd ensembles and catalytic selectivity similar to that of monometallic Pd. At higher Zn loadings, or higher reduction temperatures, the PdZn nanoparticle surface is fully covered by the PdZn alloy, which is inactive for structure-

sensitive reactions like neopentane hydrogenolysis/isomerization and propane hydrogenolysis. The PdZn intermetallic surface alloy, however, has high catalytic activity for structure-insensitive reactions like propane dehydrogenation. The high propane dehydrogenation to propylene selectivity results from the geometric isolation of the active Pd atoms, which have only metallic Zn neighbors. From this work, catalytic reactions where there are both structure-sensitive (hydrogenolysis) and structure-insensitive (propane dehydrogenation) reactions and the structure-insensitive reaction leads to the desired products, the ideal catalyst will have single metallic sites with few ensemble sites.

6 FUTURE WORK

In this study, we have studied both geometric and electronic effects on the kinetics of catalysts. Pt and Pd (and their alloys) catalysts have been the catalysts studied and neopentane hydrogenolysis and propane dehydrogenation were the reaction systems evaluated. The work done has provided several insights:

1. Neopentane isomerization selectivity improved with increasing particle size for both Pt and Pd catalysts as was found in previous literature. A correlation was found between CO initial heat of adsorption and isomerization selectivity which is independent of metal and particle size. Although this improvement can be accomplished by adjusting particle size, the bonding (electronic) properties of the catalyst may be the dominant factor in determining kinetics for monometallic catalysts.

2. Adjusting electronic properties through alloying Pt with Pd and Pd with Au results in slight improvements to neopentane isomerization selectivity. Although there were changes in the kinetics, they were not significant changes in behavior, but rather optimizations of the active metal in the catalyst, Pt for the PtPd catalyst and Pd for the PdAu.

3. Significantly altering palladium's geometric structure by the addition of zinc produced significant changes in kinetics. Forming the intermetallic alloy turned off structure sensitive pathways almost completely (neopentane hydrogenolysis, isomerization and propane hydrogenolysis), but structure insensitive pathways (propane dehydrogenation) were active.

This study has given insights into the role of geometric and electronic effects on catalysis. Changes in the electronic properties of the catalyst can cause changes in behavior, but

will not alter the fundamental behavior of the active metal. Neopentane isomerization selectivity of Pt was slightly improved by alloying with Pd, however, the behavior of the catalyst still was very similar to pure Pt. Alloying Au with Pd caused a similar improvement in selectivity relative to particle size. This improvement did not exceed the best pure Pd selectivity obtained in the particle size study and did not significantly alter the behavior of Pd. When palladium and zinc were not in an intermetallic structure, the catalyst behaved similarly to pure Pd as seen in the neopentane hydrogenolysis behavior of the 3%Pd-1.8%Zn catalyst. However, when the intermetallic structure was formed, a major shift in surface geometry resulted and a fundamental shift in the catalytic behavior for both neopentane hydrogenolysis and propane dehydrogenation was observed. From these studies we can posit that electronic effects can cause minor shifts or optimizations in behavior of an active metal, but causing major changes or deviations requires altering the geometric structure of the catalyst.

Future studies should examine the specifics of PdZn intermetallic alloy formation. Although the characterization in Chapter 5 strongly indicates that the intermetallic alloy forms on the nanoparticle surface first then moves inward, it is unknown if a mixed alloy of PdZn forms initially then the intermetallic or if the intermetallic structure forms from segregated Pd and Zn. In order to evaluate structural changes, a lower surface area support like alumina will be used to give clearer and better looking characterization. From our study, it is apparent that excess zinc allows the intermetallic structure to form more readily. One method to observe structure change is to run EXAFS of the Pd-Zn catalysts at increasing reduction temperatures. Data from Chapter 5 and previous literature have shown that higher reduction temperatures trigger the formation of the intermetallic structure.[214, 220] Two PdZn catalysts with different loadings were synthesized to perform this study. 4%Pd-2%Zn and 4%Pd-12%Zn were supported

on a spherical δ-alumina from Alfa Aesar (Nanodur, SA: 45 m^2/g). The catalysts were synthesized by sequential IWI and the low surface area of the support required multiple impregnation steps for both Zn and Pd. The zinc was added first using $Zn(NO_3)_2$ in one impregnation for the 4%Pd-2%Zn catalyst and in two impregnations for the 4%Pd-12%Zn catalyst. The palladium was then added using 10% $Pd(NH_3)_4(NO_3)_2$ in H_2O solution in four impregnation steps. The catalysts were dried at 125°C for at least an hour between impregnation steps. The finished catalysts were then calcined at 300°C for 3 hours. Figures 45 and 46 show the Pd K-edge EXAFS spectra of both PdZn catalysts at varying reduction temperatures and show the changes in structure. Similar to data in Chapter 5, the Pd spectra at low temperatures are similar to monometallic Pd with only a change in the peak ratio indicating the presence of zinc. As the temperature increases to 350°C the peak ratios change significantly and the PdZn peak becomes more apparent. At 500°C, the PdZn peak becomes dominant and the bulk of the catalyst has the intermetallic structure. Increasing the zinc loading from 2% to 12% in Figure 46 shows the intermetallic structure forming at lower reduction temperatures. These spectra show a clear change in structure with increasing reduction temperature and also the zinc loading as we suggested in Chapter 5. As stated previously, EXAFS is a bulk technique and so will not be able to discern different phases of PdZn with high resolution, only that the two metals are near one another. It can indicate when the bulk of the PdZn is intermetallic.

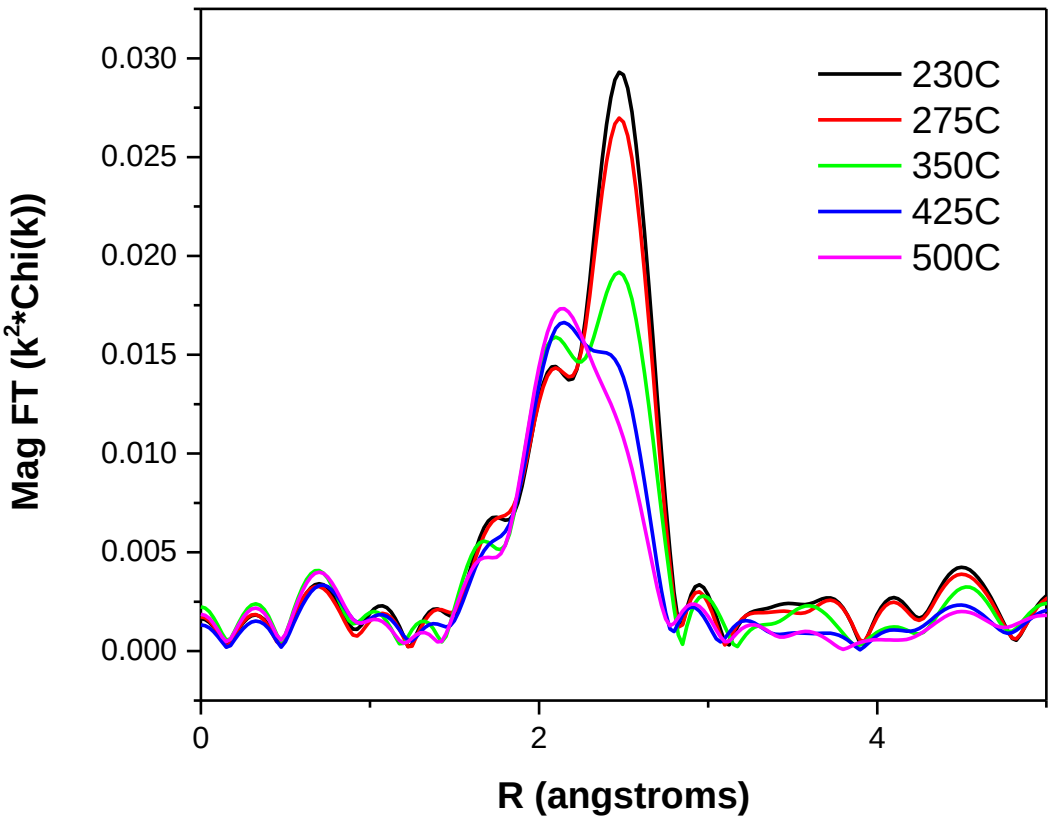

Figure 45: Pd K-edge EXAFS spectra of the 4%Pd-2%Zn catalyst at varying reduction temperatures: 230°C (black), 275°C (red), 350°C (green), 425°C (blue) and 500°C (magenta)

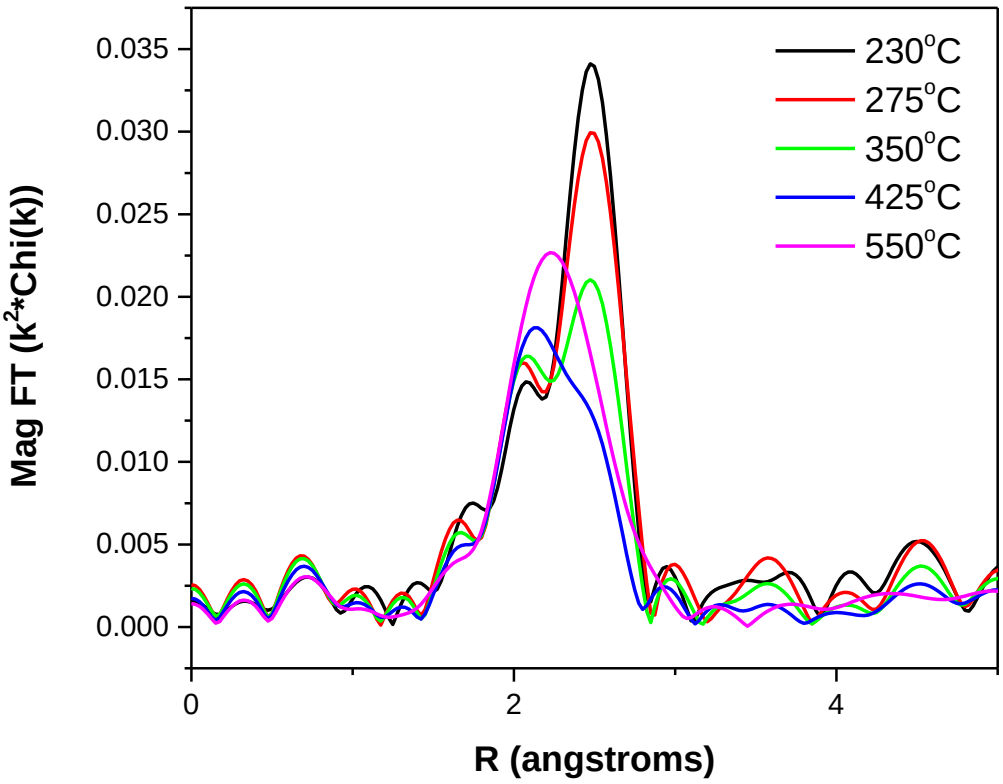

Figure 46: Pd K-edge EXAFS spectra of the 4%Pd-12%Zn catalyst at varying reduction temperatures: 230°C (black), 275°C (red), 350°C (green), 425°C (blue) and 500°C (magenta)

A disadvantage of EXAFS is that it gives information about local structure (although we have seen this is highly useful) without providing information about the long range order of the system. Therefore, X-ray Diffraction is better able to differentiate between a mixed PdZn alloy and an intermetallic structure. As reported by Bollman et al. Metallic Pd should display a peak at about 39.9° and the PdZn intermetallic alloy has peaks at 41.4° and 44.2°.[168] If Pd forms a mixed alloy with the zinc prior to the intermetallic structure then intermediate peaks will form between the metallic Pd peak and the PdZn intermetallic peak. If the intermetallic structure forms initially without a mixed alloy, then the peaks at 41.4° and 44.2° will increase with a

corresponding decrease in the metallic Pd peak at 39.9°. Taking XRD spectra at increasing reduction temperatures will allow us to evaluate when these changes in structure take place and that combined with EXAFS can give a more complete picture of the structure of the PdZn intermetallic alloy.

The work with PdZn shows that the intermetallic phase is inactive for both pathways of neopentane conversion as well as propane hydrogenolysis. It was suggested that the isolation of palladium atoms on the surface was responsible for this change in reactivity. Further investigation into the mechanisms of these reactions can give further insight into why intermetallic PdZn is unable to perform these reactions. Using H_2-D_2 exchange can allow us to look into H activation and diffusion on the surface. Hydrogen dissociation is one of the initial steps of the hydrogenolysis pathway.[184] If hydrogen is unable to dissociate readily it may limit hydrogenolysis. Adding zinc may introduce a barrier to dissociate H_2 (calculations indicate that this barrier is on the order of 0.1 eV). Isotope exchange has been used to study intermetallic compounds previously. Onda et al. studied acetylene hydrogenation over NiSn intermetallic catalysts.[221] H_2-D_2 equilibrium experiments were done to evaluate the ability of NiSn to dissociate hydrogen. They found that the order of rates of acetylene hydrogenation and HD formation were the same with pure nickel being the most active and decreasing with additional Sn being added. It was hypothesized that the electron density of the active atoms was responsible for this change and not the physical distance between the active atoms. Adding tin caused the Ni electron density at the Fermi level to decrease (due to charge transfer between Sn and Ni) and so decrease activity for hydrogen dissociation. The data in Chapter 5 suggests that the increase in distance between Pd atoms (from 2.75 to 2.84 Å) is responsible for the change in behavior. It

would be interesting to perform a similar isotope exchange experiment on the PdZn to see if there is a similar relationship between electron density and hydrogen dissociation.

The PdZn study also raises interesting questions about structure sensitivity. The intermetallic structure was unable to perform structure sensitive reactions, but was able to do propane dehydrogenation, a structure insensitive reaction. Creating this intermetallic structure with other metals or using other reactions could expand these findings to give a fundamental understanding of how to alter catalyst kinetics. There is an increasing amount of literature on intermetallic catalysts that can be used to guide future experiments. Ota et al. have used PdGa intermetallics to perform semi-hydrogenation of acetylene.[222] The PdGa catalysts exhibited an ethylene selectivity increase from 20% to 70% as well as increased stability and activity. Ni_3Sn has also shown high selectivity for this reaction.[221] Komatsu et al. tested intermetallic catalysts for oxidative acetoxylation of toluene to benzyl acetate and found that Pd_3Bi, Pd_3Pb, PdCd and Pd_3Tl intermetallic structures were selective for this reaction while pure Pd is not able to do this reaction.[203] A geometric effect was credited to this change in reactivity as well. Intermetallic catalysts have been used for Fischer-Tropsch synthesis as well. Komatsu's group also tested a number of intermetallic catalysts and found that RuTi had the highest selectivity to higher hydrocarbons.[223] The RuTi system has also been used for the selective hydrogenation of crotonaldehyde.[224]

These studies show the possibility for a wide range of systems and applications for intermetallic catalysts. The data from the PdZn study gives an interesting starting point to the fundamentals of catalyst kinetics. Future studies can be focused on determining the nature of intermetallic structure and applying this knowledge to other intermetallic systems to gain a better

understanding of the role of geometric and electronic effects. The end goal is to gain a fundamental understanding of the role of geometric and electronic effects in bimetallic catalysts.

CITED LITERATURE

[1] D. Childers, A. Saha, N. Schweitzer, R.M. Rioux, J.T. Miller, R.J. Meyer, Correlating Heat of Adsorption of CO to Reaction Selectivity: Geometric Effects vs Electronic Effects in Neopentane Isomerization over Pt and Pd Catalysts, ACS Catal., 3 (2013) 2487-2496.
[2] T.P. Wu, D.J. Childers, C. Gomez, A.M. Karim, N.M. Schweitzer, A.J. Kropf, H. Wang, T.B. Bolin, Y.F. Hu, L. Kovarik, R.J. Meyer, J.T. Miller, General Method for Determination of the Surface Composition in Bimetallic Nanoparticle Catalysts from the L Edge X-ray Absorption Near-Edge Spectra, Acs Catalysis, 2 (2012) 2433-2443.
[3] G.A. Somorjai, J.Y. Park, Molecular Factors of Catalytic Selectivity, Angew. Chem.-Int. Edit., 47 (2008) 9212-9228.
[4] G.A. Somorjai, C.J. Kliewer, Reaction selectivity in heterogeneous catalysis, React. Kinet. Catal. Lett., 96 (2009) 191-208.
[5] N. Musselwhite, G.A. Somorjai, Investigations of Structure Sensitivity in Heterogeneous Catalysis: From Single Crystals to Monodisperse Nanoparticles, Top. Catal., 56 (2013) 1277-1283.
[6] J.A. Dumesic, H. Topsoe, S. Khammouma, M. Boudart, SURFACE, CATALYTIC AND MAGNETIC-PROPERTIES OF SMALL IRON PARTICLES .2. STRUCTURE SENSITIVITY OF AMMONIA-SYNTHESIS, Journal of Catalysis, 37 (1975) 503-512.
[7] M. Boudart, M.A. McDonald, STRUCTURE SENSITIVITY OF HYDROCARBON SYNTHESIS FROM CO AND H2, J. Phys. Chem., 88 (1984) 2185-2195.
[8] E. Iglesia, M. Boudart, STRUCTURE-SENSITIVITY AND ENSEMBLE EFFECTS IN REACTIONS OF STRONGLY ADSORBED INTERMEDIATES - CATALYTIC DEHYDROGENATION AND DEHYDRATION OF FORMIC-ACID ON NICKEL, J. Phys. Chem., 95 (1991) 7011-7016.
[9] D.J. Sajkowski, M. Boudart, STRUCTURE SENSITIVITY OF THE CATALYTIC-OXIDATION OF ETHENE BY SILVER, Catal. Rev.-Sci. Eng., 29 (1987) 325-360.
[10] J. Kleis, J. Greeley, N.A. Romero, V.A. Morozov, H. Falsig, A.H. Larsen, J. Lu, J.J. Mortensen, M. Dulak, K.S. Thygesen, J.K. Norskov, K.W. Jacobsen, Finite Size Effects in Chemical Bonding: From Small Clusters to Solids, Catalysis Letters, 141 (2011) 1067-1071.
[11] D.C. Koningsberger, D.E. Ramaker, J.T. Miller, J. de Graaf, B.L. Mojet, The direct influence of the support on the electronic structure of the active sites in supported metal catalysts: evidence from Pt-H anti-bonding shape resonance and Pt-COFTIR data, Top. Catal., 15 (2001) 35-42.
[12] D.C. Koningsberger, J. de Graaf, B.L. Mojet, D.E. Ramaker, J.T. Miller, The metal-support interaction in Pt/Y zeolite: evidence for a shift in energy of metal d-valence orbitals by Pt-H shape resonance and atomic XAFS spectroscopy, Appl. Catal. A-Gen., 191 (2000) 205-220.
[13] S. Kruger, S. Vent, F. Nortemann, M. Staufer, N. Rosch, The average bond length in Pd clusters Pd-n, n=4-309: A density-functional case study on the scaling of cluster properties, J. Chem. Phys., 115 (2001) 2082-2087.
[14] T. Teranishi, M. Miyake, Size control of palladium nanoparticles and their crystal structures, Chemistry of Materials, 10 (1998) 594-600.
[15] R. Lamber, S. Wetjen, N.I. Jaeger, SIZE DEPENDENCE OF THE LATTICE-PARAMETER OF SMALL PALLADIUM PARTICLES, Physical Review B, 51 (1995) 10968-10971.
[16] R.E. Benfield, A. Filipponi, D.T. Bowron, R.J. Newport, S.J. Gurman, G. Schmid, EXAFS investigations of high-nuclearity Pd clusters, Physica B: Condensed Matter, 208–209 (1995) 671-673.
[17] G.C.A. Schuit, L.L. Van Reijen, The Structure and Activity of Metal-on-Silica Catalysts, in: W.G.F.V.I.K. D.D. Eley, B.W. Paul (Eds.) Advances in Catalysis, Academic Press, 1958, pp. 242-317.

[18] J.H. Sinfelt, Heterogeneous catalysis: Some aspects of catalysis by metals, C R C Critical Reviews in Solid State Sciences, 4 (1973) 311-332.
[19] S. Dahl, A. Logadottir, R.C. Egeberg, J.H. Larsen, I. Chorkendorff, E. Tornqvist, J.K. Norskov, Role of steps in N-2 activation on Ru(0001), Phys Rev Lett, 83 (1999) 1814-1817.
[20] S. Dahl, E. Tornqvist, I. Chorkendorff, Dissociative adsorption of N-2 on Ru(0001): A surface reaction totally dominated by steps, Journal of Catalysis, 192 (2000) 381-390.
[21] S. Schauermann, N. Nilius, S. Shaikhutdinov, H.J. Freund, Nanoparticles for Heterogeneous Catalysis: New Mechanistic Insights, Accounts Chem. Res., 46 (2013) 1673-1681.
[22] C.R. Henry, C. Chapon, C. Goyhenex, R. Monot, SIZE EFFECT IN THE CO CHEMISORPTION ON PALLADIUM CLUSTERS SUPPORTED ON MAGNESIUM-OXIDE, Surf. Sci., 272 (1992) 283-288.
[23] C.R. Henry, B. Mutaftschiev, Adsorption-desorption kinetics on stepped surfaces by modulated molecular beam techniques, Surf. Sci., 163 (1985) 409-434.
[24] E.K. Parks, B.J. Winter, T.D. Klots, S.J. Riley, The structure of nickel clusters, The Journal of Chemical Physics, 94 (1991) 1882-1902.
[25] B. Hammer, O.H. Nielsen, J.K. Norskov, Structure sensitivity in adsorption: CO interaction with stepped and reconstructed Pt surfaces, Catalysis Letters, 46 (1997) 31-35.
[26] B. Hammer, Y. Morikawa, J.K. Norskov, CO chemisorption at metal surfaces and overlayers, Phys Rev Lett, 76 (1996) 2141-2144.
[27] Y. Morikawa, J.J. Mortensen, B. Hammer, J.K. Norskov, CO adsorption and dissociation on Pt(111) and Ni(111) surfaces, Surf. Sci., 386 (1997) 67-72.
[28] B. Hammer, J.K. Norskov, Theoretical surface science and catalysis - Calculations and concepts, in: B.C. Gates, H. Knozinger (Eds.) Advances in Catalysis, Vol 45: Impact of Surface Science on Catalysis, 2000, pp. 71-129.
[29] B. Hammer, J.K. Norskov, Electronic factors determining the reactivity of metal surfaces, Surface Science, 343 (1995) 211-220.
[30] J.Y. Park, Y.J. Lee, P.R. Karandikar, K.W. Jun, K.S. Ha, H.G. Park, Fischer-Tropsch catalysts deposited with size-controlled Co3O4 nanocrystals: Effect of Co particle size on catalytic activity and stability, Appl. Catal. A-Gen., 411 (2012) 15-23.
[31] F.J. Gracia, L. Bollmann, E.E. Wolf, J.T. Miller, A.J. Kropf, In situ FTIR, EXAFS, and activity studies of the effect of crystallite size on silica-supported Pt oxidation catalysts, Journal of Catalysis, 220 (2003) 382-391.
[32] P. Claus, H. Hofmeister, Electron microscopy and catalytic study of silver catalysts: Structure sensitivity of the hydrogenation of crotonaldehyde, Journal of Physical Chemistry B, 103 (1999) 2766-2775.
[33] M.N. Padilla-Serrano, F. Maldonado-Hodar, C. Moreno-Castilla, Influence of Pt particle size on catalytic combustion of xylenes on carbon aerogel-supported Pt catalysts, Applied Catalysis B-Environmental, 61 (2005) 253-258.
[34] J.A. Rodriguez, D.W. Goodman, SURFACE SCIENCE STUDIES OF THE ELECTRONIC AND CHEMICAL-PROPERTIES OF BIMETALLIC SYSTEMS, Journal of Physical Chemistry, 95 (1991) 4196-4206.
[35] J.A. Rodriguez, D.W. Goodman, THE NATURE OF THE METAL METAL BOND IN BIMETALLIC SURFACES, Science, 257 (1992) 897-903.
[36] J.H. Sinfelt, BIMETALLIC CATALYSTS, Sci.Am., 253 (1985) 90-&.
[37] K. Balakrishnan, J. Schwank, Neopentane reactions over bimetallic Pt-Sn/Al_2O_3 and Pt-Au/SiO_2 catalysts, Journal of Catalysis, 132 (1991) 451-464.
[38] A. Gross, Reactivity of bimetallic systems studied from first principles, Topics in Catalysis, 37 (2006) 29-39.
[39] J.L. Carter, G.B. McVicker, W. Weissman, W.S. Kmak, J.H. Sinfelt, BIMETALLIC CATALYSTS - APPLICATION IN CATALYTIC REFORMING, Applied Catalysis, 3 (1982) 327-346.

[40] F. Tao, M.E. Grass, Y.W. Zhang, D.R. Butcher, J.R. Renzas, Z. Liu, J.Y. Chung, B.S. Mun, M. Salmeron, G.A. Somorjai, Reaction-Driven Restructuring of Rh-Pd and Pt-Pd Core-Shell Nanoparticles, Science, 322 (2008) 932-934.
[41] J.H. Sinfelt, D.J.C. Yates, J.L. Carter, CATALYTIC HYDROGENOLYSIS AND DEHYDROGENATION OVER COPPER-NICKEL ALLOYS, Journal of Catalysis, 24 (1972) 283-&.
[42] M.J.P. Botman, K. Devreugd, H.W. Zandbergen, R. Deblock, V. Ponec, THE EFFECT OF ALLOYING PT WITH RE ON THE INTERMEDIATES IN HYDROCARBON REACTIONS - REACTIONS OF 2,2-DIMETHYLBUTANE, Journal of Catalysis, 116 (1989) 467-479.
[43] C.T. Campbell, BIMETALLIC SURFACE-CHEMISTRY, Annu. Rev. Phys. Chem., 41 (1990) 775-837.
[44] C.P. O'Brien, B.H. Howard, J.B. Miller, B.D. Morreale, A.J. Gellman, Inhibition of hydrogen transport through Pd and Pd47Cu53 membranes by H2S at 350 °C, Journal of Membrane Science, 349 (2010) 380-384.
[45] C.P. O'Brien, J.B. Miller, B.D. Morreale, A.J. Gellman, The Kinetics of H-2-D-2 Exchange over Pd, Cu, and PdCu Surfaces, Journal of Physical Chemistry C, 115 (2011) 24221-24230.
[46] J.B. Miller, C. Matranga, A.J. Gellman, Surface segregation in a polycrystalline Pd70Cu30 alloy hydrogen purification membrane, Surf. Sci., 602 (2008) 375-382.
[47] W. Juszczyk, D. Lomot, Z. Karpinski, J. Pielaszek, NEOPENTANE CONVERSION OVER PD/GAMMA-AL2O3, Catalysis Letters, 31 (1995) 37-45.
[48] J.H. Sinfelt, J.L. Carter, D.J.C. Yates, Catalytic hydrogenolysis and dehydrogenation over copper-nickel alloys, Journal of Catalysis, 24 (1972) 283-296.
[49] C. Xu, B.E. Koel, M.T. Paffett, ADSORPTION AND DESORPTION BEHAVIOR OF N-BUTANE AND ISOBUTANE ON PT(111) AND SN/PT(111) SURFACE ALLOYS, Langmuir, 10 (1994) 166-171.
[50] R.D. Cortright, R.M. Watwe, B.E. Spiewak, J.A. Dumesic, Kinetics of ethane hydrogenolysis over supported platinum catalysts, Catal. Today, 53 (1999) 395-406.
[51] J.H. Sinfelt, CATALYTIC HYDROGENOLYSIS ON METALS, Catalysis Letters, 9 (1991) 159-172.
[52] D.W. Flaherty, E. Iglesia, Transition-State Enthalpy and Entropy Effects on Reactivity and Selectivity in Hydrogenolysis of n-Alkanes, Journal of the American Chemical Society, 135 (2013) 18586-18599.
[53] D.W. Blakely, G.A. Somorjai, The dehydrogenation and hydrogenolysis of cyclohexane and cyclohexene on stepped (high miller index) platinum surfaces, Journal of Catalysis, 42 (1976) 181-196.
[54] A.K. Rovik, S.K. Klitgaard, S. Dahl, C.H. Christensen, I. Chorkendorff, Effect of alloying on carbon formation during ethane dehydrogenation, Applied Catalysis A: General, 358 (2009) 269-278.
[55] J. Anderson, N. Avery, The Isomerization of Aliphatic Hydrocarbons over Evaporated Films of Platinum and Palladium, Journal of Catalysis, 5 (1966) 18.
[56] V.M.a.A.-K. Akhmedov, S. H., Recent Advances and Future Aspects in the Selective Isomerization of High n-Alkanes, Catalysis Reviews: Science and Engineering, 49 (2007) 33-139.
[57] A. Aitani, Catalytic Naphtha Reforming, 2nd ed., Marcel Dekker, Inc., New York, 2004.
[58] V.M. Akhmedov, S.H. Al-Khowaiter, Recent advances and future aspects in the selective isomerization of high n-alkanes, Catal Rev, 49 (2007) 33-139.
[59] F.G. Ciapetta, D.N. Wallace, Catalytic naphtha reforming, Catalysis Reviews, 5 (1972) 67-158.
[60] A. Aitani, Reforming Processes, in: M. Dekker (Ed.) Catalytic Naphtha Reforming, 1995, pp. 415.
[61] F.G. Ciapetta, D.N. Wallace, Catalytic naphtha reforming, Catalysis Reviews 5(1972) 67-158.
[62] W. Juszczyk, Z. Karpinski, I. Ratajczykowa, Z. Stanasiuk, J. Zielinski, L.L. Sheu, W.M.H. Sachtler, CHARACTERIZATION OF SUPPORTED PALLADIUM CATALYSTS .3. PD/AL2O3, Journal of Catalysis, 120 (1989) 68-77.
[63] W. Juszczyk, Z. Karpinski, CHARACTERIZATION OF SUPPORTED PALLADIUM CATALYSTS .2. PD/SIO2, Journal of Catalysis, 117 (1989) 519-532.
[64] M.M. Bhasin, J.H. McCain, B.V. Vora, T. Imai, P.R. Pujado, Dehydrogenation and oxydehydrogenation of paraffins to olefins, Appl. Catal. A-Gen., 221 (2001) 397-419.

[65] V. Haensel, Conversion of hydrocarbons with platinum composite catalyst, in, Google Patents, 1952.
[66] H. Bloch, UOP discloses new way to make linear alkylbenzene, Oil Gas J, (1967) 79-81.
[67] Y.W. Zhang, Y.M. Zhou, A.D. Qiu, Y. Wang, Y. Xu, P.C. Wu, Effect of alumina binder on catalytic performance of PtSnNa/ZSM-5 catalyst for propane dehydrogenation, Ind. Eng. Chem. Res., 45 (2006) 2213-2219.
[68] X.Z. Lin, G.C. Li, C.J. Huang, W.Z. Weng, H.L. Wan, P-modified cobalt oxide: A novel and effective catalyst for oxidative dehydrogenation of propane, Chin. Chem. Lett., 24 (2013) 789-792.
[69] P. Sazama, N.K. Sathu, E. Tabor, B. Wichterlova, S. Sklenak, Z. Sobalik, Structure and critical function of Fe and acid sites in Fe-ZSM-5 in propane oxidative dehydrogenation with N2O and N2O decomposition, Journal of Catalysis, 299 (2013) 188-203.
[70] G. Wu, F. Hei, N. Zhang, N. Guan, L. Li, W. Grünert, Oxidative dehydrogenation of propane with nitrous oxide over Fe-ZSM-5 prepared by grafting: Characterization and performance, Applied Catalysis A: General, 468 (2013) 230-239.
[71] L. Cheng, G.A. Ferguson, S.A. Zygmunt, L.A. Curtiss, Structure–activity relationships for propane oxidative dehydrogenation by anatase-supported vanadium oxide monomers and dimers, Journal of Catalysis, 302 (2013) 31-36.
[72] M. Høj, A.D. Jensen, J.-D. Grunwaldt, Structure of alumina supported vanadia catalysts for oxidative dehydrogenation of propane prepared by flame spray pyrolysis, Applied Catalysis A: General, 451 (2013) 207-215.
[73] F. Zhang, R.X. Wu, Y.H. Yue, W.M. Yang, S.Y. Gu, C.X. Miao, W.M. Hua, Z. Gao, Chromium oxide supported on ZSM-5 as a novel efficient catalyst for dehydrogenation of propane with CO2, Microporous Mesoporous Mat., 145 (2011) 194-199.
[74] S. Sugiyama, Y. Hirata, K. Nakagawa, K.I. Sotowa, K. Maehara, Y. Himeno, W. Ninomiya, Application of the unique redox properties of magnesium ortho-vanadate incorporated with palladium in the unsteady-state operation of the oxidative dehydrogenation of propane, Journal of Catalysis, 260 (2008) 157-163.
[75] O.A. Barias, A. Holmen, E.A. Blekkan, Propane dehydrogenation over supported Pt and Pt-Sn catalysts: Catalyst preparation, characterization, and activity measurements, Journal of Catalysis, 158 (1996) 1-12.
[76] F.M. Ashmawy, CATALYTIC DEHYDROGENATION OF PROPANE ON CHROMIA, PALLADIUM AND PLATINUM SUPPORTED CATALYSTS, Journal of Applied Chemistry and Biotechnology, 27 (1977) 137-142.
[77] Y.W. Zhang, Y.M. Zhou, A.D. Qiu, Y. Wang, Y. Xu, P.C. Wu, Propane dehydrogenation on PtSn/ZSM-5 catalyst: Effect of tin as a promoter, Catal. Commun., 7 (2006) 860-866.
[78] L. Jiao, J.R. Regalbuto, The synthesis of highly dispersed noble and base metals on silica via strong electrostatic adsorption: I. Amorphous silica, Journal of Catalysis, 260 (2008) 329-341.
[79] J.R. Regalbuto, Catalyst Preparation: Science and Engineering, CRC Press, 2006.
[80] J.B. Rawlings, J.G. Ekerdt, Chemical Reactor Analysis and Design Fundamentals, Nob Hill Publishing, Madison, WI, 2004.
[81] M. Boudart, L.D. Ptak, REACTIONS OF NEOPENTANE ON TRANSITION METALS, Journal of Catalysis, 16 (1970) 90-&.
[82] K. Foger, J.R. Anderson, REACTIONS OF NEOPENTANE AND NEOHEXANE ON PLATINUM-Y-ZEOLITE AND PLATINUM-SILICA CATALYSTS, Journal of Catalysis, 54 (1978) 318-335.
[83] J.T. Miller, A.J. Kropf, Y. Zha, J.R. Regalbuto, L. Delannoy, C. Louis, E. Bus, J.A. van Bokhoven, The effect of gold particle size on Au-Au bond length and reactivity toward oxygen in supported catalysts, Journal of Catalysis, 240 (2006) 222-234.
[84] S.M. Davis, F. Zaera, G.A. Somorjai, SURFACE-STRUCTURE AND TEMPERATURE-DEPENDENCE OF LIGHT-ALKANE SKELETAL REARRANGEMENT REACTIONS CATALYZED OVER PLATINUM SINGLE-CRYSTAL SURFACES, Journal of the American Chemical Society, 104 (1982) 7453-7461.

[85] R.C. Egeberg, J.H. Larsen, I. Chorkendorff, Molecular beam study of N-2 dissociation on Ru(0001), Phys. Chem. Chem. Phys., 3 (2001) 2007-2011.
[86] J.B. Giorgi, T. Schroeder, M. Baumer, H.J. Freund, Study of CO adsorption on crystalline-silica-supported palladium particles, Surf Sci, 498 (2002) L71-L77.
[87] J. Rebelli, A.A. Rodriguez, S.G. Ma, C.T. Williams, J.R. Monnier, Preparation and characterization of silica-supported, group IB-Pd bimetallic catalysts prepared by electroless deposition methods, Catalysis Today, 160 (2011) 170-178.
[88] J.S. Bradley, E.W. Hill, S. Behal, C. Klein, B. Chaudret, A. Duteil, Preparation and Characterization of Organosols of Monodispersed Nanoscale Palladium - Particle-Size Effects in the Binding Geometry of Adsorbed Carbon-Monoxide, Chem Mater, 4 (1992) 1234-1239.
[89] T.K. Lear, Thomas; Baumer, Marcus; Rupprechter, Gunther; Freund, Hans-Joachim; Lennon, David, The application of infrared spectroscopy to probe the surface morphology of alumina-supported palladium catalysts, Journal of Chemical Physics, 123 (2005) 13.
[90] J.F. Lu, Baosong; Kung, M.C.; Xiao Guomin; Elam, Jeffery; Kung, H.H.; Stair, P.C., Coking- and Sintering-Resistant Palladium Catalysts Achieved Through Atomic Layer Deposition, Science, 335 (2012) 4.
[91] D.M. Haaland, Infrared Studies of Co Adsorbed on Pt/Al2o3 - Evidence for Co Bonded in 3-Fold Coordination, Surf Sci, 185 (1987) 1-14.
[92] K. Balakrishnan, A. Sachdev, L. Schwank, Chemisorption and Ftir Study of Bimetallic Pt-Au/Sio2 Catalysts, Journal of Catalysis, 121 (1990) 441-455.
[93] J. Singh, J.A. van Bokhoven, Structure of alumina supported platinum catalysts of different particle size during CO oxidation using in situ IR and HERFD XAS, Catalysis Today, 155 (2010) 199-205.
[94] S. Veldurthi, C.H. Shin, O.S. Joo, K.D. Jung, Promotional effects of Cu on Pt/Al2O3 and Pd/Al2O3 catalysts during n-butane dehydrogenation, Catalysis Today, 185 (2012) 88-93.
[95] J.S. Bradley, J.M. Millar, E.W. Hill, S. Behal, Surface-Chemistry on Transition-Metal Colloids - an Infrared and Nmr-Study of Carbon-Monoxide Adsorption on Colloidal Platinum, Journal of Catalysis, 129 (1991) 530-539.
[96] A.M. Bradshaw, Ir Reflection Absorption-Spectroscopy of Adsorbed Molecules, Surf Sci, 158 (1985) 624-627.
[97] C.L. Kao, R.J. Madix, The adsorption dynamics of molecular methane, propane, and neopentane on Pd(111): Theory and experiment, J Phys Chem B, 106 (2002) 8248-8257.
[98] K.L. Street, V. Fiorin, M.R.S. McCoustra, M.A. Chesters, Neopentane adsorption on Pt(111), Surface Science, 433 (1999) 176-179.
[99] P. Chou, M.A. Vannice, Calorimetric Heat of Adsorption Measurements on Palladium 2. Influence of Crystallite Size and Support on CO Adsorption, J Catal, 104 (1987) 17-30.
[100] B. Sen, M.A. Vannice, The Influence of Platinum Crystallite Size on H_2 and CO Heats of Adsorption and CO Hydrogenation, J Catal, 130 (1991) 9-20.
[101] B. Sen, M.A. Vannice, THE INFLUENCE OF PLATINUM CRYSTALLITE SIZE ON H-2 AND CO HEATS OF ADSORPTION AND CO HYDROGENATION, Journal of Catalysis, 130 (1991) 9-20.
[102] M.A. Vannice, P. Chou, CO, O_2 and H_2 Heats of Adsorption on Supported Pd, Acs Symposium Series, 298 (1986) 76-88.
[103] M.A. Vannice, L.C. Hasselbring, B. Sen, Direct Measurements of Heats of Adsorption on Platinum Catalysts. 2. CO on Pt Dispersed on SiO_2, Al_2O_3, SiO_2-Al_2O_3 and TiO_2, J Catal, 97 (1986) 66-74.
[104] M.A. Vannice, L.C. Hasselbring, B. Sen, Direct Measurement of Heats of Adsorption on Platinum Catalysts. 1. H_2 on Pt Dispersed on SiO_2, Al_2O_3, SiO_2-Al_2O_3 and TiO_2, J Catal, 95 (1985) 57-70.
[105] M.A. Vannice, L.C. Hasselbring, B. Sen, Metal Support Effects on H_2 and CO Heats of Adsorption on TiO_2-Supported Platinum, Journal of Physical Chemistry, 89 (1985) 2972-2973.

[106] M.A. Vannice, B. Sen, P. Chou, Modifications Required on a Power-Compensated Differential Scanning Calorimeter to Obtain Heat of Adsorption Measurements, Review of Scientific Instruments, 58 (1987) 647-653.
[107] J.M. Hill, J.Y. Shen, R.M. Watwe, J.A. Dumesic, Microcalorimetric, infrared spectroscopic, and DFT studies of ethylene adsorption on Pd and Pd/Sn catalysts, Langmuir, 16 (2000) 2213-2219.
[108] J.Y. Shen, J.M. Hill, R.M. Watwe, B.E. Spiewak, J.A. Dumesic, Microcalorimetric, infrared spectroscopic, and DFT studies of ethylene adsorption on Pt/SiO(2) and Pt-Sn/SiO(2) catalysts, Journal of Physical Chemistry B, 103 (1999) 3923-3934.
[109] S.B. Sharma, P. Ouraipyvan, H.A. Nair, P. Balaraman, T.W. Root, J.A. Dumesic, Microcalorimetric, ^{13}C NMR Spectroscopic and Reaction Kinetic Studies of Silica-Supported and L-Zeolite Supported Platinum Catalysts for n-hexane Conversion, J Catal, 150 (1994) 234-242.
[110] J. Silvestre, M. Sanchez-Castillo, R. He, F. Rodriguez-Reinoso, J.A. Dumesic, Microcalorimetric, reaction kinetic and DFT studies of Pt-ZnJX-zeolite for isobutane dehydrogenation. (vol 74, pg 17, 2001), Catal Lett, 82 (2002) 153-153.
[111] J. Silvestre-Albero, M.A. Sanchez-Castillo, R. He, A. Sepulveda-Escribano, F. Rodriguez-Reinoso, J.A. Dumesic, Microcalorimetric, reaction kinetics and DFT studies of Pt-Zn/X-zeolite for isobutane dehydrogenation, Catal Lett, 74 (2001) 17-25.
[112] M.S. Li, J.Y. Shen, Microcalorimetric and infrared spectroscopic studies of CO and C2H4 adsorption on Pd/SiO2 and Pd-Ag/SiO2 catalysts, Mater. Chem. Phys., 68 (2001) 204-209.
[113] M. Gravellerumeaumaillot, V. Pitchon, G.A. Martin, H. Praliaud, COMPLEMENTARY STUDY BY CALORIMETRY AND INFRARED-SPECTROSCOPY OF ALKALI-METAL DOPED PD/SIO2 SOLIDS - ADSORPTION OF HYDROGEN AND CARBON-MONOXIDE, Appl. Catal. A-Gen., 98 (1993) 45-59.
[114] P. Chou, M.A. Vannice, CALORIMETRIC HEAT OF ADSORPTION MEASUREMENTS ON PALLADIUM .2. INFLUENCE OF CRYSTALLITE SIZE AND SUPPORT ON CO ADSORPTION, Journal of Catalysis, 104 (1987) 17-30.
[115] S.M. Davis, W.D. Gillespie, G.A. Somorjai, DEUTERIUM-ISOTOPE EFFECTS FOR HYDROCARBON REACTIONS CATALYZED OVER PLATINUM SINGLE-CRYSTAL SURFACES, Journal of Catalysis, 83 (1983) 131-140.
[116] J. Greeley, J.K. Norskov, A general scheme for the estimation of oxygen binding energies on binary transition metal surface alloys, Surf Sci, 592 (2005) 104-111.
[117] P. Liu, J.K. Norskov, Ligand and ensemble effects in adsorption on alloy surfaces, Phys Chem Chem Phys, 3 (2001) 3814-3818.
[118] G.C. Wang, J. Li, X.F. Xu, R.F. Li, J. Nakamura, The relationship between adsorption energies of methyl on metals and the metallic electronic properties: A first-principles DFT study, J Comput Chem, 26 (2005) 871-878.
[119] F. Studt, F. Abild-Pedersen, T. Bligaard, R.Z. Sorensen, C.H. Christensen, J.K. Norskov, Identification of non-precious metal alloy catalysts for selective hydrogenation of acetylene, Science, 320 (2008) 1320-1322.
[120] T.T.T. Wong, W.M.H. Sachtler, The Effects of Protons on the Hydrogenolysis of Neopentane over Rhodium Catalysts - Rh/Hy, Rh/Nahy, and Rh/Sio2, Journal of Catalysis, 141 (1993) 407-418.
[121] R. He, H. Kusaka, M. Mavrikakis, J.A. Dumesic, Microcalorimetric, infrared spectroscopic and DFT studies of CO adsorption on Rh and Rh-Te catalysts, Journal of Catalysis, 217 (2003) 209-221.
[122] A. Bourane, M. Nawdali, D. Bianchi, Heats of adsorption of the linear CO species adsorbed on a Ir/Al2O3 catalyst using in situ FTIR spectroscopy under adsorption equilibrium, J Phys Chem B, 106 (2002) 2665-2671.
[123] G.C. Bond, R. Yahya, Hydrogenolysis of Alkanes .7. Hydrogenolysis of Propane and of Normal-Butane over Ir/Tio2 and Os/Tio2 Catalysts, J Chem Soc Faraday T, 87 (1991) 775-781.

[124] R.D. Cortright, P.E. Levin, J.A. Dumesic, Kinetic studies of isobutane dehydrogenation and isobutene hydrogenation over Pt/Sn-based catalysts, Ind Eng Chem Res, 37 (1998) 1717-1723.
[125] F. Gao, D.W. Goodman, Pd-Au bimetallic catalysts: understanding alloy effects from planar models and (supported) nanoparticles, Chemical Society Reviews, 41 (2012) 8009-8020.
[126] X.M. Chen, Z.X. Cai, X. Chen, M. Oyama, Green synthesis of graphene-PtPd alloy nanoparticles with high electrocatalytic performance for ethanol oxidation, Journal of Materials Chemistry A, 2 (2014) 315-320.
[127] X.Q. Huang, Y.J. Li, Y.J. Li, H.L. Zhou, X.F. Duan, Y. Huang, Synthesis of PtPd Bimetal Nanocrystals with Controllable Shape, Composition, and Their Tunable Catalytic Properties, Nano Letters, 12 (2012) 4265-4270.
[128] R.M. Navarro, B. Pawelec, J.M. Trejo, R. Mariscal, J.L.G. Fierro, Hydrogenation of aromatics on sulfur-resistant PtPd bimetallic catalysts, Journal of Catalysis, 189 (2000) 184-194.
[129] V.L. Barrio, P.L. Arias, J.F. Cambra, M.B. Guemez, B. Pawelec, J.L.G. Fierro, Hydrodesulfurization and hydrogenation of model compounds on silica-alumina supported bimetallic systems, Fuel, 82 (2003) 501-509.
[130] H. Kobayashi, M. Yamauchi, H. Kitagawa, Y. Kubota, K. Kato, M. Takata, Hydrogen absorption in the core/shell interface of Pd/Pt nanoparticles, Journal of the American Chemical Society, 130 (2008) 1818-+.
[131] J.R. Theis, R.W. McCabe, The effects of high temperature lean exposure on the subsequent HC conversion of automotive catalysts, Catal. Today, 184 (2012) 262-270.
[132] G.W. Graham, H.W. Jen, O. Ezekoye, R.J. Kudla, W. Chun, X.Q. Pan, R.W. McCabe, Effect of alloy composition on dispersion stability and catalytic activity for NO oxidation over alumina-supported Pt-Pd catalysts, Catalysis Letters, 116 (2007) 1-8.
[133] Z. Karpinski, W. Juszczyk, J. Pielaszek, REACTION OF NEOPENTANE WITH HYDROGEN OVER PD, PT, IR AND RH, Journal of the Chemical Society-Faraday Transactions I, 83 (1987) 1293-1305.
[134] W.D. Williams, M. Shekhar, W.S. Lee, V. Kispersky, W.N. Delgass, F.H. Ribeiro, S.M. Kim, E.A. Stach, J.T. Miller, L.F. Allard, Metallic Corner Atoms in Gold Clusters Supported on Rutile Are the Dominant Active Site during Water-Gas Shift Catalysis, Journal of the American Chemical Society, 132 (2010) 14018-14020.
[135] N.A. Bhore, M.T. Klein, K.B. Bischoff, Species Rank in Reaction Pathways: Application of Delplot Analysis, Chem Eng. Sci, 45 (1990) 2109-2116.
[136] Characterization of Solid Catalysts, in: H.K. Gerhard Ertl, Ferdi Schüth, Jens Weitkamp (Ed.) Handbook of heterogeneous catalysis, Wiley-VCH 2008, pp. 439-441.
[137] N. Guo, B.R. Fingland, W.D. Williams, V.F. Kispersky, J. Jelic, W.N. Delgass, F.H. Ribeiro, R.J. Meyer, J.T. Miller, Determination of CO, H_2O and H_2 coverage by XANES and EXAFS on Pt and Au during water gas shift reaction, Physical Chemistry Chemical Physics, 12 (2010) 5678-5693.
[138] Y. Lei, J. Jelic, L. Nitsche, R.J. Meyer, J.T. Miller, Effect of Particle Size and Adsorbates on the X-ray Absorption Near Edge Structure of Supported Pt Nanoparticles, Topics in Catalysis, 54 (2011) 334-348.
[139] A. Palazov, C.C. Chang, R.J. Kokes, The infrared spectrum of carbon monoxide on reduced and oxidized palladium, Journal of Catalysis, 36 (1975) 338-350.
[140] M.T. Schaal, M.P. Hyman, M. Rangan, S. Ma, C.T. Williams, J.R. Monnier, J.W. Medlin, Theoretical and experimental studies of Ag–Pt interactions for supported Ag–Pt bimetallic catalysts, Surf. Sci., 603 (2009) 690-696.
[141] J. Sehested, K.E. Larsen, A.L. Kustov, A.M. Frey, T. Johannessen, T. Bligaard, M.P. Andersson, J.K. Norskov, C.H. Christensen, Discovery of technical methanation catalysts based on computational screening, Top. Catal., 45 (2007) 9-13.

[142] N. Schweitzer, H.L. Xin, E. Nikolla, J.T. Miller, S. Linic, Establishing Relationships Between the Geometric Structure and Chemical Reactivity of Alloy Catalysts Based on Their Measured Electronic Structure, Top. Catal., 53 (2010) 348-356.
[143] M. Bonarowska, J. Pielaszek, W. Juszczyk, Z. Karpinski, Characterization of Pd-Au/SiO2 catalysts by X-ray diffraction, temperature-programmed hydride decomposition, and catalytic probes, Journal of Catalysis, 195 (2000) 304-315.
[144] P. Dash, T. Bond, C. Fowler, W. Hou, N. Coombs, R.W.J. Scott, Rational Design of Supported PdAu Nanoparticle Catalysts from Structured Nanoparticle Precursors, Journal of Physical Chemistry C, 113 (2009) 12719-12730.
[145] N. El Kolli, L. Delannoy, C. Louis, Bimetallic Au-Pd catalysts for selective hydrogenation of butadiene: Influence of the preparation method on catalytic properties, Journal of Catalysis, 297 (2013) 79-92.
[146] A.M. Venezia, L.F. Liotta, G. Pantaleo, V. La Parola, G. Deganello, A. Beck, Z. Koppany, K. Frey, D. Horvath, L. Guczi, Activity of SiO2 supported gold-palladium catalysts in CO oxidation, Appl. Catal. A-Gen., 251 (2003) 359-368.
[147] A. Sarkany, O. Geszti, G. Safran, Preparation of Pd-shell-Au-core/SiO2 catalyst and catalytic activity for acetylene hydrogenation, Appl. Catal. A-Gen., 350 (2008) 157-163.
[148] K. Luo, T. Wei, C.W. Yi, S. Axnanda, A.W. Goodman, Preparation and characterization of silica supported Au-Pd model catalysts, Journal of Physical Chemistry B, 109 (2005) 23517-23522.
[149] S.W.T. Price, J.M. Rhodes, L. Calvillo, A.E. Russell, Revealing the Details of the Surface Composition of Electrochemically Prepared Au@Pd Core@Shell Nanoparticles with in Situ EXAFS, Journal of Physical Chemistry C, 117 (2013) 24858-24865.
[150] A.F. Lee, C.J. Baddeley, C. Hardacre, R.M. Ormerod, R.M. Lambert, G. Schmid, H. West, STRUCTURAL AND CATALYTIC PROPERTIES OF NOVEL AU/PD BIMETALLIC COLLOID PARTICLES - EXAFS, XRD, AND ACETYLENE COUPLING, J. Phys. Chem., 99 (1995) 6096-6102.
[151] M.S. Chen, D. Kumar, C.W. Yi, D.W. Goodman, The promotional effect of gold in catalysis by palladium-gold, Science, 310 (2005) 291-293.
[152] X. Yang, C. Huang, Z.Y. Fu, H.Y. Song, S.J. Liao, Y.L. Su, L. Du, X.J. Li, An effective Pd-promoted gold catalyst supported on mesoporous silica particles for the oxidation of benzyl alcohol, Applied Catalysis B-Environmental, 140 (2013) 419-425.
[153] P. Dolle, R. Baudoing-Savois, M. De Santis, M.C. Saint-Lager, M. Abel, J.C. Bertolini, P. Delichère, Strained Pd films, by epitaxial growth on Au(1 1 0), to control catalytic properties, Surf Sci, 518 (2002) 1-13.
[154] Z. Li, F. Gao, O. Furlong, W.T. Tysoe, Adsorption of carbon monoxide Au/Pd(1 0 0) alloys in ultrahigh vacuum: Identification of adsorption sites, Surf Sci, 604 (2010) 136-143.
[155] B. Zhu, G. Thrimurthulu, L. Delannoy, C. Louis, C. Mottet, J. Creuze, B. Legrand, H. Guesmi, Evidence of Pd segregation and stabilization at edges of AuPd nano-clusters in the presence of CO: A combined DFT and DRIFTS study, Journal of Catalysis, 308 (2013) 272-281.
[156] F. Gao, Y.L. Wang, D.W. Goodman, CO Oxidation over AuPd(100) from Ultrahigh Vacuum to Near-Atmospheric Pressures: CO Adsorption-Induced Surface Segregation and Reaction Kinetics, Journal of Physical Chemistry C, 113 (2009) 14993-15000.
[157] G. Mazzone, I. Rivalta, N. Russo, E. Sicilia, Interaction of CO with PdAu(111) and PdAu(100) bimetallic surfaces: A theoretical cluster model study, J. Phys. Chem. C, 112 (2008) 6073-6081.
[158] H.L. Abbott, A. Aumer, Y. Lei, C. Asokan, R.J. Meyer, M. Sterrer, S. Shaikhutdinov, H.J. Freund, CO Adsorption on Monometallic and Bimetallic Au−Pd Nanoparticles Supported on Oxide Thin Films†, The Journal of Physical Chemistry C, 114 (2010) 17099-17104.
[159] V. Soto-Verdugo, H. Metiu, Segregation at the surface of an Au/Pd alloy exposed to CO, Surf Sci, 601 (2007) 5332-5339.

[160] D. Yuan, X. Gong, R. Wu, Ensemble effects on ethylene dehydrogenation on PdAu(001) surfaces investigated with first-principles calculations and nudged-elastic-band simulations, Phys Rev B, 75 (2007) 233401.
[161] T. Wei, J. Wang, D.W. Goodman, Characterization and Chemical Properties of Pd−Au Alloy Surfaces†, The Journal of Physical Chemistry C, 111 (2007) 8781-8788.
[162] M. Neurock, D.H. Mei, Effects of alloying Pd and Au on the hydrogenation of ethylene: An ab initio-based dynamic Monte Carlo study, Top. Catal., 20 (2002) 5-23.
[163] M. Garcia-Mota, N. Lopez, Temperature and pressure effects in CO titration of ensembles in PdAu(111) alloys using first principles, Phys Rev B, 82 (2010).
[164] K. Balakrishnan, J. Schwank, NEOPENTANE REACTIONS OVER BIMETALLIC PT-SN/AL2O3 AND PT-AU/SIO2 CATALYSTS, Journal of Catalysis, 132 (1991) 451-464.
[165] T. Ward, L. Delannoy, R. Hahn, S. Kendell, C.J. Pursell, C. Louis, B.D. Chandler, Effects of Pd on Catalysis by Au: CO Adsorption, CO Oxidation, and Cyclohexene Hydrogenation by Supported Au and Pd-Au Catalysts, ACS Catal., 3 (2013) 2644-2653.
[166] F. Menegazzo, M. Manzoli, A. Chiorino, F. Boccuzzi, T. Tabakova, M. Signoretto, F. Pinna, N. Pernicone, Quantitative determination of gold active sites by chemisorption and by infrared measurements of adsorbed CO, Journal of Catalysis, 237 (2006) 431-434.
[167] M.A. Vannice, C.C. Twu, Extinction coefficients and integrated intensities for linear- to bridge-bonded CO on platinum, Journal of Chemical Physics, 75 (1981) 5944-5948.
[168] L. Bollmann, J.L. Ratts, A.M. Joshi, W.D. Williams, J. Pazmino, Y.V. Joshi, J.T. Miller, A.J. Kropf, W.N. Delgass, F.H. Ribeiro, Effect of Zn addition on the water-gas shift reaction over supported palladium catalysts, Journal of Catalysis, 257 (2008) 43-54.
[169] M.R. Knecht, M.G. Weir, A.I. Frenkel, R.M. Crooks, Structural rearrangement of bimetallic alloy PdAu nanoparticles within dendrimer templates to yield core/shell configurations, Chemistry of Materials, 20 (2008) 1019-1028.
[170] T. Lear, R. Marshall, J.A. Lopez-Sanchez, S.D. Jackson, T.M. Klapotke, M. Baumer, G. Rupprechter, H.J. Freund, D. Lennon, The application of infrared spectroscopy to probe the surface morphology of alumina-supported palladium catalysts (vol 123, pg 174706, 2005), J. Chem. Phys., 124 (2006).
[171] J.L. Lu, B.S. Fu, M.C. Kung, G.M. Xiao, J.W. Elam, H.H. Kung, P.C. Stair, Coking- and Sintering-Resistant Palladium Catalysts Achieved Through Atomic Layer Deposition, Science, 335 (2012) 1205-1208.
[172] A. Hugon, L. Delannoy, J.-M. Krafft, C. Louis, Selective Hydrogenation of 1,3-Butadiene in the Presence of an Excess of Alkenes over Supported Bimetallic Gold−Palladium Catalysts, The Journal of Physical Chemistry C, 114 (2010) 10823-10835.
[173] S. Marx, F. Krumeich, A. Baiker, Surface Properties of Supported, Colloid-Derived Gold/Palladium Mono- and Bimetallic Nanoparticles, Journal of Physical Chemistry C, 115 (2011) 8195-8205.
[174] A.M. Venezia, V. La Parola, G. Deganello, B. Pawelec, J.L.G. Fierro, Synergetic effect of gold in Au/Pd catalysts during hydrodesulfurization reactions of model compounds, Journal of Catalysis, 215 (2003) 317-325.
[175] G. Rupprechter, M. Morkel, H.J. Freund, R. Hirschl, Sum frequency generation and density functional studies of CO-H interaction and hydrogen bulk dissolution on Pd(111), Surf Sci, 554 (2004) 43-59.
[176] W.Y. Yu, G.M. Mullen, C.B. Mullins, Interactions of Hydrogen and Carbon Monoxide on Pd-Au Bimetallic Surfaces, Journal of Physical Chemistry C, 118 (2014) 2129-2137.
[177] W.Y. Yu, G.M. Mullen, C.B. Mullins, Hydrogen Adsorption and Absorption with Pd-Au Bimetallic Surfaces, Journal of Physical Chemistry C, 117 (2013) 19535-19543.

[178] M.E. Bjorketun, G.S. Karlberg, J. Rossmeisl, I. Chorkendorff, H. Wolfschmidt, U. Stimming, J.K. Norskov, Hydrogen evolution on Au(111) covered with submonolayers of Pd, Physical Review B, 84 (2011).
[179] N.A. Bhore, M.T. Klein, K.B. Bischoff, THE DELPLOT TECHNIQUE - A NEW METHOD FOR REACTION PATHWAY ANALYSIS, Ind. Eng. Chem. Res., 29 (1990) 313-316.
[180] T. Akita, T. Hiroki, S. Tanaka, T. Kojima, M. Kohyama, A. Iwase, F. Hori, Analytical TEM observation of Au-Pd nanoparticles prepared by sonochemical method, Catal. Today, 131 (2008) 90-97.
[181] J. Greeley, M. Mavrikakis, Alloy catalysts designed from first principles, Nature Materials, 3 (2004) 810-815.
[182] B. Hammer, Special sites at noble and late transition metal catalysts, Topics in Catalysis, 37 (2006) 3-16.
[183] R.C. Egeberg, S. Dahl, A. Logadottir, J.H. Larsen, J.K. Norskov, I. Chorkendorff, N-2 dissociation on Fe(110) and Fe/Ru(0001): what is the role of steps?, Surf Sci, 491 (2001) 183-194.
[184] D.W. Flaherty, D.D. Hibbitts, E.I. Gürbüz, E. Iglesia, Theoretical and kinetic assessment of the mechanism of ethane hydrogenolysis on metal surfaces saturated with chemisorbed hydrogen, Journal of Catalysis, 311 (2014) 350-356.
[185] O.Z. Didenko, G.R. Kosmambetova, P.E. Strizhak, Size effect in CO oxidation over magnesia-supported ZnO nanoparticles, Journal of Molecular Catalysis a-Chemical, 335 (2011) 14-23.
[186] M.S. Chen, D.W. Goodman, Structure-activity relationships in supported Au catalysts, Catal. Today, 111 (2006) 22-33.
[187] D.W. Goodman, Model catalysts: from imagining to imaging a working surface, Journal of Catalysis, 216 (2003) 213-222.
[188] A.A. Peterson, L.C. Grabow, T.P. Brennan, B.G. Shong, C.C. Ooi, D.M. Wu, C.W. Li, A. Kushwaha, A.J. Medford, F. Mbuga, L. Li, J.K. Norskov, Finite-Size Effects in O and CO Adsorption for the Late Transition Metals, Top. Catal., 55 (2012) 1276-1282.
[189] M. Casarin, C. Maccato, A. Vittadini, Theoretical investigation of the chemisorption of H-2 and CO on the ZnO(10(1)over-bar0) surface, Inorganic Chemistry, 37 (1998) 5482-5490.
[190] F.M. Poveda, A. Sierraalta, J.L. Villaveces, F. Ruette, Modelling carbon chemisorption on a nickel catalyst. MINDO/SR semiempirical calculations, Journal of Molecular Catalysis a-Chemical, 106 (1996) 109-118.
[191] H.J. Wei, C. Gomez, R.J. Meyer, A Comparative Density Functional Theory Study of Water Gas Shift Over PdZn(111) and NiZn(111), Top. Catal., 55 (2012) 313-321.
[192] A. Sarkany, Z. Zsoldos, B. Furlong, J.W. Hightower, L. Guczi, HYDROGENATION OF 1-BUTENE AND 1,3-BUTADIENE MIXTURES OVER PD/ZNO CATALYSTS, Journal of Catalysis, 141 (1993) 566-582.
[193] J.A. Rodriguez, INTERACTIONS IN BIMETALLIC BONDING - ELECTRONIC AND CHEMICAL-PROPERTIES OF PDZN SURFACES, J. Phys. Chem., 98 (1994) 5758-5764.
[194] M. Nilsson, K. Jansson, P. Jozsa, L.J. Pettersson, Catalytic properties of Pd supported on ZnO/ZnAl2O4/Al2O3 mixtures in dimethyl ether autothermal reforming, Applied Catalysis B-Environmental, 86 (2009) 18-26.
[195] N. Iwasa, T. Akazawa, S. Ohyama, K. Fujikawa, N. Takezawa, DEHYDROGENATION OF METHANOL TO METHYL FORMATE OVER SUPPORTED NI, PD AND PT CATALYSTS - ANOMALOUS CATALYTIC FUNCTIONS OF PDZN AND PTZN ALLOYS, React. Kinet. Catal. Lett., 55 (1995) 245-250.
[196] N. Iwasa, S. Masuda, N. Ogawa, N. Takezawa, STEAM REFORMING OF METHANOL OVER PD/ZNO - EFFECT OF THE FORMATION OF PDZN ALLOYS UPON THE REACTION, Appl. Catal. A-Gen., 125 (1995) 145-157.
[197] N. Iwasa, S. Masuda, N. Takezawa, STEAM REFORMING OF METHANOL OVER NI, CO, PD AND PT SUPPORTED ON ZNO, React. Kinet. Catal. Lett., 55 (1995) 349-353.

[198] M. Lenarda, E. Moretti, L. Storaro, P. Patrono, F. Pinzari, E. Rodríguez-Castellón, A. Jiménez-López, G. Busca, E. Finocchio, T. Montanari, R. Frattini, Finely dispersed Pd-Zn catalyst supported on an organized mesoporous alumina for hydrogen production by methanol steam reforming, Applied Catalysis A: General, 312 (2006) 220-228.
[199] K. Fottinger, J.A. van Bokhoven, M. Nachtegaal, G. Rupprechter, Dynamic Structure of a Working Methanol Steam Reforming Catalyst: In Situ Quick-EXAFS on Pd/ZnO Nanoparticles, J. Phys. Chem. Lett., 2 (2011) 428-433.
[200] O.P. Tkachenko, A.Y. Stakheev, L.M. Kustov, I.V. Mashkovsky, M. van den Berg, W. Grunert, N.Y. Kozitsyna, Z.V. Dobrokhotova, V.I. Zhilov, S.E. Nefedov, M.N. Vargaftik, Moiseev, II, An easy way to Pd-Zn nanoalloy with defined composition from a heterobimetallic Pd(mu-OOCMe)(4)Zn(OH2) complex as evidenced by XAFS and XRD, Catalysis Letters, 112 (2006) 155-161.
[201] Z.-X. Chen, K.M. Neyman, A.B. Gordienko, N. Rösch, Surface structure and stability of PdZn and PtZn alloys: Density-functional slab model studies, Phys Rev B, 68 (2003) 075417.
[202] N. Iwasa, T. Mayanagi, W. Nomura, M. Arai, N. Takezawa, Effect of Zn addition to supported Pd catalysts in the steam reforming of methanol, Applied Catalysis A: General, 248 (2003) 153-160.
[203] T. Komatsu, K. Inaba, T. Uezono, A. Onda, T. Yashima, Nano-size particles of palladium intermetallic compounds as catalysts for oxidative acetoxylation, Appl. Catal. A-Gen., 251 (2003) 315-326.
[204] V. Lebarbier, R. Dagle, T. Conant, J.M. Vohs, A.K. Datye, Y. Wang, CO/FTIR spectroscopic characterization of Pd/ZnO/Al2O3 catalysts for methanol steam reforming, Catalysis Letters, 122 (2008) 223-227.
[205] C. Weilach, S.M. Kozlov, H.H. Holzapfel, K. Fottinger, K.M. Neyman, G. Rupprechter, Geometric Arrangement of Components in Bimetallic PdZn/Pd(111) Surfaces Modified by CO Adsorption: A Combined Study by Density Functional Calculations, Polarization-Modulated Infrared Reflection Absorption Spectroscopy, and Temperature-Programmed Desorption, Journal of Physical Chemistry C, 116 (2012) 18768-18778.
[206] M. Boudart, H.S. Hwang, SOLUBILITY OF HYDROGEN IN SMALL PARTICLES OF PALLADIUM, Journal of Catalysis, 39 (1975) 44-52.
[207] M.W. Tew, J.T. Miller, J.A. van Bokhoven, Particle Size Effect of Hydride Formation and Surface Hydrogen Adsorption of Nanosized Palladium Catalysts: L-3 Edge vs K Edge X-ray Absorption Spectroscopy, J. Phys. Chem. C, 113 (2009) 15140-15147.
[208] S. Penner, B. Jenewein, H. Gabasch, B. Klotzer, D. Wang, A. Knop-Gericke, R. Schlogl, K. Hayek, Growth and structural stability of well-ordered PdZn alloy nanoparticles, Journal of Catalysis, 241 (2006) 14-19.
[209] W. Palczewska, In Hydrogen Effects in Catalysis, Marcel Dekker, New York, 1988.
[210] Y.C. Huang, W.P. Ding, Z.X. Chen, Effect of Zn on the adsorption of CO on Pd(111), Journal of Chemical Physics, 133 (2010).
[211] A. Tamtogl, M. Kratzer, J. Killman, A. Winkler, Adsorption/desorption of H-2 and CO on Zn-modified Pd(111), Journal of Chemical Physics, 129 (2008).
[212] H. Gabasch, A. Knop-Gericke, R. Schlögl, S. Penner, B. Jenewein, K. Hayek, B. Klötzer, Zn Adsorption on Pd(111): ZnO and PdZn Alloy Formation, The Journal of Physical Chemistry B, 110 (2006) 11391-11398.
[213] H. Liu, Y.M. Zhou, Y.W. Zhang, L.Y. Bai, M.H. Tang, Effect of Preparation Processes on Catalytic Performance of PtSnNa/ZSM-5 for Propane Dehydrogenation, Ind. Eng. Chem. Res., 48 (2009) 5598-5603.
[214] M.W. Tew, H. Emerich, J.A. van Bokhoven, Formation and Characterization of PdZn Alloy: A Very Selective Catalyst for Alkyne Semihydrogenation, Journal of Physical Chemistry C, 115 (2011) 8457-8465.

[215] G.C. Bond, Diagnostic use of compensation phenomena in heterogeneous catalysis - Reactions of alkanes on platinum and palladium catalysts, Appl. Catal. A-Gen., 191 (2000) 23-34.
[216] A.J. Sandee, T.J. Chintada, C. Groen, J.G. Donkervoort, R. Terorde, Optimized Palladium on activated carbon formulation for N-hydrogenolysis reactions, Chimica Oggi-Chemistry Today, 31 (2013) 20-23.
[217] R. Burch, Z. Paal, THE USE OF 2,2-DIMETHYLBUTANE (NEOHEXANE) AS A PROBE MOLECULE OF METAL-CATALYSTS, Appl. Catal. A-Gen., 114 (1994) 9-33.
[218] J.H. Sinfelt, KINETICS OF ETHANE HYDROGENOLYSIS, Journal of Catalysis, 27 (1972) 468-&.
[219] T. Conant, A.M. Karim, V. Lebarbier, Y. Wang, F. Girgsdies, R. Schlogl, A. Datye, Stability of bimetallic Pd-Zn catalysts for the steam reforming of methanol, Journal of Catalysis, 257 (2008) 64-70.
[220] A. Karim, T. Conant, A. Datye, The role of PdZn alloy formation and particle size on the selectivity for steam reforming of methanol, Journal of Catalysis, 243 (2006) 420-427.
[221] A. Onda, T. Komatsu, T. Yashima, Characterization and catalytic properties of Ni-Sn intermetallic compounds in acetylene hydrogenation, Phys. Chem. Chem. Phys., 2 (2000) 2999-3005.
[222] A. Ota, M. Armbruster, M. Behrens, D. Rosenthal, M. Friedrich, I. Kasatkin, F. Girgsdies, W. Zhang, R. Wagner, R. Schlogl, Intermetallic Compound Pd2Ga as a Selective Catalyst for the Semi-Hydrogenation of Acetylene: From Model to High Performance Systems, Journal of Physical Chemistry C, 115 (2011) 1368-1374.
[223] T. Komatsu, Y. Fukui, Fischer-Tropsch synthesis on RuTi intermetallic compound catalyst, Appl. Catal. A-Gen., 279 (2005) 173-180.
[224] J. Ruiz-Martinez, Y. Fukui, T. Komatsu, A. Sepulveda-Escribano, Ru-Ti intermetallic catalysts for the selective hydrogenation of crotonaldehyde, Journal of Catalysis, 260 (2008) 150-156.

APPENDIX

Reprint permission for Figure 1

SPRINGER LICENSE
TERMS AND CONDITIONS

Mar 27, 2014

This is a License Agreement between David Childers ("You") and Springer ("Springer") provided by Copyright Clearance Center ("CCC"). The license consists of your order details, the terms and conditions provided by Springer, and the payment terms and conditions.

All payments must be made in full to CCC. For payment instructions, please see information listed at the bottom of this form.

License Number	3356881463587
License date	Mar 27, 2014
Licensed content publisher	Springer
Licensed content publication	Catalysis Letters
Licensed content title	Finite Size Effects in Chemical Bonding: From Small Clusters to Solids
Licensed content author	J. Kleis
Licensed content date	Jan 1, 2011
Volume number	141
Issue number	8
Type of Use	Thesis/Dissertation
Portion	Figures
Author of this Springer article	No
Order reference number	
Original figure numbers	Fig. 1
Title of your thesis / dissertation	An Exploration of Geometric and Electronic Effects in Metal Nanoparticle Catalysts
Expected completion date	Apr 2014
Estimated size(pages)	150
Total	0.00 USD

Reprint permission for Figure 2

ELSEVIER LICENSE
TERMS AND CONDITIONS

Mar 27, 2014

This is a License Agreement between David Childers ("You") and Elsevier ("Elsevier") provided by Copyright Clearance Center ("CCC"). The license consists of your order details, the terms and conditions provided by Elsevier, and the payment terms and conditions.

All payments must be made in full to CCC. For payment instructions, please see information listed at the bottom of this form.

Supplier	Elsevier Limited The Boulevard,Langford Lane Kidlington,Oxford,OX5 1GB,UK
Registered Company Number	1982084
Customer name	David Childers
Customer address	2537 Bennett Ave Evanston, IL 60201
License number	3357280633368
License date	Mar 27, 2014
Licensed content publisher	Elsevier
Licensed content publication	Applied Catalysis
Licensed content title	Bimetallic catalysts; application in catalytic reforming
Licensed content author	J.L. Carter,G.B. McVinker,W. Weissman,M.S. Kmak,J.H. Sinfelt
Licensed content date	15 August 1982
Licensed content volume number	3
Licensed content issue number	4
Number of pages	20
Start Page	327
End Page	346
Type of Use	reuse in a thesis/dissertation
Intended publisher of new work	other
Portion	figures/tables/illustrations
Number of figures/tables/illustrations	1
Format	print
Are you the author of this	No

Reprint permission for Figure 3

ELSEVIER LICENSE
TERMS AND CONDITIONS

Mar 27, 2014

This is a License Agreement between David Childers ("You") and Elsevier ("Elsevier") provided by Copyright Clearance Center ("CCC"). The license consists of your order details, the terms and conditions provided by Elsevier, and the payment terms and conditions.

All payments must be made in full to CCC. For payment instructions, please see information listed at the bottom of this form.

Supplier	Elsevier Limited The Boulevard,Langford Lane Kidlington,Oxford,OX5 1GB,UK
Registered Company Number	1982084
Customer name	David Childers
Customer address	2537 Bennett Ave Evanston, IL 60201
License number	3357280075364
License date	Mar 27, 2014
Licensed content publisher	Elsevier
Licensed content publication	Journal of Catalysis
Licensed content title	Catalytic hydrogenolysis and dehydrogenation over copper-nickel alloys
Licensed content author	J.H. Sinfelt,J.L. Carter,D.J.C. Yates
Licensed content date	February 1972
Licensed content volume number	24
Licensed content issue number	2
Number of pages	14
Start Page	283
End Page	296
Type of Use	reuse in a thesis/dissertation
Intended publisher of new work	other
Portion	figures/tables/illustrations
Number of figures/tables/illustrations	1
Format	print

Reprint permission for Figure 4

THE AMERICAN ASSOCIATION FOR THE ADVANCEMENT OF SCIENCE LICENSE TERMS AND CONDITIONS

Mar 27, 2014

This is a License Agreement between David Childers ("You") and The American Association for the Advancement of Science ("The American Association for the Advancement of Science") provided by Copyright Clearance Center ("CCC"). The license consists of your order details, the terms and conditions provided by The American Association for the Advancement of Science, and the payment terms and conditions.

All payments must be made in full to CCC. For payment instructions, please see information listed at the bottom of this form.

License Number	3357250109943
License date	Mar 27, 2014
Licensed content publisher	The American Association for the Advancement of Science
Licensed content publication	Science
Licensed content title	Reaction-Driven Restructuring of Rh-Pd and Pt-Pd Core-Shell Nanoparticles
Licensed content author	Feng Tao, Michael E. Grass, Yawen Zhang, Derek R. Butcher, James R. Renzas, Zhi Liu, Jen Y. Chung, Bongjin S. Mun, Miquel Salmeron, Gabor A. Somorjai
Licensed content date	Nov 7, 2008
Volume number	322
Issue number	5903
Type of Use	Thesis / Dissertation
Requestor type	Scientist/individual at a research institution
Format	Print
Portion	Text Excerpt
Number of pages requested	1
Order reference number	
Title of your thesis / dissertation	An Exploration of Geometric and Electronic Effects in Metal Nanoparticle Catalysts
Expected completion date	Apr 2014
Estimated size(pages)	150
Total	0.00 USD

Reprint permission for Figure 5

Reprint permission for Figures 6 and 7

Catalytic naphtha reforming

Order detail ID:	65555435
Order License Id:	3430881185031
ISBN:	978-0-8247-5058-9
Publication Type:	Book
Publisher:	CRC PRESS LLC
Author/Editor:	ANTOS, GEORGE J.

Permission Status: Granted

Permission type: Republish or display content
Type of use: Republish in a thesis/dissertation

Requestor type	Academic institution
Format	Print, Electronic
Portion	chart/graph/table/figure
Number of charts/graphs/tables/figures	2
Title or numeric reference of the portion(s)	Part I Figure 1, Part I Figure 6
Title of the article or chapter the portion is from	Naphtha Reforming Chemistry
Editor of portion(s)	Antos, G.; Aitani, A.
Author of portion(s)	Prestvik, R.; Moljord, K.; Grande, K.; Holmen, A.

Volume of serial or monograph	N/A
Page range of portion	3 and 14
Publication date of portion	2004
Rights for	Main product
Duration of use	Life of current edition
Creation of copies for the disabled	no
With minor editing privileges	no
For distribution to	Worldwide
In the following language(s)	Original language of publication
With incidental promotional use	no
Lifetime unit quantity of new product	0 to 499
Made available in the following markets	Online and UIC Library
The requesting person/organization	David Childers
Order reference number	None
Author/Editor	David Childers
The standard identifier	Thesis/dissertation
Title	An Exploration of Geometric and Electronic Effects in Metal Nanoparticle Catalysts
Publisher	UIC
Expected publication date	Aug 2014
Estimated size (pages)	175

Reprint permission for Figure 9

Copyright Clearance Center RightsLink®

Home | Account Info | Help

Title: Dehydrogenation and oxydehydrogenation of paraffins to olefins
Author: M.M Bhasin,J.H McCain,B.V Vora,T Imai,P.R Pujadó
Publication: Applied Catalysis A: General
Publisher: Elsevier
Date: 30 November 2001
Copyright © 2001, Elsevier

Logged in as:
David Childers
LOGOUT

Order Completed

Thank you very much for your order.

This is a License Agreement between David Childers ("You") and Elsevier ("Elsevier"). The license consists of your order details, the terms and conditions provided by Elsevier, and the payment terms and conditions.

Get the printable license.

License Number	3356891360415
License date	Mar 27, 2014
Licensed content publisher	Elsevier
Licensed content publication	Applied Catalysis A: General
Licensed content title	Dehydrogenation and oxydehydrogenation of paraffins to olefins
Licensed content author	M.M Bhasin,J.H McCain,B.V Vora,T Imai,P.R Pujadó
Licensed content date	30 November 2001
Licensed content volume number	221
Licensed content issue number	1–2
Number of pages	23
Type of Use	reuse in a thesis/dissertation
Portion	figures/tables/illustrations
Number of figures/tables/illustrations	1
Format	print
Are you the author of this Elsevier article?	No
Will you be translating?	No
Title of your thesis/dissertation	An Exploration of Geometric and Electronic Effects in Metal Nanoparticle Catalysts
Expected completion date	Apr 2014
Estimated size (number of pages)	150
Elsevier VAT number	GB 494 6272 12
Permissions price	0.00 USD
VAT/Local Sales Tax	0.00 USD / 0.00 GBP
Total	0.00 USD

Reprint permission for Figure 11

Copyright Clearance Center RightsLink®

Home | Account Info | Help

Title: Propane dehydrogenation on PtSn/ZSM-5 catalyst: Effect of tin as a promoter

Author: Yiwei Zhang,Yuming Zhou,Anding Qiu,Yu Wang,Yi Xu,Peicheng Wu

Publication: Catalysis Communications

Publisher: Elsevier

Date: November 2006

Logged in as:
David Childers

LOGOUT

Order Completed

Thank you very much for your order.

This is a License Agreement between David Childers ("You") and Elsevier ("Elsevier"). The license consists of your order details, the terms and conditions provided by Elsevier, and the payment terms and conditions.

Get the printable license.

License Number	3356900120201
License date	Mar 27, 2014
Licensed content publisher	Elsevier
Licensed content publication	Catalysis Communications
Licensed content title	Propane dehydrogenation on PtSn/ZSM-5 catalyst: Effect of tin as a promoter
Licensed content author	Yiwei Zhang,Yuming Zhou,Anding Qiu,Yu Wang,Yi Xu,Peicheng Wu
Licensed content date	November 2006
Licensed content volume number	7
Licensed content issue number	11
Number of pages	7
Type of Use	reuse in a thesis/dissertation
Portion	figures/tables/illustrations
Number of figures/tables/illustrations	1
Format	print
Are you the author of this Elsevier article?	No
Will you be translating?	No
Title of your thesis/dissertation	An Exploration of Geometric and Electronic Effects in Metal Nanoparticle Catalysts
Expected completion date	Apr 2014
Estimated size (number of pages)	150
Elsevier VAT number	GB 494 6272 12
Permissions price	0.00 USD
VAT/Local Sales Tax	0.00 USD / 0.00 GBP
Total	0.00 USD

Reprint permission for Figure 12

ELSEVIER LICENSE
TERMS AND CONDITIONS

Mar 27, 2014

This is a License Agreement between David Childers ("You") and Elsevier ("Elsevier") provided by Copyright Clearance Center ("CCC"). The license consists of your order details, the terms and conditions provided by Elsevier, and the payment terms and conditions.

All payments must be made in full to CCC. For payment instructions, please see information listed at the bottom of this form.

Supplier	Elsevier Limited The Boulevard,Langford Lane Kidlington,Oxford,OX5 1GB,UK
Registered Company Number	1982084
Customer name	David Childers
Customer address	2537 Bennett Ave Evanston, IL 60201
License number	3357270463965
License date	Mar 27, 2014
Licensed content publisher	Elsevier
Licensed content publication	Journal of Catalysis
Licensed content title	The synthesis of highly dispersed noble and base metals on silica via strong electrostatic adsorption: I. Amorphous silica
Licensed content author	Ling Jiao,John R. Regalbuto
Licensed content date	10 December 2008
Licensed content volume number	260
Licensed content issue number	2
Number of pages	13
Start Page	329
End Page	341
Type of Use	reuse in a thesis/dissertation
Intended publisher of new work	other
Portion	figures/tables/illustrations
Number of figures/tables/illustrations	1
Format	print

Reprint permission for Figure 15

ELSEVIER LICENSE
TERMS AND CONDITIONS

Mar 27, 2014

This is a License Agreement between David Childers ("You") and Elsevier ("Elsevier") provided by Copyright Clearance Center ("CCC"). The license consists of your order details, the terms and conditions provided by Elsevier, and the payment terms and conditions.

All payments must be made in full to CCC. For payment instructions, please see information listed at the bottom of this form.

Supplier	Elsevier Limited The Boulevard,Langford Lane Kidlington,Oxford,OX5 1GB,UK
Registered Company Number	1982084
Customer name	David Childers
Customer address	2537 Bennett Ave Evanston, IL 60201
License number	3356900355613
License date	Mar 27, 2014
Licensed content publisher	Elsevier
Licensed content publication	Journal of Catalysis
Licensed content title	Reactions of neopentane on transition metals
Licensed content author	M. Boudart,L.D. Ptak
Licensed content date	January 1970
Licensed content volume number	16
Licensed content issue number	1
Number of pages	7
Start Page	90
End Page	96
Type of Use	reuse in a thesis/dissertation
Intended publisher of new work	other
Portion	figures/tables/illustrations
Number of figures/tables/illustrations	1
Format	print
Are you the author of this	No

Reprint permission for Figure 16

ELSEVIER LICENSE
TERMS AND CONDITIONS

Mar 27, 2014

This is a License Agreement between David Childers ("You") and Elsevier ("Elsevier") provided by Copyright Clearance Center ("CCC"). The license consists of your order details, the terms and conditions provided by Elsevier, and the payment terms and conditions.

All payments must be made in full to CCC. For payment instructions, please see information listed at the bottom of this form.

Supplier	Elsevier Limited The Boulevard,Langford Lane Kidlington,Oxford,OX5 1GB,UK
Registered Company Number	1982084
Customer name	David Childers
Customer address	2537 Bennett Ave Evanston, IL 60201
License number	3356900547794
License date	Mar 27, 2014
Licensed content publisher	Elsevier
Licensed content publication	Journal of Catalysis
Licensed content title	Reactions of neopentane and neohexane on platinum/Y-zeolite and platinum/silica catalysts
Licensed content author	K. Foger,J.R. Anderson
Licensed content date	13 October 1978
Licensed content volume number	54
Licensed content issue number	3
Number of pages	18
Start Page	318
End Page	335
Type of Use	reuse in a thesis/dissertation
Intended publisher of new work	other
Portion	figures/tables/illustrations
Number of figures/tables/illustrations	1
Format	print

Reprint permission for [1]

Copyright Clearance Center RightsLink®

Home | Create Account | Help

ACS Publications High quality. High impact.

Title: Correlating Heat of Adsorption of CO to Reaction Selectivity: Geometric Effects vs Electronic Effects in Neopentane Isomerization over Pt and Pd Catalysts

Author: David Childers, Arindom Saha, Neil Schweitzer, Robert M. Rioux, Jeffrey T. Miller, and Randall J. Meyer

Publication: ACS Catalysis

Publisher: American Chemical Society

Date: Nov 1, 2013

Copyright © 2013, American Chemical Society

User ID

Password

Enable Auto Login

LOGIN

Forgot Password/User ID?

If you're a copyright.com user, you can login to RightsLink using your copyright.com credentials. Already a RightsLink user or want to learn more?

PERMISSION/LICENSE IS GRANTED FOR YOUR ORDER AT NO CHARGE

This type of permission/license, instead of the standard Terms & Conditions, is sent to you because no fee is being charged for your order. Please note the following:

- Permission is granted for your request in both print and electronic formats, and translations.
- If figures and/or tables were requested, they may be adapted or used in part.
- Please print this page for your records and send a copy of it to your publisher/graduate school.
- Appropriate credit for the requested material should be given as follows: "Reprinted (adapted) with permission from (COMPLETE REFERENCE CITATION). Copyright (YEAR) American Chemical Society." Insert appropriate information in place of the capitalized words.
- One-time permission is granted only for the use specified in your request. No additional uses are granted (such as derivative works or other editions). For any other uses, please submit a new request.

Reprint permission for [2]

Copyright Clearance Center RightsLink®

Home | Create Account | Help

ACS Publications High quality High impact

Title: General Method for Determination of the Surface Composition in Bimetallic Nanoparticle Catalysts from the L Edge X-ray Absorption Near-Edge Spectra

Author: Tianpin Wu, David J. Childers, Carolina Gomez, Ayman M. Karim, Neil M. Schweitzer, A. Jeremy Kropf, Hui Wang, Trudy B. Bolin, Yongfeng Hu, Libor Kovarik, Randall J. Meyer, and Jeffrey T. Miller

Publication: ACS Catalysis

Publisher: American Chemical Society

Date: Nov 1, 2012

Copyright © 2012, American Chemical Society

User ID

Password

Enable Auto Login

LOGIN

Forgot Password/User ID?

If you're a copyright.com user, you can login to RightsLink using your copyright.com credentials. Already a RightsLink user or want to learn more?

PERMISSION/LICENSE IS GRANTED FOR YOUR ORDER AT NO CHARGE

This type of permission/license, instead of the standard Terms & Conditions, is sent to you because no fee is being charged for your order. Please note the following:

- Permission is granted for your request in both print and electronic formats, and translations.
- If figures and/or tables were requested, they may be adapted or used in part.
- Please print this page for your records and send a copy of it to your publisher/graduate school.
- Appropriate credit for the requested material should be given as follows: "Reprinted (adapted) with permission from (COMPLETE REFERENCE CITATION). Copyright (YEAR) American Chemical Society." Insert appropriate information in place of the capitalized words.
- One-time permission is granted only for the use specified in your request. No additional uses are granted (such as derivative works or other editions). For any other uses, please submit a new request.

VITA

NAME: David J. Childers

EDUCATION: Ph.D., Chemical Engineering, University of Illinois at Chicago, Chicago, Illinois, 2014

B.S., Chemical Engineering, University of Michigan, Ann Arbor, Michigan, 2009

PRESENTATIONS: 2014 Spring Symposium of Catalysis Club of Chicago, Naperville, IL, 2014.

2013 AIChE Annual Meeting, San Francisco, CA, 2013

23rd North American Catalysis Society Meeting, Louisville, KY, 2013

PROFESSIONAL American Institute of Chemical Engineers (AIChE)

MEMBERSHIP: Catalysis Club of Chicago (CCC)

PUBLICATIONS: S. Kraft, G. Zhang, **D. Childers**, F. Dogan, J. Miller, S. Ngyuen, A. Hock, Rhodium Catechol Containing Porous Organic Polymers: Defined Catalysis for Single-Site and Supported Nanoparticle Materials. *ACS Organometallics* 33 (2014) 2517-2522.

J. Liu, Z. Guo, **D. Childers**, N. Schweitzer, C. Marshall, R. Klie, J. Miller, R. Meyer, Correlating the Degree of Metal-promoter Interaction to Ethanol Selectivity over MnRh/CNTs CO Hydrogenation Catalysts. *Journal of Catalysis* 313 (2014) 149-158.

D. Childers, A. Saha, N. Schweitzer, R. Rioux, J. Miller, R. Meyer, Correlating Heat of Adsorption of CO to Reaction Selectivity: Geometric Effects vs. Electronic Effects in Neopentane

Isomerization over Pt and Pd Catalysts. *ACS Catalysis* 3 (2013) 2487-2496.

T. Wu, **D. Childers**, C. Gomez, A. Karim, N. Schweitzer, A. Kropf, H. Wang, T. Bolin, Y. Hu, L. Kovarik, R. Meyer, J. Miller, General Method for Determination of the Surface Composition in Bimetallic Nanoparticle Catalysts from the L Edge X-ray Absorption Near-Edge Spectra. *ACS Catalysis* 2 (2012) 2433-2443.